

**Synthesis and characterization of designed peptides as  
inhibitors of IAPP fibrillogenesis**

**João Filipe Lopes da Cruz Morais**

Thesis to obtain the Master of Science Degree in  
**Biological Engineering**

Supervisor: Prof. Aphrodite Kapurniotu/ Prof. Arsénio do Carmo Sales Mendes Fialho

**Examination Committee**

Chairperson: Prof. Duarte Miguel De França Teixeira dos Prazeres

Supervisor: Prof. Arsénio do Carmo Sales Mendes Fialho

Members of the Committee: Prof. Nuno Filipe Santos Bernardes

**October 2018**



# Preface

The work presented in this thesis was performed at the Department of Peptide Biochemistry of Technical University of Munich (Munich, Germany), during the period April-September 2018, under the supervision of Prof. Aphrodite Kapurniotu, and within the frame of the Erasmus programme. The thesis was co-supervised at Instituto Superior Técnico by Prof. Arsénio Fialho.

# Abstract

Type 2 diabetes (T2D) and Alzheimer's disease (AD) are characterized by the accumulation of amyloid fibrils constituted mainly by islet amyloid polypeptide (IAPP; T2D) and amyloid  $\beta$  peptide (A $\beta$ ; AD). This work aimed at the optimization of solubility by maintaining the inhibitory properties of a peptide, named "peptide A", recently developed in the Kapurniotu lab.

The optimization of the solubility was done through the addition of dipeptide tags to peptide A. Analogs with tag 1 and 2, called "peptide 1" and "2", were synthesized and studied. The addition of the tags did not alter the secondary structure. However, solubility was decreased and ThT binding showed that only peptide 2 can inhibit IAPP fibrillogenesis.

The study on the optimization of the inhibitory properties of peptide A was done by mutations in position X. Peptides "3" and "4" with aromatic or charged residues in position X were synthesized. The mutations with residues with different properties allowed the change of the secondary structure. The solubility studies showed, however, contradictory results. Also, peptides 3 and 4 interacted with IAPP, but only peptide 4 could inhibit the IAPP fibrillogenesis at the same molar ratio as peptide A.

In conclusion, the length of the peptide played an important role in both solubility and inhibitory properties. The shorter peptide showed a higher solubility, whereas the longer peptides showed a higher inhibitory property. In addition, inhibitory properties were affected by the nature of the amino acid residue at position X.

Key words: IAPP; designed inhibitors; IAPP fibrillogenesis; secondary structure.

# Resumo

A diabetes do tipo 2 (DT2) e doença de Alzheimer (DA) são caracterizadas pela acumulação de fibras amiloides constituídas maioritariamente por amilina e beta amiloide ( $A\beta$ ). Este trabalho teve como objectivo a optimização da solubilidade e das propriedades inibitórias dum inibidor previamente desenvolvidos no laboratório da Prof. Kapurniotu, designado por péptido A.

A optimização da solubilidade foi realizada através da adição de uma cauda de diaminoácidos ao N-terminal do péptido. Análogos com as caudas 1 e 2, designados de péptidos 1 e 2, foram sintetizados e analisados. A adição de aminoácidos não alterou a estrutura do péptido. No entanto, a solubilidade dos péptidos diminuiu e os resultados do ThT mostraram que apenas o péptido 2 foi capaz de inibir a fibrilogénese da amilina.

O estudo da optimização das propriedades inibitórias foi efectuada através de mutações na posição X. Os péptidos 3 e 4 com um aminoácido aromático e polar com carga foram sintetizados. A adição de aminoácidos com diferentes polaridades permitiu alterar a estrutura do péptido. No entanto, o valor da solubilidade apresentou resultados contraditórios. Ambos os péptidos foram capazes de interagirem com o IAPP, mas apenas o péptido 4 foi capaz de inibir fibrilogénese à mesma concentração que o péptido A.

Em suma, o tamanho do péptido desempenha um papel importante nas suas propriedades. Os péptidos mais pequenos apresentaram uma maior solubilidade, enquanto que os péptidos maiores apresentaram melhores propriedades inibitórias. Para além disso, as propriedades inibitórias dos péptidos foram afectadas pela natureza dos aminoácidos na posição X.

Palavras-chaves: IAPP; designado de inibidores; IAPP fibrilogénese; estrutura secundária.

# Acknowledgments

I would like to thank to my family, especially to my parents without them this opportunity would not have been possible. Without their financial support and help I couldn't go abroad to do my thesis. To my brother I thank for all the support and help he gave throughout all my life.

My adaptation was facilitated by all my Erasmus friends, who always supported me and made this experience one of the best experiences in my life.

I am grateful to Prof. Aphrodite Kapurniotu for accepting me in her group and for giving me the opportunity to work in this project. Within her group, I would like to thank Valentina Armiento, the best supervisor I could have asked for. Without her knowledge, guidance and friendship I could not have succeed. A deeply thanks to the rest of the co-workers in Prof. Kapurniotu lab for all the help throughout my thesis and for the good moments. A special thanks to Karin Tas and Kathleen Hille for the TEM grid and the MALDI-TOF results.

# Table of Content

<b>Preface</b> .....	<b>iii</b>
<b>Abstract</b> .....	<b>iv</b>
<b>Resumo</b> .....	<b>v</b>
<b>Acknowledgments</b> .....	<b>vi</b>
<b>Table of Content</b> .....	<b>vii</b>
<b>List of figures</b> .....	<b>x</b>
<b>List of Tables</b> .....	<b>xii</b>
<b>List of Acronyms</b> .....	<b>xiii</b>
<b>1. Introduction</b> .....	<b>1</b>
1.1. Protein synthesis .....	1
1.2. Protein folding.....	1
1.3. Misfolded proteins.....	2
1.4. Amyloid Formation.....	4
1.4.1. Thermodynamics properties and kinetics.....	4
1.5. Alzheimer's disease.....	6
1.5.1. Amyloid cascade hypothesis.....	6
1.5.2. Amyloid $\beta$ .....	8
1.5.3. Structure of A $\beta$ monomers .....	9
1.6. Diabetes type 2.....	11
1.6.1. Islet amyloid polypeptide.....	11
1.6.2. Residues important for amyloid formation .....	12
1.6.3. Structure of hIAPP .....	13
1.6.4. Mechanism of cell toxicity .....	15
1.7. Cross interaction.....	16
1.8. Peptide inhibitors .....	18
1.9. Aim of this work .....	20
<b>2. Material and Methods</b> .....	<b>21</b>
2.1. Material.....	21
2.2. Methods.....	24
2.2.1. Synthesis of the peptides through solid phase peptide synthesis .....	24
2.2.2. Cleavage.....	28
2.2.3. Purification using HPLC .....	29

2.2.4.	Mass spectrometry .....	30
2.2.5.	Aliquots preparation .....	31
2.2.6.	Circular dichroism .....	31
2.2.7.	Thioflavin-T assay.....	33
2.2.8.	Transmission electron microscopy.....	34
2.2.9.	Centrifugation assay .....	34
2.2.10.	Fluorescence titration.....	35
<b>3.</b>	<b>Results.....</b>	<b>36</b>
3.1.	Synthesis and purification.....	36
3.1.1.	Analogs with tags.....	36
3.1.1.	Analogs with mutations in specific residues .....	46
3.2.	Effect of the modifications on the secondary structure and solubility of the analogs .....	52
3.2.1.	Secondary structure and solubility of the analogs with tags.....	53
3.2.1.	Secondary structure and solubility of analogs with mutations in specific residues.....	54
3.3.	Effect of the interaction between IAPP and the analogs in the secondary structure .....	56
3.3.1.	Interaction between IAPP and the analogs with tags .....	56
3.3.1.	Interaction between IAPP and the analogs with mutations in specific residues .....	57
3.4.	Effect of the modifications in the inhibition of the IAPP fibrillogenesis .....	59
3.4.1.	Inhibitory properties of the analogs with tags .....	59
3.4.1.	Inhibitory properties of the analogs with mutations in specific residues .....	62
3.5.	Effect of the modifications on the self-assembly and binding of the analogs to IAPP .....	64
3.6.	Determination of the solubility by a centrifugation assay .....	66
<b>4.</b>	<b>Discussion.....</b>	<b>70</b>
4.1.	Synthesis and purification.....	70
4.2.	Effect of the modifications on the secondary structure and solubility of the analogs .....	71
4.2.1.	Secondary structure and solubility of the analogs with tags.....	71
4.2.2.	Secondary structure and solubility of the analogs with mutations in specific residues .....	72
4.3.	Effect of the modifications in the inhibition of the IAPP fibrillogenesis .....	73
4.3.1.	Inhibitory properties of the analogs with tags .....	73
4.3.2.	Inhibitory properties of the analogs with mutations in specific residues .....	73
4.4.	Effect of the interaction between IAPP and the analogs in the secondary structure .....	74
4.5.	Effect of the modifications on the analogs self-assembly and the binding affinity of the analogs to IAPP .....	75
4.5.1.	Addition of tags .....	75
4.5.2.	Mutations in specific residues .....	76
4.6.	Determination of the solubility by a centrifugation assay .....	77



<b>5. Conclusion and future perspective .....</b>	<b>78</b>
<b>6. References .....</b>	<b>80</b>

## List of figures

**Figure 1.1** – Energy landscape scheme of protein folding and aggregation.

**Figure 1.2** – The scheme represents the formation of amorphous and native-like deposits and amyloid fibrils.

**Figure 1.3** – Scheme of amyloid kinetics.

**Figure 1.4** – Scheme representing the two different paths of APP.

**Figure 1.5** – Representation of A $\beta$ <sub>40</sub> structure obtained through solid-state NMR studies.

**Figure 1.6** – Atomic model of a cross section of a A $\beta$ <sub>42</sub> fibril by solid-state NMR and cryo–electron microscopy.

**Figure 1.7** – Amino acid sequence of the PrePro-hiAPP, Pro-hiAPP and mature hiAPP.

**Figure 1.8** – Scheme of  $\beta$ -hairpin structure of hiAPP.

**Figure 1.9** – Structural model of hiAPP obtained from studies with steric zippers.

**Figure 1.10** – Sequence of IAPP and A $\beta$  with the identical amino acids in blue and the similar residues in green.

**Figure 2.1** – General scheme of solid phase peptide synthesis.

**Figure 2.2** – Generic scheme of the peptide bond formation accomplished through the activation of the carboxyl group.

**Figure 2.3** – Far UV CD spectra of the different types of secondary structures.

**Figure 3.1** – Purification of 500  $\mu$ g crude, dissolved in 100  $\mu$ L TFA and 400  $\mu$ L 80% B, with a Reprosil Gold 200 column (C18, 10  $\mu$ m 250 x8 mm), using Schnell A $\beta$  program.

**Figure 3.2** – MALDI-TOF results obtained from the three fractions of the purification of the peptide 1 crude, in an acetone matrix.

**Figure 3.3** – Repurification of 500  $\mu$ g peptide 1, dissolved in 100  $\mu$ L TFA and 400  $\mu$ L 80% B, with a Reprosil Gold 200 column (C18, 10  $\mu$ m 250 x8 mm), using Langsame A $\beta$  program 214 nm.

**Figure 3.4** – MALDI-TOF results obtained for the repurification of the peptide 1, in an acetone matrix.

**Figure 3.5** – Purification of 500  $\mu$ g fluorescence labelled peptide 1 crude, dissolved in 100  $\mu$ L TFA and 400  $\mu$ L 80% B, with a Reprosil column Gold 200 (C18, 10  $\mu$ M 250 x8 mm), using Schnell A $\beta$  program 214 nm and 433 nm.

**Figure 3.6** – MALDI-TOF results obtained for the purification of the fluorescence labelled peptide 1, in acetone matrix.

**Figure 3.7** – Purification of 500  $\mu$ g of fluorescence labelled peptide 1 crude dissolved in 100  $\mu$ L TFA and 400  $\mu$ L 80% B with a Reprosil Gold 200 (C18, 10  $\mu$ M 250 x8 mm) using Langsame A $\beta$  214 nm and 433 nm.

**Figure 3.8** – MALDI-TOF results obtained for the purification of the fluorescence labelled peptide 1, in an acetone matrix.

**Figure 3.9** – Repurification of 500  $\mu$ g of peptide 2 crude dissolved in 100  $\mu$ L TFA and 400  $\mu$ L 80% B with a Reprosil Gold 200 (C18, 10  $\mu$ M 250 x8 mm) using Langsame A $\beta$  Long 214 nm.

**Figure 3.10** – MALDI-TOF results obtained for the purification of peptide 2, in an acetone matrix.

**Figure 3.11** – Purification of 500 µg of fluorescence labelled peptide 2 crude dissolved in 100 µL TFA and 400 µL 80% B with a Reprosil Gold 200 (C18, 10 µM 250 x8 mm) using Schnell Aβ 214 nm and 433 nm.

**Figure 3.12** – MALDI-TOF results obtained for the purification of the fluorescence labelled peptide 2, in an acetone matrix.

**Figure 3.13** – Purification of 500 µg peptide 3 crude dissolved in 100 µL TFA and 400 µL 80% B with a Reprosil Gold 200 (C18, 10 µM 250 x8 mm) using Schnell Aβ (A) and Langsame Aβ (B) and the detection was at 214 nm.

**Figure 3.14** – MALDI-TOF results obtained for the purification of the peptide 3, in an acetone matrix.

**Figure 3.15** – Purification of 500 µg of fluorescence labelled peptide 3 crude dissolved in 100 µL TFA and 400 µL 80% B with a Reprosil Gold 200 (C18, 10 µM 250 x8 mm) using LangsameSamuel Aβ 214 nm and 433 nm.

**Figure 3.16** – MALDI-TOF results obtained for the purification of the fluorescence labelled JF<sup>31</sup>, in an acetone matrix.

**Figure 3.17** – Purification of 500 µg of peptide 4 crude dissolved in 100 µL TFA and 400 µL 80% B with a Reprosil Gold 200 (C18, 10 µM 250 x8 mm) using Schnell Aβ and the detection was at the wavelength of 214 nm.

**Figure 3.18** – MALDI-TOF results obtained for the purification of the peptide 4, in an acetone matrix.

**Figure 3.19** – Purification of 500 µg of fluorescence labelled peptide 4 crude dissolved in 100 µL TFA and 400 µL 80% B with a Reprosil Gold 200 (C18, 10 µM 250 x8 mm) using Schnell Aβ 214 nm and 433 nm.

**Figure 3.20** – MALDI-TOF results obtained for the purification of the fluorescence labelled peptide 4, in an acetone matrix.

**Figure 3.21** – Far UV CD – concentration dependence spectra obtained for all analogs.

**Figure 3.22** – Far UV CD spectra obtained for the interaction of IAPP and the analogs.

**Figure 3.23** – ThT assay of the mixture IAPP with peptide 1 and TEM images.

**Figure 3.24** – ThT assay of the mixture IAPP with peptide 2 and TEM images.

**Figure 3.25** – ThT assay of the mixture between IAPP and the peptide 3 and TEM images.

**Figure 3.26** – ThT assay of the mixture IAPP with peptide 4 and TEM images.

**Figure 3.27** – Correlation between the fluorescence emission in arbitrary units (a.u.) and the peptide mass in µg.

**Figure 3.28** – Centrifugation assay performed with 20 µM of peptide.

**Figure 4.1** – Comparison of the secondary structures of the analogs at 5 µM.

**Figure 4.2** – Comparison of the secondary structure of the analog A and the analogs with mutations in position 31 at 5 µM.

**Figure 4.3** – Representation of the two local minimums obtained from the IAPP and the peptide mixture.

**Figure 4.4** – Comparison of binding affinities of the synthesized analogs 1 and 2 with the control peptides, A and B.

**Figure 4.5** – Comparison of binding affinities of the synthesized analogs 3 and 4 with the peptide A.

## List of Tables

**Table 2.1** – List of devices used during the experiments with the correspondent supplier.

**Table 2.2** – List of materials used with the correspondent supplier.

**Table 2.3** – List of software used with the correspondent supplier.

**Table 2.4** – List of chemicals used with the correspondent abbreviation and supplier.

**Table 2.5** – List of solutions used with the correspondent application and its components.

**Table 2.6** – Description of the HPLC programs used to elute the peptides, with the flow in mL/min, the duration of the elution gradient in min and the initial and final conditions of the elution gradient.

**Table 2.7** – Description of the HPLC programs used to clean the column, with the flow in mL/min, the duration of the program in min and the washing conditions.

**Table 3.1** – App.  $K_d$  values obtained for three different experiments: the determination of the binding affinity between the fluorescence labelled peptide and IAPP; the binding affinity between the fluorescence IAPP and the peptide and the binding activity between the fluorescence labelled peptide and the peptide.

**Table 3.2** – Summary of the experiments performed for the analogs.

## List of Acronyms

<b>A<math>\beta</math></b>	Amyloid beta
<b>AD</b>	Alzheimer's disease
<b>App. K<sub>D</sub></b>	Apparent K <sub>D</sub>
<b>CD</b>	Circular dichroism
<b>CPE</b>	carboxypeptidase E
<b>DIEA</b>	N,N-diisopropylethylamine
<b>ddH<sub>2</sub>O</b>	Distilled water
<b>DMF</b>	Dimethylformamide
<b>EGCG</b>	(-)-Epigallocatechin 3-Gallate
<b>ER</b>	Endoplasmic reticulum
<b>ERAD</b>	Endoplasmic reticulum associated protein degradation
<b>HATU</b>	2-(7-aza-1H-benzotriazole-1-yl)-1,1,3,3-tetramethyluronium hexafluorophosphate
<b>HBTU</b>	(2-(1H-benzotriazol-1-yl)-1,1,3,3-tetramethyluronium hexafluorophosphate
<b>HFIP</b>	1,1,3,3,3-hexafluoro-2-isopropanol
<b>HPLC</b>	High pressure liquid chromatography
<b>IAPP</b>	Islet amyloid polypeptide
<b>K<sub>D</sub></b>	Dissociation constant
<b>MALDI</b>	Matrix assisted laser desorption ionization
<b>MRE</b>	Mean residue ellipticity
<b>MS</b>	Mass spectrometry
<b>nm</b>	Nanometer
<b>PAM</b>	Peptidyl amidating mono-oxygenase
<b>SD</b>	Standard deviation
<b>SPPS</b>	Solid phase peptide synthesis
<b>T2D</b>	Type 2 Diabetes
<b>TEM</b>	Transmission electron microscopy
<b>ThT</b>	Thioflavin-T
<b>TFA</b>	Trifluoroacetic acid
<b>TOF</b>	Time of flight
<b>UPR</b>	unfolded protein response



# 1. Introduction

## 1.1. Protein synthesis

In the living organism, the synthesis of proteins involves the transcription and processing of the mRNA, followed by the translation of mRNA into the amino acids sequence in the ribosomes. In the eukaryote cells, the synthesis can be performed in the cytoplasm or in the endoplasmic reticulum (ER) by the free or immobilized ribosomes, respectively. The proteins synthesized in the cytoplasm are folded after detachment of the ribosome. This process depends on the amino acid sequence since the interaction of some residues allows the protein to acquire a semi-folded state. The folding of these proteins is mediated by a class of proteins named chaperones<sup>1</sup>. They can also rescue misfolded proteins or aggregates to fold properly again<sup>2,3</sup>.

On the other hand, proteins can also be synthesis in the ER, where chaperones and folding catalysts will help proteins to fold correctly and after that they are translocated to the Golgi. The folding process is mediated by several check-points that are important to ensure the correct folding of proteins throughout the different stages<sup>4,5</sup>. The folding quality control is processed by glycosylation and deglycosylation that allows the cell to distinguish the well folded proteins from the others<sup>4</sup>. The misfolded proteins are ubiquitinated and then are transported to the proteasome where they undergo proteolysis. These two antagonist processes, synthesis and degradation of proteins, play an important role as regulatory mechanisms for the well function of eukaryotic cells, not only due to the elimination of damage proteins but also because the degradation of proteins act as a mechanism of intracellular regulation.<sup>6</sup> Hence, the folding of proteins is a complex process accomplished through a sequence of equilibria that goes from the amino acid sequence to the partially fold-state and then to a fold state<sup>7</sup>. Despite the molecular mechanism to prevent misfolded proteins our aggregates, some proteins are able to escape them, forming unwanted structures that are associated with several diseases. Hence, several studies have been carried out in order to understand the mechanisms of folding and misfolding.

## 1.2. Protein folding

In the majority of the cases the native structure of the protein is the most stable structure under physiological conditions<sup>8</sup>. The transition between random coil and the native structure does not involve sequential steps, instead consists in the screening of different conformations that minimizes the free energy for that protein, as it's shown in figure 1.1<sup>9,10</sup>. In the beginning, the amino acid sequence provides different folding possibilities. The interactions between a small number of amino acids will allow the formation of a folding nucleus, by which the rest of the amino acids will fold in order to obtain the native folded protein<sup>11</sup>. During this process, the decrease of entropy must be compensated by the increase of enthalpy resulting from the intra e intermolecular interactions between the residues. Hence, the driving force of this process is the decrease of free energy<sup>12</sup>. Through this process, the number of putative fold structures decreases until the native structure is achieved<sup>13</sup>. However, since the free energy depends upon the interactions established between the amino acids, alterations of cellular conditions, such as

protein concentration or temperature, may alter the free energy minimum. This alteration will induce a different fold conformation that may tend to aggregate. Hence, the native state of a protein may not be, in different conditions, the global energy minimum. Protein aggregates are formed due to the establishment of intermolecular interactions between the different oligomers. These interactions are responsible for the stabilization of the protein, making it more stable than the native state, as it is shown in figure 1.1. Therefore, the conformation that a protein acquires depends strongly on the interactions established between the amino acids<sup>13</sup>. If the interactions are mainly intramolecular the protein will tend to fold into its native structure, whereas if the predominant interactions are intermolecular, then the protein will tend to aggregate. *In vivo*, the cellular mechanism, mediated by chaperones, are responsible to lift the aggregates to a higher level of energy which enables them to follow a new folding path and consequently, fold correctly<sup>14</sup>.

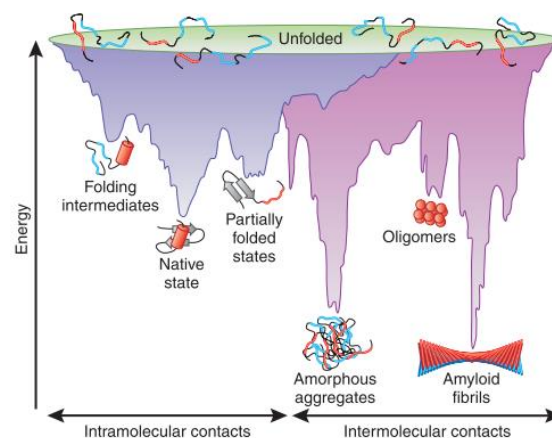


Figure 1.1 – Energy landscape scheme of protein folding and aggregation. The purple section represents the folding of the native state and it's due to the intramolecular interactions between residues of the protein. The pink section represents the formation of aggregates or amyloid fibrils. The formation of those structures depends on intermolecular interactions. This structure can have a lower energy than the native state of the protein and therefore, are thermodynamically more stable. There is an overlap between both regions, which indicates that the formation of amyloid fibrils or aggregates can occur due to intermediates during the *de novo* folding or of the destabilization of native state. However, there are cellular mechanism to prevent the formation of those structures. Figure taken from *F Ulrich Hartl et. al, (2009)*<sup>13</sup>.

### 1.3. Misfolded proteins

As noted above, the proteins can have several states between its linear structure to its globular native structure. However, there are proteins which do not fold into a globular state or do not fold completely, designated as intrinsically disordered or partially folded protein, respectively. Intrinsically disordered proteins are important signalling and regulatory molecules and their lack of structure is crucial for their function<sup>15,16</sup>. This type of proteins can also be originated by the proteolytic degradation of globular fold proteins, like the case of amyloid-beta peptide<sup>7</sup>.



Even though, these proteins tend to aggregate and are involved in several diseases associated with protein aggregation, the evolution of their sequences occurred to increase their solubility and therefore, to maintain their optimal function<sup>17</sup>. Protein aggregation can occur in all protein stages and it depends on the aggregation monomer, i. e., disordered, partial folded or native folded proteins, and their aggregation can originate amorphous and native-like aggregates or amyloid fibrils, as it is shown in figure 1.2.

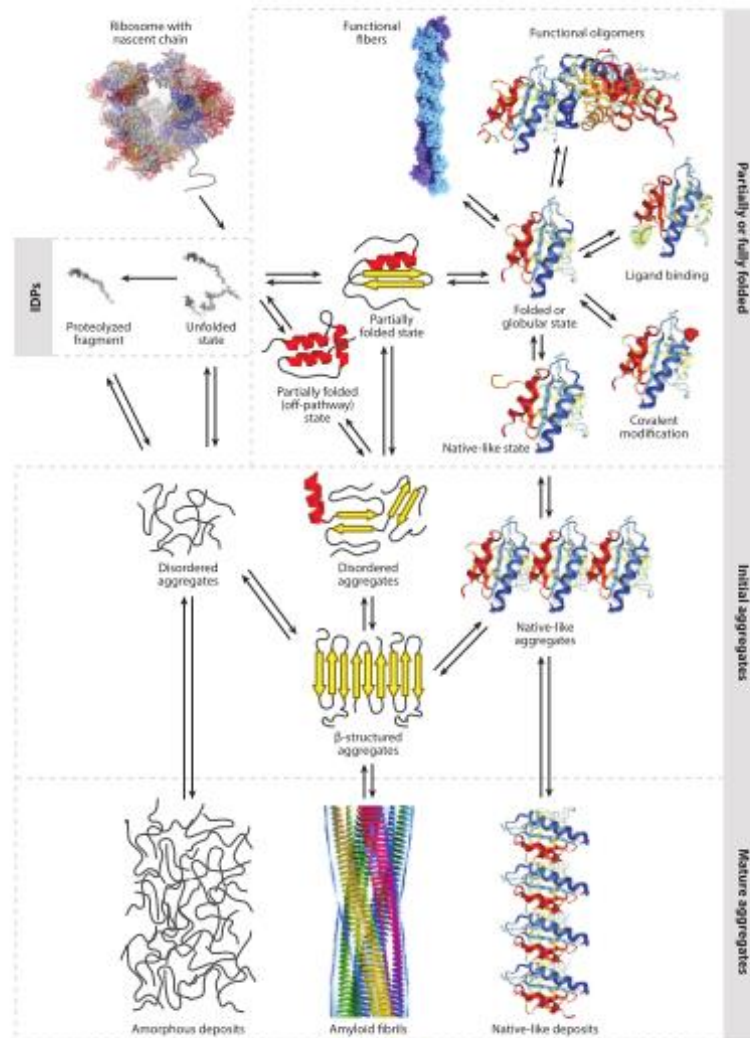


Figure 1.2 – The scheme represents the formation of amorphous and native-like deposits and amyloid fibrils. The scheme is divided in different boxes: the intrinsically disordered proteins (IDPs), the partially or fully folded proteins, initial oligomers and mature aggregates. Initially, the linear sequence is synthesized in the ribosome and afterwards can fold to originate intermediates and the native state of the protein, which can remain unfolded or can form aggregates responsible for deposits. The aggregation of native-like state can also originate deposits. These processes are regulated by cellular mechanisms, which aim to prevent the formation of the different deposits and allow the formation of proteins native state. Figure taken from *Fabrizio Chiti et al. (2012)*<sup>7</sup>.

## 1.4. Amyloid Formation

As mentioned before, several proteins can aggregate and form amyloid fibrils, which are constituted by protofilaments. Typically, they were between 2 and 8 protofilaments<sup>18</sup>. Nevertheless, fibrils constituted by a single protofilament have also been observed<sup>19,20</sup>. These fibrils are defined, according to biophysicists, as displaying a cross- $\beta$  fiber diffraction pattern<sup>21</sup>. The cross- $\beta$  architecture stabilizes the fibrils formation due to the development of continuous hydrogen bonds between the  $\beta$ -sheets<sup>22</sup>. Moreover, the hydrogen bonds along the fibril axis are strong interactions between the polypeptide chains which make the distance between the polypeptide chains approximately constant, even for different polypeptide sequences. On the other hand, the interactions between different fibrils are weak interactions and therefore, the distance between the fibrils varies considerably with the sequence of the side chain groups and their interactions<sup>23,24</sup>. Other important characteristic of the amyloid fibrils is their ability to bind with dyes, such as, the thioflavin-T<sup>7</sup>.

The  $\beta$ -strand structure can be either parallel or antiparallel, i.e. the adjacent sheets run in the same direction or in opposite directions. Another important feature of amyloid proteins is that the sheets are usually "in register", i.e. the strands align in order to allow the alignment of the same side chain residues, optimizing the intermolecular interactions. The distance between the side chain residues differs depending if the strands are parallel or antiparallel<sup>25</sup>.

To enter the amyloid state, proteins need to expose their amine and carboxylic terminus to allow the formation of hydrogen bonds with other protein groups. Nevertheless, the exposure of the terminus regions is not enough to make proteins enter the amyloid state; the reaction has to be thermodynamically favourable.<sup>21</sup>

### 1.4.1. Thermodynamics properties and kinetics

A process is thermodynamically favourable if the free energy of the products is lower than the free energy of the reactants. Hence, the amyloid formation occurs because the free energy of the amyloid is lower than the free energy of the protein native state, which makes the amyloid more stable than the protein native state<sup>18</sup>. Since the free energy depends of the concentration of species involved in the equilibrium, the concentration of the peptides must be high to counter balance the decrease of entropy resulting from fibers formation<sup>21</sup>.

The kinetics of the amyloid formation is described by a sigmoidal kinetics divided in three parts: the lag phase, the growth phase and the plateau phase. The lag phase is characterized by the association of the monomers to form the nuclei. This phase is thermodynamically disfavoured and the nuclei formation will determine the overall kinetics profile. In the growth phase, polymerization will occur and elongation of the fibrils, in a thermodynamically favourable process. After the depletion of the monomers, the concentration of fibrils will be constant, which means that the plateau phase is reached<sup>26,27</sup>.

The nucleation process starts with the aggregation of soluble monomers into insoluble structures, the nuclei, that will induce the elongation of the fibril. This process of transition between the soluble phase to a condense phase is known as primary nucleation and is characterized by the lag phase. However, the nucleation process involves different processes, such as, fragmentation, branching and secondary nucleation<sup>18</sup>. During the fibrils elongation, characteristics of growth phase, there may occur fragmentation of those fibrils increasing the number of nuclei available for the fibrils formation, and consequently, the fibrils rate formation<sup>27,28</sup>. The fragmentation process and the secondary nucleation processes – fibrils catalyse the formation of new aggregates on their surface by the ability of some fibrils to create new ends through branching – are responsible for increasing the aggregation rate. The figure 1.3 summarizes the overall process described previously. Furthermore, it's important to emphasize that the different kinetics phases are the result of different processes and is their combination that will determine the kinetics parameters, such as the fibrils formation rate. This process is usually followed by the binding of ThT to cross- $\beta$  aggregates.

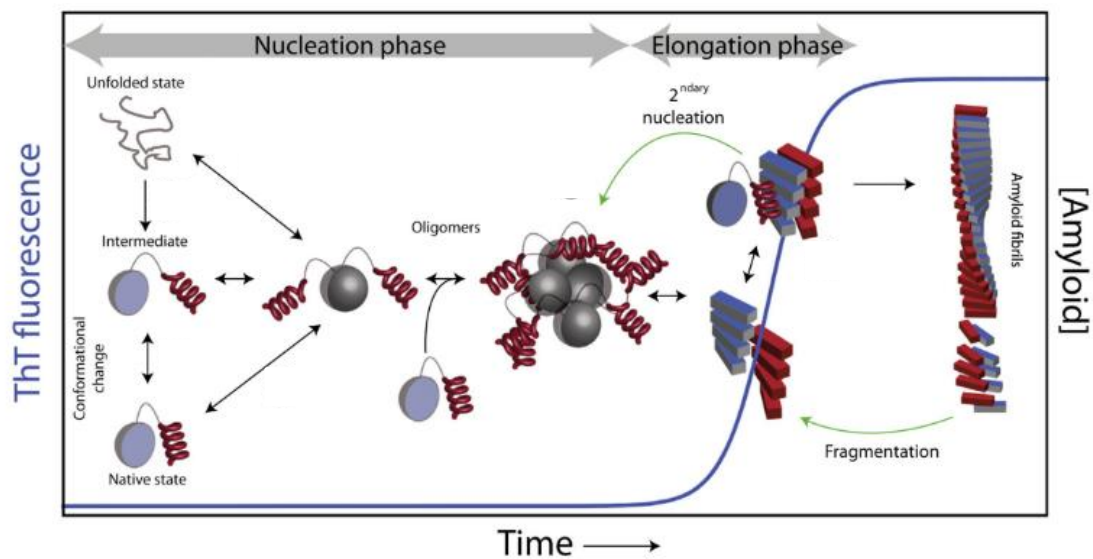


Figure 1.3 – Scheme of amyloid kinetics. The lag phase, or nucleation phase, is characterized by the formation of the nuclei, nucleation. The grow phase or elongation phase is where the polymerization and elongation take places. The secondary nucleation and fragmentation processes will increase the number of nuclei and therefore, the formation of fibrils. Afterwards, the plateau phase is reached and is characterized by depletion of monomers and the concentration of amyloid fibrils will remain constant. This process can be monitored by ThT fluorescence, which consists in the binding of Thioflavin-T, a dye, to proteins with a  $\beta$ -sheet structure, such as amyloid fibrils. Figure taken from *Karamanos et al. (2015)*<sup>29</sup>.

## 1.5. Alzheimer's disease

Alzheimer disease (AD) was first described by Alois Alzheimer, a German psychiatrist in 1907. AD is a neurodegenerative disease and is the main cause of dementia in the western world<sup>30,31</sup>. From a histological point a view, AD is characterized by three different hallmarks: the extracellular amyloid- $\beta$  ( $A\beta$ ) plaques, the neurofibrillary tangles and the synapses lost<sup>31</sup>. The  $A\beta$  plaques are extracellular insoluble constitute by aggregates amyloid-beta peptides<sup>32</sup>. The second biomarker is an intracellular deposit formed of filaments of hyperphosphorylated tau, which is localized manly in neurons. The last hallmark is a consequence of the first two biomarkers.

### 1.5.1. Amyloid cascade hypothesis

The amyloid cascade hypothesis postulates that the accumulation of amyloid fibrils in the brain is the main cause of Alzheimer's disease<sup>33</sup>.

Amyloid-beta ( $A\beta$ ) are natural peptides formed as a result of cellular metabolism, whose length vary at the C-terminus, between 36 to 43 amino acids<sup>34</sup>. These peptides are produced through the cleavage of amyloid precursor protein (APP). APP is a type I membrane glycoprotein constitute by several isoforms, which are the result of alternative splicing and consists in a large extracellular glycosylated N-terminus and a shorter cytoplasmic C-terminus<sup>35</sup>. This membrane protein regulates the synapses plasticity, iron export and anterograde neuronal transport<sup>36-38</sup>.

There are two different pathways for the processing of APP, as it is shown in figure 1.4. In the non-amyloidogenic pathway the  $\alpha$ -secretase cleaves the APP in a cytoplasmic region originating two segments, the soluble form of APP, the sAPP $\alpha$ , and C83 (the membrane fragment constituted by 83 amino acids). Afterwards, the  $\gamma$ - secretase cleaves the C83, originating the p3 and AICD, a nuclear signaller. On the other hand, in the amyloidogenic pathway the  $\beta$ -secretase BACE-1 (beta-side amyloid precursor protein-cleaving enzyme 1), cleaves the APP peptide originating two segments, the sAPP $\beta$  and the C99, a membrane fragment<sup>34</sup>. Afterwards, the  $\gamma$ - secretase, a protein complex with presenilin 1 at the active-site, cleaves the C99 in multiple sites which will originate the  $A\beta$  peptide and the AICD<sup>39</sup>.

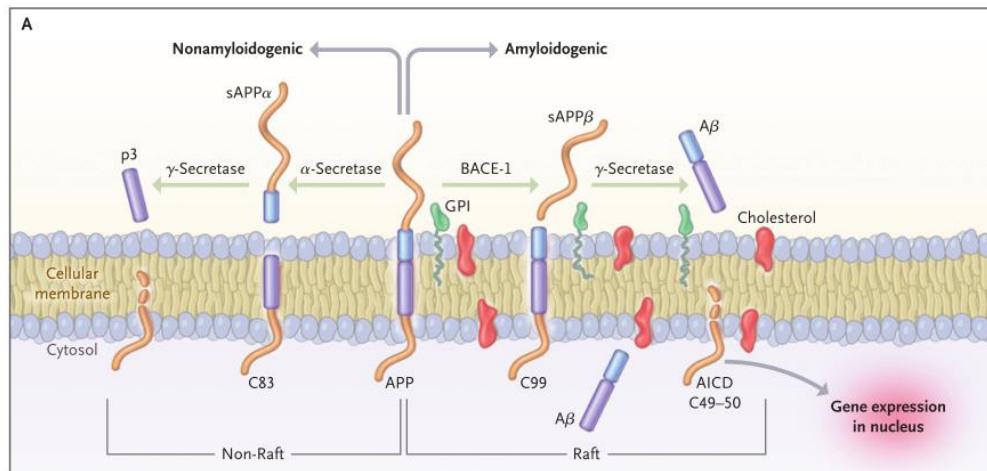


Figure 1.4 – Scheme representing the two different paths of APP. In the non-amyloidogenic pathway the APP is cleaved by the  $\alpha$ -secretase, originating two fragments, the ectodomain, the sAPP $\alpha$ , and C83. Afterwards, the  $\gamma$ -secretase cleaves the C83, originating the p3 and AICD, a nuclear signal. In the amyloidogenic pathway the  $\beta$ -secretase BACE-1 cleaves the APP peptide originating two segments, the sAPP $\beta$  and the C99. After that, the  $\gamma$ -secretase cleaves the C83 in multiple sites which will originate the A $\beta$  peptide and the AICD. Figure taken from Frank M. La Ferla et. al (2010)<sup>34</sup>.

The dysregulation between the production and clearance of A $\beta$  lead to the increase of A $\beta_{42}$ /A $\beta_{40}$  ratio and the excess of the amyloid peptides with induce their oligomerization, along with the deposition of A $\beta$  deposits, in the brain parenchyma. Firstly, these fibres will deposit as benign diffuse paques and after obtaining other A $\beta$  fibres an inflammatory response is triggered. The change in extracellular stimulus that neurons received will change their normal function, namely the ionic homeostasis important in the brain plasticity. Moreover, those alterations may increase the oxidative stress aggravating the cellular damages. Simultaneously, alteration in the kinase/phosphatase pathways will induce oligomerization and hyperphosphorylation of tau protein, which is responsible for the cellular malfunction and death. The neuronal death cause by the accumulation of those two types of fibrils contribute to the long-term dementia associated with AD<sup>40</sup>.

This hypothesis is corroborated by the discovery that mutations could lead to the AD, albeit the genetic mutations are responsible for only a small fraction, around 2-5%, of all AD cases<sup>41</sup>. Mutations in presenilin 1 and 2 (PSEN1 and PSEN2) – both proteins form the active site of  $\gamma$ -secretase – can increase the production of A $\beta$  peptides<sup>42,43</sup>. Alterations in APOE genes, a class of genes important for the clearance of A $\beta$  peptides, can reduce the clearance of the peptide inducing its aggregation<sup>44</sup>. Altogether these results corroborate the importance of A $\beta$  in the AD, supporting the amyloid beta cascade hypothesis.

Nevertheless, this theory has been insufficient to create efficient therapeutics against AD<sup>45</sup>. The flaws of this theory are regarding the interaction between A $\beta$  and tau protein and the presence of A $\beta$  plaques in post mortem brains of people without cognitive impairment at the death<sup>46</sup>. Even though, tau pathology is correlated with several other neurodegenerative diseases, is still not clear how the two proteins

interact with each other. The experimental evidences suggested that A $\beta$  trigger the formation of neurofibrillary tangles, and consequently, the neural dysfunction and death<sup>47</sup>. On the other hand, some studies have suggested that the toxicity is due to the existence of soluble A $\beta$  oligomers and not directly to the amount of A $\beta$  plaques, explaining the presence of the A $\beta$  plaques in post mortem brains of people without AD.

### 1.5.2. Amyloid $\beta$

The A $\beta$  have different isoforms that differ in the amino acid number. The A $\beta$  constituted by 40 amino acids, A $\beta$ <sub>40</sub>, is the most abundant isoform in the brain, while the A $\beta$  isoform constituted by 42 amino acids, A $\beta$ <sub>42</sub>, is the most prevalent amyloid isoform found in amyloid plaques<sup>34</sup>. Those two isoforms differ in two amino acids in the C-terminal region.

The oligomerization of A $\beta$  monomers originates oligomers. These peptides, with small size, are highly soluble that can spread throughout the brain.<sup>48</sup> The polymerization of oligomers is responsible for the formation of protofilaments and the polymerization of those filaments produce the amyloid plaques<sup>8</sup>. These plaques are insoluble and its accumulation in the extracellular matrix induces histological damages in Alzheimer's patients<sup>48</sup>. These fibrils are highly resistant to denaturation and proteolytic cleavage and are thermostable<sup>49,50</sup>.

Previous studies have shown that the A $\beta$  oligomers levels correlate better with the disease severity rather than the level of amyloid plaques<sup>51</sup>. Furthermore, the presence of amyloid fibrils does not affect the cognition, while the presence of A $\beta$  oligomers in solution are responsible for the neuronal death, and consequently, memory loss and dementia<sup>51</sup>. Hence, the intermediates forms of A $\beta$ , such as A $\beta$  oligomers, play a vital role in the toxicity of A $\beta$  in the Alzheimer's disease, albeit the amyloid plaques aren't toxic. There are still controversial about the role of the amyloid plaques. Nevertheless, some results support the hypothesis that the oligomers are in equilibrium with the plaques and that the plaques can trap the A $\beta$  oligomers, inhibiting their toxicity<sup>52</sup>. However, the trap oligomers can solubilize in solution, causing neuronal death<sup>53</sup>.

### 1.5.3. Structure of A $\beta$ monomers

The development and improvement of techniques that allow the determination of protein structure, such as NMR, X-ray crystallography and cryo-electron microscopy permitted the development and improvement of A $\beta$  models<sup>20,25,54–58</sup>. The continuous improvement of those models is essential to better understand the real structure of A $\beta$  monomers in order to develop efficient drugs to prevent the malignant consequences of their accumulation. Despite the A $\beta$  polymorphism, the several structures of A $\beta$  agree in a common U-shaped- $\beta$ -strand-turn- $\beta$ -Strand structure<sup>58</sup>.

*Daniel Huster et. al* (2012) proposed the A $\beta_{40}$  fibrils structure based on solid-state NMR, as it shown in figure 1.5<sup>59</sup>. The results showed a  $\beta$ -turn structure, where it is possible to observe the different structures commonly attributed to A $\beta$ . The unstructured N-terminal of peptide is constituted by the residue 1-10, the two  $\beta$ -sheets, from residues 11-22 and 30-38, respectively, linked by a random coil structure from residues 23-28<sup>59</sup>. The random coil is constituted by polar amino acids and the Lys28 and the Asp23 establish a salt bridge connection, responsible for the stability of the  $\beta$ -turn<sup>60</sup>. The unstructured N-terminus is made by a both polar and non-polar amino acids. The two  $\beta$ -sheets are rich in hydrophobic amino acids which plays an important role in oligomerization of the A $\beta$  monomers, through the establishment of hydrogen bonds with the same amino acids from other monomers.

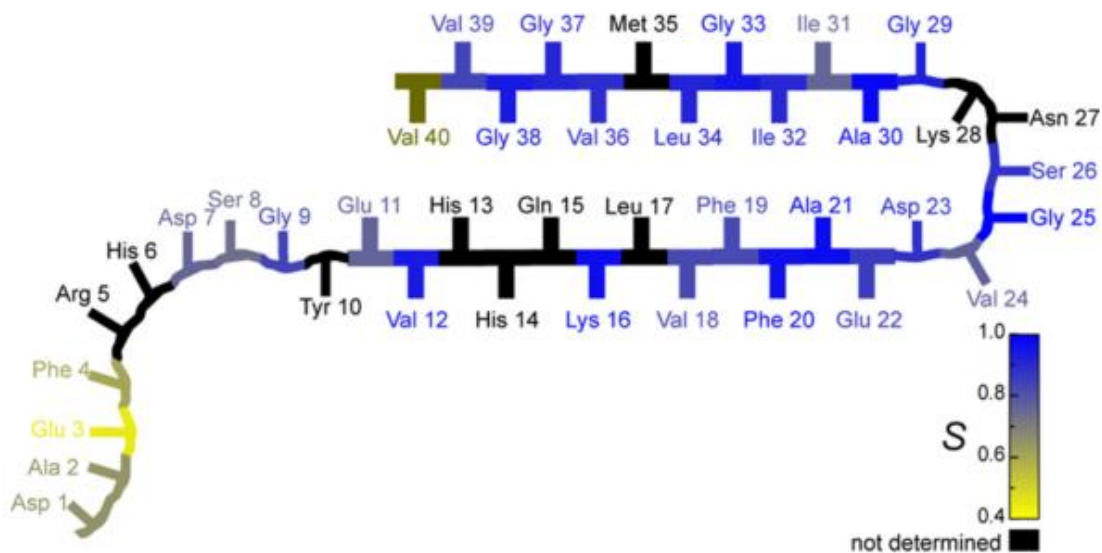


Figure 1.5 – Representation of A $\beta_{40}$  structure obtained through solid-state NMR studies. The thick lines represent the two  $\beta$ -sheet structures and the thin lines are the N-terminus and the loop, which connects both  $\beta$ -sheet. The structure agrees with the U-shaped- $\beta$ -strand-turn- $\beta$ -Strand structure. Figure taken from *Daniel Huster et. al* (2012)<sup>59</sup>.

Gunnar F. Schröder et al. (2017) determined the structure of two subunits of A $\beta$ <sub>42</sub> from a fibril structure using cryo–electron microscopy and solid-state NMR, shown in figure 1.6 a)<sup>61</sup>. The second technique was performed to complement the results obtained by the first technique. The interaction of the two monomers showed different amino acids facing the hydrophobic core compared to the previous structure. It's important to emphasize the existence of different polymorphism, which were described for the two-brain seed–derived A $\beta$ <sub>42</sub> fibrils preparation<sup>61</sup>. Three hydrophobic clusters have been proposed as a stabilizer of the fibril structure, namely the Ala2, Val36, Phe4, and Leu34; the Leu17, Ile31, and Phe19; and the Ala30, Ile32, Met35 and Val40. In figure 1.6 b) is represented the interaction between Ala 2 at the N-terminal of one monomer and the Ala42 at the C-terminal of the other one. This interaction is stabilized by a salt bridge between Asp1 and Lys28. The other salt bridges are between Asp7 and Arg5 and Glu11, His6 and His13<sup>61</sup>. The last one is important to stabilize the kink of the N-terminus on the beginning  $\beta$ -sheet, as it has been previously published.<sup>55</sup>

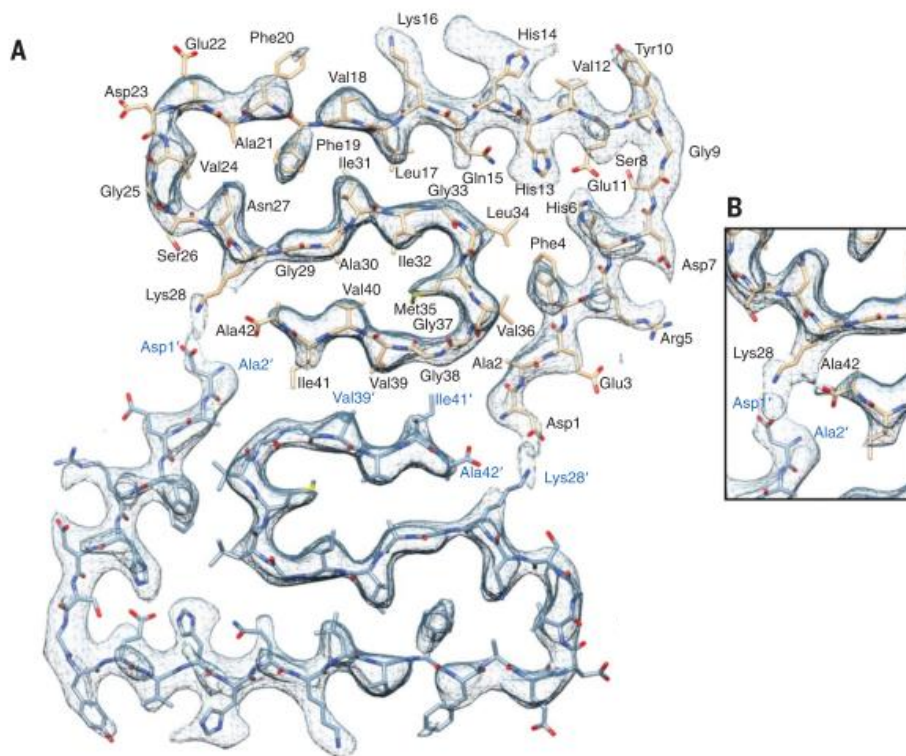


Figure 1.6 – Atomic model of a cross section of a A $\beta$ <sub>42</sub> fibril by solid-state NMR and cryo–electron microscopy. A – Cross section of a protofilament showing the A $\beta$ <sub>42</sub> sequence and its structure, along with EM density map. B – Detailed view of the interaction between N and the C terminus, focusing the importance of Lys28 side-chain group in this interaction. Figure taken from Gunnar F. Schröder et. al, (2017)<sup>61</sup>.



## 1.6. Diabetes type 2

The type 2 diabetes (T2D) is a disease characterized by the hyperglycemia that is the combination of reduced insulin secretion, impaired muscle and adipose tissue insulin action, and increased glucose output<sup>62</sup>. The reduction in insulin secretion is caused by the dysfunction and death of  $\beta$ -cells. Over the last decades the number of patients which developed this disease increase significantly. In 2010, the number of patients worldwide with this condition was around 285 million people, where 90% of the patients had T2D<sup>63,64</sup>. This number is expected to increase, reaching the 439 million of patients by 2030, which will be around 7,7% of the total population with 20–79 years. Moreover, the T2D was considered an adult disease and over the last years the number of young people developing this disease had increased significantly<sup>65</sup>. Thus, the age at which people develop this disease has been decreasing. The reasons for this decrease are related with the western life style, namely the sedentarism (the lack of physical exercise), smoking, a diet rich in fat and sugar and obesity. To avoid this trend, several attempts have been made to develop more efficient treatments in order to cure the patients and to decrease the social and economic impact that this disease will have in the future<sup>65</sup>.

### 1.6.1. Islet amyloid polypeptide

The post-mortem pancreas of patients with T2D showed the presence of amyloid aggregates of a peptide produced in the pancreas, the islet amyloid polypeptide (IAPP)<sup>66–70</sup>. Subsequent studies showed the amylogenesis of IAPP is related with the dysfunction and death of  $\beta$ -cells, in the islets of Langerhans<sup>71,72</sup>.

The IAPP is coded by single copy gene on the short arm of the chromosome 12<sup>73</sup>. Initially, an 89 amino acid peptide, the preproIAPP, is synthesized in the ER. This sequence is constituted by a signal peptide and two flanking regions which will be cleaved, originating the proIAPP<sup>74</sup>. This sequence is cleaved by three enzymes, hormone convertase PC1/3. The PC1/3 will cleave the C-terminus, leaving Gly-Lys-Arg sequence at the C-terminus. On the other hand, the N-terminus is cleaved only by the PC2, on the carboxylic site of the Lys10-Arg11. The two basic amino acids present in the C-terminus of the peptide are removed by the carboxypeptidase E (CPE). This process is followed by the amidation of the C-terminus by the peptidyl amidating mono-oxygenase complex (PAM). The mature IAPP, constituted by 37 residues, is obtained after the formation of the disulphide bond. The modifications of the proIAPP into IAPP will occur in the Golgi complex and in the insulin secretory granule<sup>74</sup>. The figure 1.7 outlines the IAPP synthesis.

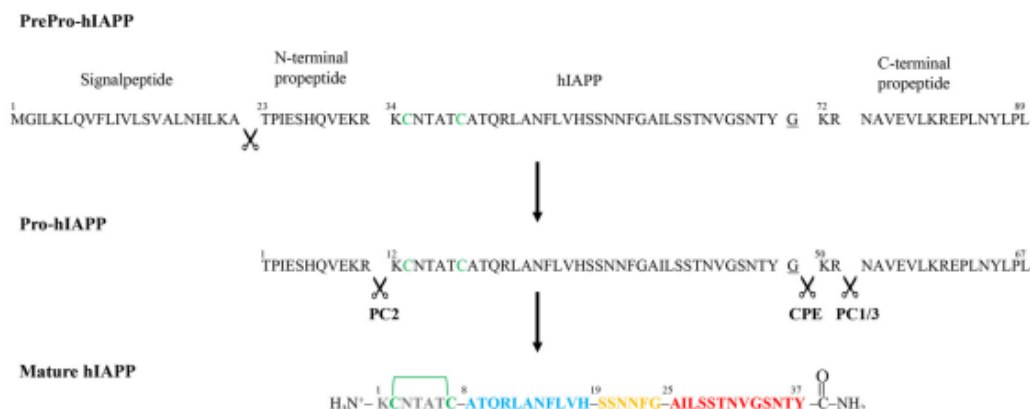


Figure 1.7 – Amino acid sequence of the PrePro-hIAPP, Pro-hIAPP and mature hIAPP. The cleavage of the signal peptide and the two flanking regions will originate the Pro-hIAPP. This molecule will be cleaved in the Golgi complex and in the insulin secretory granule. The hormone convertase PC1/3 and the carboxypeptidase E (CPE) are the enzymes involved in the process. The PC1/3 is responsible for cleaving the C-terminus leaving the tripeptide Gly-Lys-Arg on the C-terminus. On the other hand, the PC2 will cleave between the Arg11 and the Lys12. The CPE will remove the two dibasic amino acids from the C-terminus region. The amidation of the C-terminus and the disulphide bond are required to the formation of the mature hIAPP. Figure taken from *Michaela Pressa et al. (2018)*<sup>75</sup>.

The IAPP is stored together with insulin in  $\beta$ -cells secretory granules and is released together with the insulin as a response to specific stimulus<sup>76,77</sup>. The IAPP concentration inside the  $\beta$ -cells secretory granules is much higher than the concentration to induce amyloid formation *in vitro*<sup>78,79</sup>. The inhibition of amyloid formation can be explained by two different factors: the low pH of the  $\beta$ -cells secretory granules that decrease significantly the amyloid rate formation and the presence of insulin since it acts as an inhibitor of IAPP aggregation<sup>80</sup>.

The physiological role of IAPP in human is not fully understood, however evidences showed that IAPP is important in controlling gastric emptying, maintaining glucose homeostasis, in the suppression of glucan release and in controlling satiety<sup>81,82</sup>.

### 1.6.2. Residues important for amyloid formation

The IAPP is a hormone constituted by 37 amino acids, soluble and natively unfolded in solution. The amino acid composition differs from organism to organism and those differences are responsible for the ability of forming amyloid<sup>83</sup>. The human IAPP, hIAPP, is highly amyloidogenic while the rat IAPP doesn't form amyloid fibrils. The differences are between the residues 20 and 29, where the rat IAPP displays 3 proline residues, which are  $\beta$ -sheet destabilisers and can inhibit the fibrils formation. Therefore, the hIAPP 20-29 residues are important to the amyloid formation, but subsequent studies have shown that region is not the only amyloidogenic region. The residues 11-20 are important as well for the fibrils formation and the residues 14-20 can form fibrils<sup>84</sup>. Another study showed the amylogenesis of IAPP is

pH dependant, being faster at low pH (4) and slower at higher values of pH (8,8) , which is relevant due to the fact that the pH of granules where IAPP is stored is low (5,5) and when it's in circulation the pH is physiological one, 7,4<sup>84,85</sup>. Moreover, the deamidation of Asn can also play an important role in the amyloid formation for two reasons: it can alter the conformation of hIAPP amyloid fibrils and studies *in vitro* showed that deamination can increase the hIAPP fibrils formation and turn non-amylogenic hIAPP fragments in amylogenic ones<sup>86,87</sup>.

### 1.6.3. Structure of hIAPP

The IAPP is a natively unfolded protein and in its monomeric form was described as a random coil. However, following studies have shown that the secondary structure wasn't a classical random coil since NMR results had shown that in solution the N terminus region, between residues 5 and 20, displayed the helical  $\Psi$  and  $\phi$  angles, albeit the lower  $\alpha$ -helix content<sup>72,82</sup>. Nevertheless, it's important to emphasize that the structure of this peptide depends significantly on the experimental conditions used.

*Kajava et al.* (2005) proposed a  $\beta$ -hairpin with three  $\beta$ -strands as a model for hIAPP structure. This model was created in order to optimize the number of apolar amino acids in the inner part the fibrils and simultaneously have the polar residues Asn and Gln inside the fibril<sup>88</sup>. These premises would allow the optimization of the hydrogen bonds between the residues. Moreover, the three  $\beta$ -strands was also taken in account based on the exitance of three potential amyloidogenic regions, each one, with a  $\beta$ -strand structure<sup>89</sup>. The figure 1.8 showed the structure of hIAPP. In this model, the first eight residues had a random coil structure. The disulphuric bond between the Cyst2 and Cyst7 suggested the presence of a loop in this region, which was contradictory with the presence of this amino acids in the  $\beta$ -strand structure. The three  $\beta$ -strands were located in the regions 12–17, 22–27 and 31–37, which was coherent with the amyloidogenic regions, and they were linked by two loops.

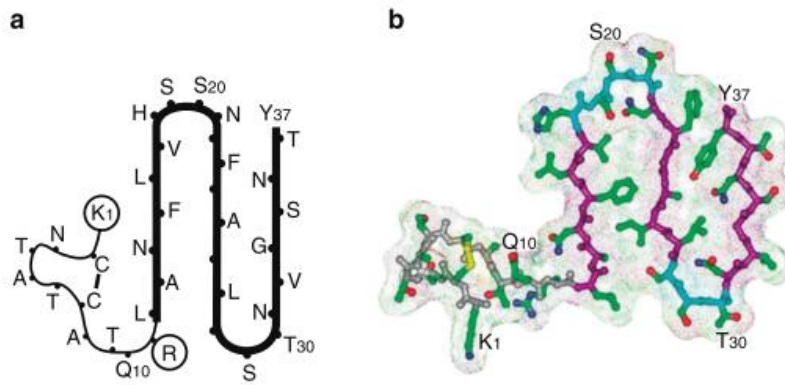


Figure 1.8 – Scheme of  $\beta$ -hairpin structure of hIAPP. a – The first 11 residues constitute the loop and are shown as a thin line, where the circles mean the presence of charge residues. The cysteines in position 2 establish a disulphuric bond with the cysteine in position 7. The three  $\beta$ -strands, linked by two loops, are constituted mainly by the apolar amino acids and are represented as thick line. b – Ball-and-stick representation of  $\beta$ -hairpin structure, where the loop and  $\beta$ -strand backbone are blue and purple, respectively. Carbon, oxygen, nitrogen and sulphur atoms are in green, red, blue and yellow, respectively. Figure taken from *Andrey V. Kajava et. al. (2005)*<sup>89</sup>.

*Heisenberg et al. (2008)*, proposed a different hIAPP model based on X-ray crystallographic studies of two penta- or hexapeptide “steric zippers”<sup>90</sup>. As it is shown in figure 1.9 B the monomer hIAPP is constituted by two  $\beta$ -strand connected by a loop. The first eleven residues don’t belong to the  $\beta$ -sheet structure due to the presence of the disulphuric bond that will impose a conformation hindrance. In this model, the region between residues 20 to 29, important to the hIAPP amyloidogenicity, isn’t incorporated in the  $\beta$ -sheets structures, instead, it appears in the loop region. The figure 1.9 C show the residues which play an important role in the interaction between the two hIAPP monomers. The amino acids in the steric zipper are Leu27, Ser29, Asn 31 and Gly 33. Since this structure is devoid of water molecules, the hydrogen bonds and the hydrophobic interactions are essential for the stabilization of the amyloid fibril formation.

Thus, different hIAPP structures have been proposed. The differences of the different structures depend on the technique used to determine it, the samples used since polymorphism is responsible for the residues position disagreement and the premises used for the construction of the model.

The IAPP fibrils display the ordinary cross- $\beta$  diffraction pattern<sup>91</sup>. The fibrils are made by three protofilaments in a left-handed coil with a pitch of 25–50 nm<sup>91</sup>. The first 7 residues are not part of the  $\beta$ -sheet core since the disulfuric bond imposed a conformational restriction that prevents the residues to have the necessary conformation in order to form the hydrogen bond required to the  $\beta$ -sheet structure<sup>74</sup>. The amyloid fibrils are constituted by parallel in register arrangement of the  $\beta$ -strand. Each protofilament has two chains where the peptides establish hydrogen bond with peptides from the other chain, but without intrachain hydrogen bounds<sup>92</sup>. The figure 1.9 A show a representation of the fibrils structure.

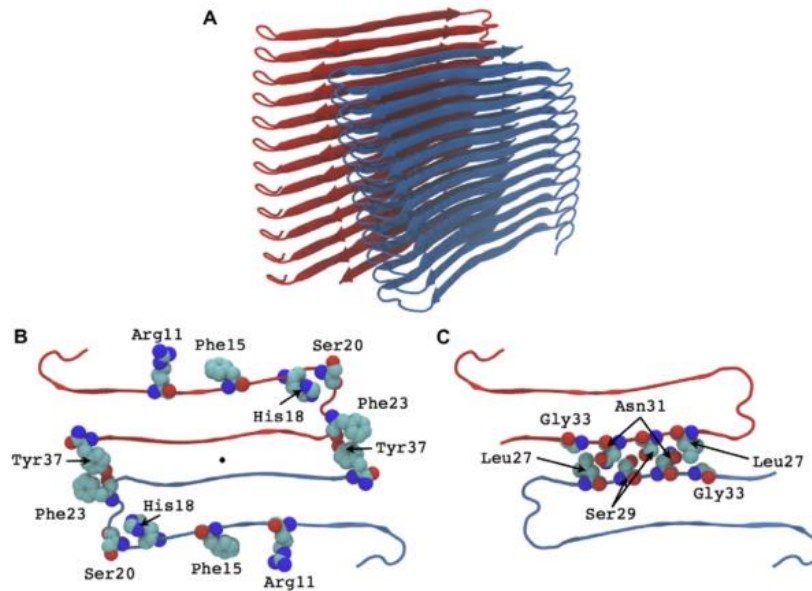


Figure 1.9 – Structural model of hIAPP obtained from studies with steric zippers. A – ribbons model of the fibrils structure. The red and the blue structures correspond to different fibrils. B – cross section of a fibril layer showing important amino acids, namely Arg11, Phe15, His18, Ser20, Phe23 and Tyr37 and the position of their side-chain group. The colour code is the same as the one used in A. C – cross section of a fibril layer showing the important residues in the steric zipper interface. The residues shown are the Leu27, Ser29, Asn 31 and Gly 33. Figure taken from *David Heisenberg et. al. (2008)*.<sup>90</sup>

#### 1.6.4. Mechanism of cell toxicity

The toxicity of the IAPP is not well understood, however it's thought to interfere with cellular processes through the alteration of signalling pathways and/or cellular mechanism. Some of the processes involved in cellular death are the ER stress, defect in autophagy, increased the production of proinflammatory cytokines, damage of cellular membrane and activation of apoptosis signalling pathways<sup>93</sup>.

The presence of hIAPP have been reported to induce ER stress, endoplasmic reticulum associated protein degradation (ERAD) and the unfolded protein response (UPR) and consequently  $\beta$ -cell death. Although several studies have shown a relation between the ER stress and apoptosis of  $\beta$ -cell, the role of hIAPP in toxicity isn't clear yet<sup>94</sup>. Some studies shown that the overexpression of hIAPP in rat trigger cell death mechanism, while other showed absence of ER stress of cultured islets that produce hIAPP<sup>95-97</sup>. The oligomers produced in the ER and in the Golgi complex can go to the cytosol, where they will damage the organelles membrane. The damage of mitochondria membrane will induce oxidative stress due to the production of reactive oxygen species ROS, which will oxidize the proteins. Thus, the protein activity will decrease significantly and that will affect several cellular pathways<sup>98</sup>.

Dysfunction of autophagy was also reported in other amyloid diseases. The increase production and accumulation of toxic hIAPP inside the cell will induce the autophagy mechanism – a cellular protective mechanism – in order to eliminate them from the cell. However, this mechanism cannot eliminate efficiently all the aggregates and the remaining aggregates will lead to autophagy-mediated lysosomal dysfunction and therefore, cell death<sup>99,100</sup>.

The production of proinflammatory cytokines can also play an important role in the induction of apoptosis. The accumulation of hIAPP aggregates is responsible for triggering an inflammatory response. This response will induce an inflammasome activity – the inflammasome are multiprotein assemblies that produce caspase-1 as a result of the inflammatory stimuli. Afterwards, the caspase-1 cleave the cytokine IL-1 $\beta$ , which will induce cellular dysfunction and death<sup>101,102</sup>. Moreover, the intra and extracellular hIAPP is able to induce apoptosis signal pathways, such as the JNK pathway<sup>103</sup>.

Lastly, the hIAPP had been proposed to change the membrane permeability and therefore, its integrity<sup>104,105</sup>. Two different mechanisms were proposed to explain the membrane disruption. The first one is the pore hypothesis, where the hIAPP interact with the cellular membrane, forming pores that will allow an uncontrolled flux of ions across the membrane that will damage the cell and may trigger apoptosis mechanisms. The experimental evidences suggest the pores development occurs in the beginning of fibrilization since the number of pores disappeared with the fibril's formation. Therefore, the oligomers are the species responsible for this mechanism<sup>106–108</sup>. The other mechanism is designated by detergent or fragmentation mechanism and consists in the interaction of the IAPP intermediates with a cellular membrane, forming vesicle-like structures containing both peptide and lipid. This mechanism also occurs in the beginning of fibril formation<sup>109</sup>. These two mechanisms coexist inside the cell and its relevance depends on the cellular environment. However, the ability of IAPP to permeabilize the membrane will depend on several factors, such as, the lipid to peptide ratio, the lipid composition, the pH and the ionic strength<sup>74</sup>. It's necessary caution when extrapolating from biophysical experiments since the results are obtained using systems with a higher percentage of anionic lipids than the one found in  $\beta$ -cell membranes and due to the fact that the employed models are simpler than the cellular membrane since they don't have cholesterol nor gangliosides<sup>110</sup>.

Overall, the hIAPP can trigger several mechanisms that converge to the induction of cellular death mechanism in order to eliminate the malfunction cells.

## 1.7. Cross interaction

Several epidemiological studies have shown the patients with T2D have a higher probability to develop AD and vice-versa<sup>111</sup>. Moreover, both diseases have several features in common.

Both diseases are caused by the accumulation of misfolded protein aggregates; the accumulation of A $\beta$  and IAPP in the brain of AD patients and in the pancreatic islet of T2D patients, respectively. The A $\beta$  and the IAPP shared an identity and a sequence similarity of 25% and 50%, respectively. The high degree of similarity was shared between the A $\beta$ (15-21) and IAPP(10-16) and the A $\beta$ (26-32) and APP(21-27), highlighted in yellow in figure 1.10<sup>112</sup>. The region highlighted by the pink area is the area thought to be important in the self-assembly and it contemplated the amyloidogenic region<sup>25,92,113–116</sup>.

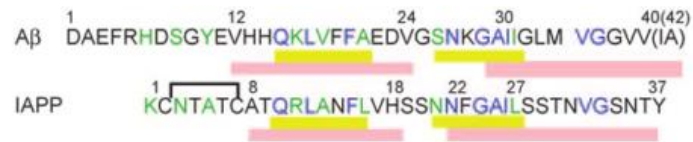


Figure 1.10 - Sequence of IAPP and A $\beta$  with the identical amino acids in blue and the similar residues in green. The region highlighted in yellow are the shortest regions with a higher degree of similarity and identity. The pink area is the one reported to be important in the interaction of both peptides. Figure taken from *Aphrodite Kapurniotu et al.* (2010)<sup>112</sup>.

The production of those aggregates follows a seeding-nucleation model, as the one explained in the chapter 1.4.1. Interestingly, amyloid proteins have the ability to influence the appearance and progression of different amyloid diseases, through a process designated by cross-interaction or cross-seeding<sup>117</sup>. This ability is related with the capacity of some amyloid proteins to nucleate the formation of a different amyloid protein, which is possible due to structural similarities between the different amyloid peptides, such as the IAPP and A $\beta$ . Several *in vitro* studies have demonstrated the existence of cross-interaction between those two amyloid peptides, where the addition of IAPP aggregates can increase the A $\beta$  aggregation *in vitro*<sup>112,118,119</sup>. It has been reported that IAPP aggregates within the A $\beta$  plaques in the brain of patients with both diseases, suggesting an *in vivo* correlation between both peptides. This is possible due to the presence of IAPP and the A $\beta$  peptides in the serum and in the cerebrospinal fluid. Moreover, the A $\beta$  peptides have been found in pancreatic islet amyloid aggregates of T2D. A recent study *in vivo* confirmed the *in vitro* results, in which the over-production of hIAPP increase the accumulation of A $\beta$  in the brain and staining of those fibrils showed the presence of hIAPP<sup>120</sup>.

Interestingly, the AD hallmarks: the presence of neurofibrillary tangles with phosphorylated tau protein and the presence of extracellular deposits constituted mainly the A $\beta$  peptide are also present in the T2D, with the differences that in the T2D the extracellular deposits are constituted mainly by hIAPP<sup>121</sup>.

Besides the peptide's similarity, both diseases had identical physiological processes. One factor that impact both diseases is the insulin. The insulin receptors are also expressed on neurons in the central nervous system<sup>122,123</sup>. These receptors are important to regulate several processes, such as, neuronal differentiation, neurotransmitter vesicle released and cellular repair mechanisms<sup>111</sup>. The neurotransmitter vesicle released are important since it regulated memory formation, information processing and cognitive processes<sup>124</sup>. Furthermore, insulin suppress cell death mechanism<sup>125–127</sup>.

Previous studies showed that a high serum insulin level could impair cognitive functions. This result suggested that the high level of insulin in the serum was responsible for the increase of the of A $\beta$  levels, which led to impairment of the cognitive functions. This was due to the fact that insulin act as a regulator of gene transcription and an alteration on insulin levels dysregulated the transcription of housekeeping gene. As a consequence, the degradation of A $\beta$  aggregates will be reduced due to the down regulation of insulin-degrading enzyme, an enzyme capable of degrading A $\beta$ <sup>128-130</sup>.

Moreover, the insulin will affect the transcription of genes responsible for the reduction of the release of neurotransmitters, which will lead to the weakening of synapses and phosphorylation of tau protein<sup>111</sup>. Overall, these results showed the importance of insulin abnormalities in the development of AD. Regarding the T2D, an abnormal production of insulin, a common feature of this condition, induce the hIAPP amyloidogenicity since the insulin inhibition effect is no longer present<sup>80</sup>.

On the other hand, the high levels of glucose in the plasma due to the abnormalities in the insulin pathways increased the production of advanced glycation end products which have toxic effects on the cells. Those results showed a tight physiological relationship between both diseases<sup>131,132</sup>.

## 1.8. Peptide inhibitors

The pursuit of drugs against T2D had increased in the last decades due to the increase impact of this condition in the worldwide population. The IAPP was thought to trigger the mechanism which will lead to cell death. Therefore, to prevent the harmful effects of T2D disease, inhibitors against IAPP have been developed. These inhibitors can be divided in two groups: the one that decrease the final amount of fibrils without affecting the lag phase and the ones that bind to the monomers, inhibiting the fibrils formation. The main disadvantageous of the first approach is related with the inability to prevent the formation of IAPP oligomers, which are thought to be the toxic species<sup>74</sup>.

Several classes of molecules have shown inhibitory properties, albeit most of the studies were performed with polyphenols and polypeptide-based inhibitors. (-)-Epigallocatechin 3-Gallate (EGCG) is a flavanol found in green tea and it was able to inhibit IAPP oligomerization and disaggregated preformed amyloid fibrils derived from IAPP<sup>74</sup>. Moreover, *in vitro* experiments showed that the presence of EGCG decrease the toxic effects of IAPP, with a significant increase of viable cells. Even though, the mechanism of action of this compound isn't clear, it was proposed to redirect the pathway of amyloid formation to a non-toxic pathway<sup>133,134</sup>.

The peptide-based inhibitors are developed based on a peptide structure and required the ability to bind to IAPP and, simultaneously, reduce the fibrillogenesis of the amyloid peptide.



The development of peptide-based inhibitors has several advantageous: they have high specificity and low toxicity; they don't accumulate in higher concentrations in tissues, they can be rational designed; the methods using to study their properties are highly developed; their small size facilitates the crossing of the blood brain barrier; they show a high chemical and biological diversity; their sequence can be easily modified in order to increase their affinity to a certain target and to prevent proteolytic degradation, among others<sup>135</sup>. These advantageous can explain the increase interested by pharmaceutical companies in peptides inhibitors, which lead to several therapeutic peptides on the market and high amount in clinical trials and preclinical evaluation<sup>136</sup>.

An important feature of IAPP-based inhibitors was the similarity with hIAPP in order to interact with it, however it should be different enough to inhibit the fibrils formation instead of oligomerize along with IAPP. Some inhibitors had been accomplished through proline mutations in the one of IAPP amyloidogenic region, between amino acids 20 and 29, since the proline allows the disruption of  $\beta$ -sheet, it's a  $\beta$ -sheet breaker. The addition of another  $\beta$ -sheet breakers, performed with N-methylated residue, was also able to prevent the amyloid formation and the hIAPP cytotoxicity<sup>137</sup>. Another studied showed that small fragments of hIAPP inhibited *in vitro* hIAPP aggregation, in high ratios, by preventing the fold into a  $\beta$ -sheet structure.

Previous studies have demonstrated *in vitro* the existence of a cross interaction between A $\beta$  and IAPP, capable of suppress the amyloid production and cytotoxic effects. Thereby, the development of inhibitors able to inhibit both diseases may be a promise therapeutics candidate to prevent the progression of the disease and consequently, the cross- interaction between them. Studies performed by *Kapurniotu et al.*, have demonstrated the efficacy of IAPP-base peptides to inhibit both A $\beta$  the IAPP fibrils formation.

A different approached used were based on the linking of the IAPP regions important in the IAPP amyloidogenicity and in the cross-interaction with A $\beta$ . Different linkers were used to join both regions and the nature of the linker was decisive in the inhibitory function, potency and targeting. This approach allowed the development of 3 inhibitors of IAPP and A $\beta$ , 4 inhibitors of A $\beta$  and 1 inhibitor of IAPP, which were capable to inhibit in the nanomolar range. The main advantageous of these peptides were the size and the lack of IAPP bioactivity, an important feature for inhibitors against AD<sup>138</sup>.

Recently, a macrocyclic peptide based on the minimal IAPP-derived recognition elements have been proposed as an inhibitor of both IAPP and A $\beta$  or just A $\beta$  with promising properties. Besides the good inhibitory properties, inhibition in the range of the nanomolar and the high values of IC<sub>50</sub>, these peptides showed a high proteolytic stability and enable the cross of the blood-brain barrier in a cell model, essential properties for the development of drugs against AD<sup>139</sup>. Thereby, the development of peptides capable of inhibiting amyloid diseases used the important regions in the interaction of the amyloid peptides as a scaffold to create new inhibitors with better pharmacological properties.

## 1.9. Aim of this work

Nowadays, the increased impact of misfolding protein diseases in our society triggered the pursuit of new treatments against those diseases. The A $\beta$  and the IAPP are examples of amyloid peptides, which are thought to be responsible for the death of neurons and  $\beta$ -cells in the Alzheimer's and T2D diseases, respectively. Moreover, the cross-interaction between IAPP and A $\beta$  was responsible for the increase propensity of patients with one of those conditions to develop the other one. Since this cross-interaction is, in part, due to the structural similarity between IAPP and A $\beta$ , it has been possible to develop inhibitors to prevent A $\beta$  and/or IAPP fibril formation by using IAPP sequences.

This thesis aimed at the biophysical characterization – conformation, interactions, solubility and fibrillogenesis studies – of four designed peptides. Towards this aim, the peptides were synthesized by solid phase peptide synthesis (SPPS), purified by high performance liquid chromatography (HPLC) and characterized by MALDI-TOF. Two different design strategies were employed: the addition of tags or the mutation of a specific residue of the previously designed peptide A, which is described in detail in annex 1. The addition of the tags aimed to increase the solubility of the peptide and the mutations in position X aimed to increase the inhibitory properties of the peptide. The structural modifications and the solubility were analysed by CD. The binding of the peptides to IAPP was followed by CD and by fluorescence spectroscopy. The inhibition of IAPP fibrillogenesis was followed by the ThT assay and TEM.

## 2. Material and Methods

### 2.1. Material

Table 2.1 - List of devices used during the experiments with the correspondent supplier.

Device	Supplier
Analytical balance	Denver Instrument/ Sartorius, Göttingen, DE
Centrifuge, 5417 C	Eppendorf tube, Hamburg, DE
Desiccator	Glaswerk Wertheim, DE
Dionex Multiple-Wavelength Detector	Thermo Scientific, Waltham, USA
Dionex Pump	Thermo Scientific, Waltham, USA
Dry freezer, Alpha 1-2 LDplus	CHRIST, Osterode, DE
Freezer, GN4113 Comfort No Frost	Liebherr, Biberach, DE
Heating block, neoBlock I 2-2503	NeoLab, Heidelberg, DE
HPLC degassing unit, DG-2080-53	Jasco, Gross-Umstadt, DE
HPLC Hardware interface, LC Net II/ADC	Jasco, Gross-Umstadt, DE
HPLC Low pressure gradient unit, LG-2080-02S	Jasco, Gross-Umstadt, DE
HPLC pump, PU-2080 Plus	Jasco, Gross-Umstadt, DE
HPLC UV/Vis detector, UV-2077Plus	Jasco, Gross-Umstadt, DE
HPLC, Ultimate 3000	ThermoFisher Scientific
Incubator, Heraeus	ThermoFisher Scientific, Waltham, USA
Lyophilisator, 2.5 Plus free zone	Labconco, Kansas City, USA
Magnetic stirrer. Ikamag RCT	IKA, Staufen, DE
MALDI-TOF mass spectrometer	Bruker Daltonics, Bremen, DE
Multichannel pipette, Transferring-8, 20-200 µL	BRAND, Wertheim, DE
Multilabel plate reader, Victor™ X3	PerkinElmer, Waltham, USA
Reprosil Gold 200 (C18, 10 µM, 250x8 mm)	Dr. mais GmbH
Peptide Synthesizer, CS336X	CS Bio, Menlo Park, USA
Pipette, Eppendorf tube Research, variable, 0.5-10µL	Eppendorf tube, Hamburg, DE
Pipette, Pipetman, variable, 100-1000 µL	Gilson, Middleton, USA
Pipette, Pipetman, variable, 20-200 µL	Gilson, Middleton, USA
Pipette, Pipetman, variable, 2-20 µL	Gilson, Middleton, USA
Shaker, CAT S20	CAT, Staufen, DE
Spectropolarimeter, J-715	Jasco, Gross-Umstadt, DE
Ultra-low freezers, HERAfreeze	Kendro, Langenselbold, DE
Ultrapure water unit, TKA MikroPure	TKA, Niederelbert, DE
Ultrasonic bath, SONOREX	Bandelin, Berlin, DE

UV-Vis Spectrophotometer, V630	Jasco, Gross-Umstadt, DE
Vortex Mixer, VX-2000	Labnet, Edison, USA

Table 2.2 - List of materials used with the correspondent supplier.

<b>Material</b>	<b>Supplier</b>
Bottles (100 mL, 500 mL), glass	Schott AG (Mainz, DE)
Cuvette, quartz	Hellma Analytics GmbH & Co. KG (Mulheim, DE)
Pasteur pipette	BRAND GmbH & Co. KG (Wertheim, DE)
Parafilm	Carl Roth GmbH & Co. KG (Karlsruhe, DE)
CellstarR Tubes 15 mL, sterile	Greiner Bio-One, Frickenhausen, DE
Filter paper	Macherey-Nagel, Düren, DE
Filter, Millex-FG, 1.5 mL	Merck, Darmstadt, DE
Injection cannula	B. Braun, Melsungen, DE
Pasteur pipettes, glass, 145 mm	BRAND, Wertheim, DE
Pipette tips, 0.5-10 µL	Axygen, Union City, USA
Pipette tips, 100-1000 µL, blue	BRAND, Wertheim, DE
Pipette tips, 2-200 µL, yellow	BRAND, Wertheim, DE
Reaction vessel, 1.5 mL	Sarstedt, Nürnberg, DE

Table 2.3 - List of software used with the correspondent supplier.

<b>Software</b>	<b>Supplier</b>
Chromeleon 7.2 Chromatography Data System	Thermo Fisher Scientific, Waltham, USA
ChromPass Chromatography Data System	Jasco, Gross-Umstadt, DE
OriginPro 2016G	OriginLab Corporation, Northampton, USA
Peptide Companion	WindowChem Software, Fairfield, USA
Perkin Elmer 2030 Workstation	PerkinElmer, Waltham, USA
Spectra Manager II	Jasco, Gross-Umstadt, DE

Table 2.4 - List of chemicals used with the correspondent abbreviation and supplier.

<b>Chemicals</b>	<b>Abbreviation</b>	<b>Supplier</b>
Fmoc-AA-OH		Iris Biotech GmbH (Matrkredwitz, DE)
Rink resin		Novabiochem
Acetic anhydride	Ac <sub>2</sub> O	Carl Roth GmbH & Co. KG (Karlsruhe, DE)
Acetone		Carl Roth GmbH & Co. KG (Karlsruhe, DE)
Acetonitrile	ACN	VWR International GmbH (Darmstadt, DE)
Carbon dioxide	CO <sub>2</sub>	Westfalen, Münster, DE
5(6)- Carboxyfluorescein	Fluo	Sigma-Aldrich Inc. (St. Louis, Mo,USA)
Chloranil		Fluka, Seelze, DE
Diethyl ether	Et <sub>2</sub> O	Sigma Aldrich, St. Louis, USA
N,N-Diisopropylethylamine	DIEA	VWR International GmbH (Darmstadt, DE)
N,N-Dimethylformamide	DMF	CLN, Langenbach, DE
Ethanol	EtOH	Carl Roth GmbH & Co. KG (Karlsruhe, DE)
	HATU	Merck, Darmstadt, DE
	HBTU	Merck, Darmstadt, DE
Hexafluoro-2-propanol	HFiP	Merck KGaA (Darmstadt, DE)
	HOBt	Sigma Aldrich, St. Louis, USA
	HBTU	Sigma Aldrich, St. Louis, USA
Methanol		VWR, Radnor, DE
Piperidine		Iris Biotech, Marktrechwitz, DE
Thioflavin T	ThT	Sigma-Aldrich Inc. (St. Louis, Mo,USA)
Trifluoroacetic acid	TFA	Sigma-Aldrich Inc. (St. Louis, Mo,USA)
Water	ddH <sub>2</sub> O	Own production

Table 2.5 - List of solutions used with the correspondent application and its components.

Application	Buffer/Solution	Components
Aliquots preparation	80% B	80% of HPLC Buffer B in 20% of HPLC Buffer A
BCA	Solution A Solution B Solution C	
MALDI	Acetone buffer	97% acetone and 0.1% TFA in ddH <sub>2</sub> O
Chloranil Test	Solution 1	2% chloranil in DMF
	Solution 2	2% acetaldehyde in DMF
Cleavage	Cleavage Solution	95% TFA in ddH <sub>2</sub> O
HPLC	Solution A	0,058% TFA in ddH <sub>2</sub> O
	Solution B	90% CAN, 0.05% TFA in ddH <sub>2</sub> O
	Solution C	80% Methanol
Kaiser Test	Solution 1	5 g Ninhydrine in 100 mL EtOH
	Solution 2	80 g Phenol in 20 mL EtOH
	Solution 3	0.130 mg KCN in 98 mL Piperidine and 2 mL dd H <sub>2</sub> O
Fmoc deprotection	Piperidine solution	25 % piperidine in DMF
Protein buffer	1xb	10 mM Na <sub>2</sub> PHO <sub>4</sub> in ddH <sub>2</sub> O
ThT assay	ThT buffer	50 mM Na <sub>2</sub> PHO <sub>4</sub> , 100 mM NaCl in ddH <sub>2</sub> O, pH=7,4
	ThT solution	1 mM ThT in ddH <sub>2</sub> O
TEM	Stain solution	2% solution of uranyl acetate dissolved in ddH <sub>2</sub> O

## 2.2. Methods

### 2.2.1. Synthesis of the peptides through solid phase peptide synthesis

Solid phase peptide synthesis is an iterative process used to synthesize peptides attached to a resin. This process consists in the addition of blocked amino acid, followed by a removal of the protective group and the addition of a new blocked amino acid. The protective groups used were the Fmoc/tBu groups. The reason for this choice is based on orthogonality of those groups – they are removed by different chemical conditions – i.e, the Fmoc group can be removed using mild basic conditions, while the tBu group is released using mild acidic conditions. Thus, this approach allows a controlled removal of the different groups, reducing the side-reactions. After the coupling step, it's required to acetylate the positions which were not coupled to decrease the amount of by-products. Before the next coupling, the

protective groups have to be removed, which can be accomplished with the addition of a base. This process is carried out until the peptide sequence is formed. Lastly, there is a cleavage with the aim to remove the side chain groups and detach the full synthesized peptide from the resin. The figure 2.1 shows the process involved in solid phase peptide synthesis<sup>117</sup>.

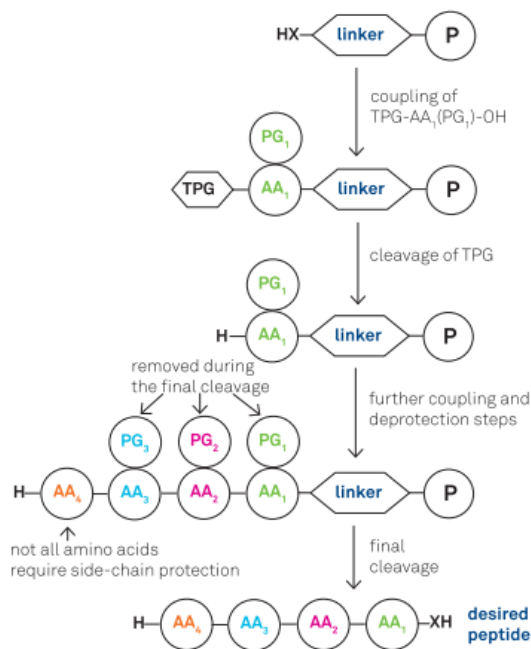


Figure 2.1 – General scheme of solid phase peptide synthesis. The first step consisted in the attachment of the first amino acid (AA) in the resin (P). The amino acids used in this process are protected amino acids in the N-terminus region (TPG) with a Fmoc group. Furthermore, some amino acids had also a protective group in the side-chain group (PG), depending on the reactivity of that group. Afterwards, the Fmoc-group was removed and a new aa was coupled. This process was repeated until the desired sequence is obtained. Lastly, the peptide is cleaved from the resin along with the removal of the side-chain protective groups. Figure taken from *Abdelmoty et al. (1994)*<sup>117</sup>.

### Attachment of the first amino acid

The attachment of the first amino acid in the resin, Rink resin, was a critical step since it will determine the number of positions in resin that are actually coupled – substitution level (SL) determination. The substitution level is a parameter which determined the emission of the benzofulvene – product resulted from the reaction between the piperidine and the Fmoc group (it will be discussed in the Fmoc-deprotection section) – at 290 nm. The benzofulvene concentration was, therefore, proportional to the positions coupled in the resin. The SL could be determined through the expression 1.

$$SL = \frac{V \cdot C}{m} \quad (1)$$

where SL is the substitution level in mmol/g, V the volume in mL, C the concentration in M and m the peptide mass used in mg. Since the concentration is determined through the Lambert-Beer law, the SL could be determined with the expression 2.

$$SL = \frac{V \cdot A_{290}}{\varepsilon \cdot b \cdot m} \quad (2)$$

where SL is the substitution level in mmol/g, V the volume in mL,  $A_{290}$  is the absorbance value at 290 nm,  $\varepsilon$  the absorption coefficient expressed in  $M^{-1}cm^{-1}$ , b the length path in cm and m the peptide mass used in mg.

The attachment of the first residue was performed using 3 equivalents of the amino acids and of the coupling reagent, HBTU. The residues and the coupling reagents were dissolved in the DMF and the reaction time was 2h. The resin was washed 3 times with DMF and twice with ether and dried for 30 min in the desiccator. To determine the substitution level, 2-3 mg of dry resin was weighed into a round bottle flasks of 10 mL, which were filled with 25% of piperidine in DMF. The flasks were shake and after 10 min a small amount was transferred to a cuvette and the absorbance was measure at 290 nm.

## Coupling

The coupling consists in the addition of a new protected amino acid to the sequence. At a molecular level, the coupling is the formation of an amide bond between the amine group of an amino acid and the carboxyl group of another one. However, this reaction isn't thermodynamically favourable since it is preceded by an acid-base reaction to form stable salts which is thermodynamically more stable<sup>140</sup>. Hence, to overcome this problem, the coupling is divided in two steps: the activation of carboxy group and the acylation of the amino group. The first step aims the reaction between the amino acid and the coupling reagent, producing an electrophilic intermediate. This process is due to the inductive (-I) effect or/ and a mesomeric (-M) effect of the coupling reagents that are responsible for the decrease of the electron density of the C=O group. This intermediate is, then, capable of react with the amino group from the other amino acid, in the second step. The attack of the carboxy group is performed by the electron lone pair of the nitrogen to form the tetrahedral zwitterionic intermediate. Afterwards, the peptide bond will be synthesised with dissociation of the nucleofuge<sup>140</sup>. The reaction is summarised in figure 2.2

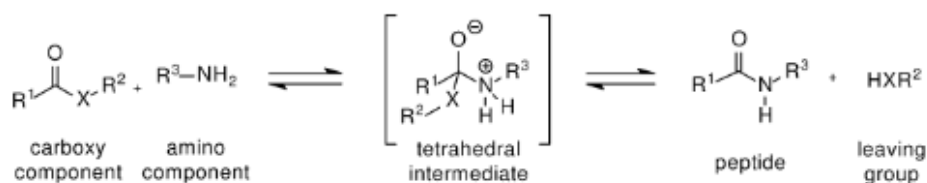


Figure 2.2 – Generic scheme of the peptide bond formation accomplished through the activation of the carboxyl group. The reaction of the carboxyl – X is O or S and R represent a chemical group – with the amine group originate a tetrahedral intermediate that will consequently, originate the peptide and the nucleofuge. Figure taken from *Norbert Sewald et al. (2002)*<sup>140</sup>.

The Aminium/Uronium reagents have been widely used as coupling reagents for SPPS. This group of coupling reagents are characterized by a high coupling rate and less side-reactions. Furthermore, the secondary products are soluble in organic solvents, such as DMF<sup>140</sup>. The mechanism of action consists



in the nucleophilic attack of the carboxylate group of the peptide attached to the resin which will originate an O-acylisouronium intermediate and a benzotriazol derivate. The O-acylisouronium will react with the benzotriazole derivative, forming and activated ester. The amino group of the other peptide will attack the carboxylic group of the peptide attached to the resin which will form the peptide bond. Nevertheless, this reaction must be performed in the presence of a base, such as DIEA – N,N-diisopropyletilamine – responsible for the carboxylate formation through an acid-base reaction<sup>140</sup>.

In this work, the coupling reagents used were HBTU – O-(Benzotriazol-1-yl)-N,N,N',N'-tetramethyluronium hexafluorophosphate – or HATU – 1-[bis-dimethylamino)methyl]pyridinium-1H-1,2,3-triazolo[4,5-b]pyridine-3-oxide hexafluorophosphate – depending on the residue and its position in the chain. The HATU was used in the hardest coupling reactions since it was the most efficient coupling reagent and had less racemization and side reactions.

In the protocol used, the coupling reagent were used in the same proportion as the protected amino acids. The number of equivalents used was 3 or 6 (the number of equivalents of the coupling reagent and the aa was the same) together with 4,5 or 9 equivalents of DIEA, respectively. The coupling steps of each peptide were described in synthesis plan, showed in annex I.

The coupling of the 5-(6)-carboxyfluorescein was performed using 3 eq. of 5-(6)-carboxyfluorescein and HATU with 4,5 eq. of DIEA for 2h. Two couplings were performed.

## Capping

The capping step was performed to block the positions in the resin that weren't filled, which will prevent the addition of amino acids to an unblocked position, avoiding the formation of sequences differing in one residue. The capping is performed with the addition of an excess of acetic anhydride responsible for the acetylation of the free positions, and a base.

The resin was load with 10 eq. of acetic anhydride (Ac<sub>2</sub>O) and DIEA. In the first amino acid (the attachment of the amino acid in the resin), the capping procedure last 40 min, while for the rest of the amino acids the acetylation had a duration of 15 min. After that, the reactants were removed, and the resin was washed 3 times with DMF for 1 min.

## Fmoc deprotection

The Fmoc deprotection consists in the removal of the Fmoc group, allowing the coupling of the next amino acid and it was performed by a base, namely, piperidine. The Fmoc deprotection follows a base induced  $\beta$ -elimination mechanism, where the piperidine removed the acidic proton from the fluorenyl ring system which leads to the formation of the benzofulvene, dioxide carbon and the unblocked peptide.

The benzofulvene is a strong electrophile able to attack irreversibly the amino acid. In order to prevent that, the piperidine will react with the benzofulvene, avoiding unwanted side reactions. Hence, the piperidine played two different roles: eliminate the Fmoc group from the N-terminus of the amino acid and prevent side reactions between benzofulvene and the amine group<sup>140</sup>. Furthermore, the fluorenyl group is a chromophore, so his release can be monitored through the UV absorbance.

The Fmoc deprotection was performed using 25% piperidine in DMF. In the case of Fmoc amino acids the deprotection was done twice, for 5 and 10 min. In the case, that no alteration of the Kaiser test was visible another 10 min was performed. On the other hand, the Fmoc-deprotection of methylated Fmoc amino acids was performed twice for 2 and 7 min, respectively.

### Confirmation

The confirmation step is extremely important since it will confirm if the step was successfully performed or not.

The couplings and the capping can be confirmed using the Kaiser test or the chloranil test. The Kaiser test is applied for primary amines, while the chloranil test is sensitive to secondary amines. The Kaiser test is based on the reaction between the amine and ninhydrin. The presence of the amine group is detected by a blue colour, and it should be visualized after the fmoc deprotection, while the absence of the amine group is visualized by the absence colour of the beads, after the coupling step. The heating until 100°C allows the exposure of some NH<sub>2</sub> groups, facilitating the detection of those groups<sup>140</sup>. On the other hand, the Chloranil test detects the presence of the amine group by the blue colouration of the beads, while the colourless beads indicate a successful coupling.

After the washing step, a small amount of resin was transferred to a small tube, where was added 2-3 drops of Kaiser test solutions. After that, the tube was heated at 108,6 °C for 5 min. The Chloranil test procedure was similar to the Kaiser test, but the Chloranil test didn't need to be heated up.

### 2.2.2. Cleavage

The cleavage of the peptide aims to separate the peptide from the resin and, simultaneously, removes the side-chain protecting group. Not all the amino acids had side-chain groups; the presence of this group depended on the reactivity of the side chain group<sup>117</sup>. The cleavage of peptide may originate by-products and in order to prevent that, scavengers must be used. The TFA, trifluoroacetic acid, is the agent utilized to the cleavage of the side groups and the cleavage of the peptide from the resin. Since the peptides synthesized didn't have sensitive side-chain groups, the standard cleavage procedure, TFA/H<sub>2</sub>O (95%/5%), was performed.

After weighing 40 mg of resin to a new syringe, swelled it with DMF for 10 min. After that, the Fmoc deprotection was performed, through the addition of 25% piperidine in DMF for 5 min and 20 min. Then,

the resin was washed 4 times with DMF for 1 min and 3 times with Et<sub>2</sub>O for 1 min. The resin was dried in the desiccator for 30 min and afterwards the cleavage solution was added inside the syringe. The cleavage had a duration of 3h, while shaking. After that, ddH<sub>2</sub>O was added inside a weighed glass vial in order to have less than 10% (v/v) of TFA in solution. The cleavage solution was added inside the glass vial and the syringe was washed with 100 µL of TFA. Finally, the solution was frozen in dry ice and afterwards was lyophilized.

The cleavage procedure of the fluorescence labelled peptide was identical to the one described previously, without the Fmoc-deprotection step.

### 2.2.3. Purification using HPLC

The peptides purification was performed by reverse phase chromatography, more specifically, high performance liquid chromatography (HPLC), using a Reprosil Gold (200 C18, 10 µm 250 x 8 mm) column. Since the stationary phase was hydrophobic it was required to use a hydrophilic mobile phase. The separation of the peptides will be accomplished through the different affinity of the peptides to the stationary and mobile phases. Thus, the peptides with a higher affinity to the stationary phase, will interact strongly with a column and will abandon it with a higher retention time. On the other hand, the hydrophilic peptides will interact strongly with the mobile phase, and consequently, will be abandoned the column with a lower retention time.

It was injected 500 µg of each sample dissolved in 20% TFA and 80% of solution B. The detection was done using the UV lamp, at 214 nm, the wavelength that the peptide backbone absorbed. The fluorescence labelled peptide was detected using also the visible lamp, at 433 nm, the wavelength that the fluorophore absorbed.

The elution was performed using a gradient elution of solution A and solution B. The gradient used are described in the table 2.7. The column regeneration was performed using two programs: the 100% B to clean the column and the washing program to ensure the full capacity of the resin on the next run. The programs features are described in the table 2.8.

The collected fractions were frozen in dry ice and afterwards were lyophilized in order to obtain the peptide in the solid phase.

Table 2.6 – Description of the HPLC programs used to elute the peptides, with the flow in mL/min, the duration of the elution gradient in min and the initial and final conditions of the elution gradient.

<b>Program name</b>	<b>Flow (mL/min)</b>	<b>Duration (min)</b>	<b>Starting conditions</b>	<b>Final conditions</b>
Schnell A $\beta$	2	30	Solution A –90% Solution B – 10%	Solution A – 10% Solution B – 90%
Langsame A $\beta$	2	37	Solution A –70% Solution B – 30%	Solution A – 30% Solution B – 70%
Langsame Samuel	2	40	Solution A –70% Solution B – 30%	Solution A – 30% Solution B – 70%
Langsame long	2	45	Solution A –70% Solution B – 30%	Solution A – 30% Solution B – 70%
10-100% B	2	25	Solution A – 90% Solution B – 10%	Solution A – 0% Solution B – 100%

Table 2.7 – Description of the HPLC programs used to clean the column, with the flow in mL/min, the duration of the program in min and the washing conditions.

<b>Program name</b>	<b>Flow (mL/min)</b>	<b>Duration (min)</b>	<b>Washing conditions</b>
100 % B	2	30	Solution B – 100%
Washing	2	15	Solution C – 100%

## 2.2.4. Mass spectrometry

The confirmation of the purity of the different fractions was performed using MALDI-TOF MS. Mass spectrometry (MS) is an analytical technique used to determine the mass of molecules. In the first place, the molecule is ionized and the ratio between mass and charge ( $m/z$ ) is measured to calculate the mass of that molecule. The MALDI (*matrix assisted laser desorption ionization*) is an ionization technique where the solution with the peptide was added on the matrix, where it crystalized. Afterwards, a laser beam focused on the sample, which will be responsible for the ionization of the sample and consequently desorption. The analyser of the ratio  $m/z$  used was the time of flight (TOF) analyser, where the mass of the compound was determined by the time required to that compound to flew through a tube<sup>141</sup>.

To prepare the samples a small fraction of the lyophilized product was transferred to an Eppendorf tube and on top of that was added 15  $\mu$ L of acetone solution (97% acetone with 0.1% TFA) and mixed.

### 2.2.5. Aliquots preparation

In the Eppendorf tube containing, at least, 1 mg of the pure peptide was added the same volume of cold 80% B +20% A solution to get a final concentration of 1  $\mu\text{g}/\mu\text{L}$ . The solution was left on ice until all the peptide was dissolved. After that, transfer 200  $\mu\text{L}$ , 100  $\mu\text{L}$  and 50  $\mu\text{L}$  to new Eppendorf tube in order to prepare the 200  $\mu\text{g}$ , 100  $\mu\text{g}$  and 50  $\mu\text{g}$  aliquots, respectively. Before lyophilized the solutions, they were frozen in dry ice. Lastly, the different aliquots were store at  $-20\text{ }^{\circ}\text{C}$ .

### 2.2.6. Circular dichroism

Circular dichroism is an optic technique that takes advantage of the ability of the proteins to absorb differently the circularly polarized light. It has been used to determine the secondary structure of proteins, peptides and nucleic acids, determination of folding and unfolding of proteins and its kinetics and interaction between biomolecules, such as protein-protein, through the alteration of their structure<sup>141</sup>.

This light has two components: the right-handed ( $E_R$ ) and left-handed ( $E_L$ ) circularized light which can describe as two vectors; and since the chromophore absorbs differently the two components of the circular light, that will originate an elliptical polarize radiation as a result of the sum of  $E_R$  and  $E_L$  vectors. In practise, the CD machine will measure the different absorbance of the two lights components<sup>142,143</sup>.

The secondary structure of proteins can be determined in the UV region, between 190 nm to 250 nm, through the detection of the peptide bond. The region 210-220 nm is the weakest energy transition, namely, a  $n \rightarrow \pi^*$  transition of the non-bonding electrons of the oxygen of the carbonyl group and it's characterized by a negative band and is sensitive to the hydrogen interactions<sup>142,143</sup>. On the other hand, the strongest interaction involves a  $\pi \rightarrow \pi^*$  transition of the  $\pi$ - electrons of the carbonyl group and shows a positive band at 192 nm and a negative band at 210 nm<sup>144</sup>.

The intensity of the peaks in those bands will depend on the proteins conformation, in other words, the secondary structure of the proteins that depends on the torsion angles phi,  $\Phi$ , and psi,  $\Psi$ , which play an important role in the definition of the secondary structure. Thus, the  $\beta$ -sheet structure is characterized by a negative band at 218 nm due to  $\pi \rightarrow \pi^*$  transitions and a positive ellipticity at 196 nm due to the  $n \rightarrow \pi^*$  transition. The  $\beta$ -turn structure is very similar to the  $\beta$ -sheet structure, with the difference at the wavelength of the negative band, that in the  $\beta$ -turn case is around 230 nm. The  $\alpha$ -helix shows a maximum band at 192 nm that can be explain through the  $\pi \rightarrow \pi^*$  transition and two negative bands at 208 and 222 nm  $\pi \rightarrow \pi^*$  and a  $n \rightarrow \pi^*$  transitions, respectively<sup>145,146</sup>. On the other hand, the random coil structure shows a negative band at 195 nm. The different types of structures are represented in figure 3<sup>147</sup>. Hence, the structure of a protein can be determined by the sum of its secondary structures.

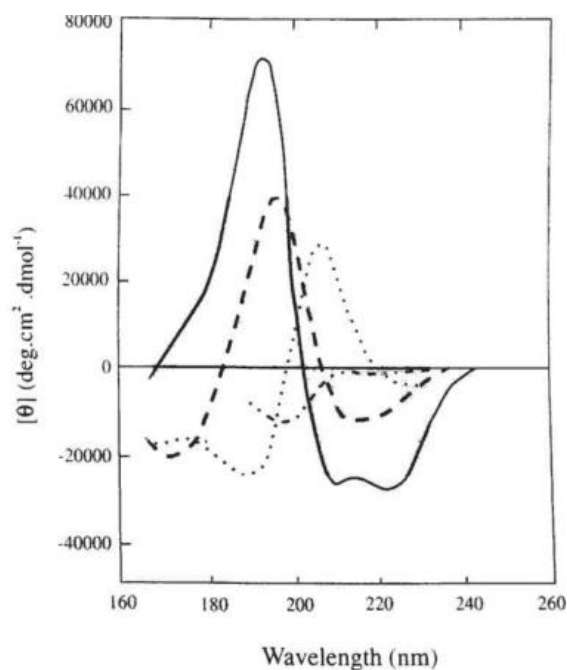


Figure 2.3 – Far UV CD spectra of the different types of secondary structures. Solid curve refers to  $\alpha$ -helix secondary structure and it's characterized by two negative bands around 222 and 208 nm. The long dashes showed the anti-parallel  $\beta$ -sheet structure with a negative band at 218 nm. The dots correspond to the  $\beta$ -turn structure characterized by a negative band at 230 nm. The short dashes correspond to a random coil structure with a negative band around 195 nm. Figure taken from *Kelly SM et al. (2000)*<sup>145</sup>.

Far-UV CD measurements were carried out using a Jasco 715 spectropolarimeter. Spectra were measured immediately following solution preparation between 195 and 250 nm, at 0.1 nm intervals, a response time of 1 second.

### Concentration dependence

The concentration measurements began with the baseline of the cuvettes with 1 cm, 0,5 cm and 0,2 cm, with a total volume of 1300  $\mu$ L, 650  $\mu$ L and 300  $\mu$ L, respectively. The baseline was performed with the buffer, 1xb containing 1% of HFiP.

The peptide stock was dissolved in HFiP in order to have a peptide concentration of 1 mM. The peptides concentration tested were 5  $\mu$ M, 10  $\mu$ M, 20  $\mu$ M, 50  $\mu$ M, 100  $\mu$ M. The first concentration was tested in the 1 cm cuvette length, the last concentration in the 0,2 cm cuvette and the rest were tested with the 0,5 cm cuvette. Firstly, the correct volume of the peptide stock was pipetted to the cuvette to have the correct peptide concentration. It's important to emphasize that the concentration of HFiP should be 1%. In the cases where the stock volume is higher than the HFiP volume allowed, the solvent should be evaporated with air and after that the correct volume of HFiP should be added. Then, the 1xb was added to the cuvette and the solution was mixed. Afterwards, the concentration dependence was measure. When the peptide started to aggregate, the measurements were stopped.

## Interaction between IAPP and peptide

This assay was performed with 1 cm cuvette with a total volume of 1300  $\mu\text{L}$ . The baseline was performed with the buffer, 1xb containing 1% of HFiP. It was prepared stock of IAPP and a 1 mM peptide stock in HFiP. Afterwards, the IAPP alone (5  $\mu\text{M}$ ), the peptide alone (10  $\mu\text{M}$ ) and the mixture of IAPP and peptide (1:2) was measure for the time points 0h, 0,25h, 0,5h, 1h, 7h, 24h. On the other hand, the IAPP alone and the IAPP and peptide mixture were, firstly, prepared in the Eppendorf tubes, i.e, the correct amount of the IAPP and peptide stocks were transferred to the correspondent Eppendorf tubes. Since the volume of HFiP pipetted is higher than the one required to have a solution with 1% HFiP, the HFiP was evaporated with air. The samples were redissolved in the correct amount of HFiP and then transferred to the cuvette along with the 1xb solution.

### 2.2.7. Thioflavin-T assay

Thioflavin-T (ThT) is a benzothiazol dye widely used to visualize and quantify the amyloid fibrils formation, not only *in vivo* but also *in vitro*, for the monitoring of amyloid kinetics<sup>148–150</sup>. The binding of this dye to  $\beta$ -sheets fibrils is responsible for the increase of the fluorescence at 482 nm, after excitation at 450 nm<sup>151</sup>. Even though, the mechanism of binding is not completely clear, it's been attributed to the rotation of the C-C bond connecting the benzothiazole and aniline rings<sup>152</sup>.

#### IAPP incubations

The IAPP aliquot was dissolved in cold HFiP and after filtration of the stock solution the concentration was determined by ultraviolet (UV) at 274 nm. The peptide aliquot was dissolved in cold HFiP in order to have a concentration of 1 $\mu\text{g}/\mu\text{L}$ .

The incubation of IAPP was performed with an IAPP concentration of 16,5  $\mu\text{M}$ . Firstly, the correct amount of volume from IAPP stock was pipetted to an Eppendorf tube. Afterwards, the HFiP was evaporated using air and then added the ThT buffer, containing 0,5% of HFiP.

Afterwards, the samples were vortexed gently 3 times and transferred 30  $\mu\text{L}$  to a 96 microwell-plate. With a multi-channel pipette 170  $\mu\text{L}$  of 20  $\mu\text{M}$  ThT solution was transferred and mixed 3 times. Finally, the fluorescence was measured in the 2030 Multilabel Reader VictorX3 (PerkinElmer Life Sciences). The measurements were performed from 24 to 24h during a week and the incubations were kept at 20  $^{\circ}\text{C}$ . The measurement procedure for the following days is the same, but in the presence of fibrils, it was required to remove them from the surface of the Eppendorf tube before transferring the solution to the microwell-plate.

## IAPP and inhibitor incubations

The protocol used to test the inhibition of IAPP with the purified peptides is the same used for the IAPP incubations alone. However, in this case the inhibitor is added inside the IAPP solution, before evaporating the HFiP with air. This assay was performed with different ratios of inhibitor, namely, 1:1, 1:2, 1:5 and 1:10.

### 2.2.8. Transmission electron microscopy

Transmission electron microscopy (TEM) is a high-resolution technique used to observe the structure of the crystal. To do that, a laser beam of electrons is charge in to a sample and the interaction with the sample will originate the image<sup>141</sup>.

Firstly, the TEM grid was held self-closing forceps and after that, 10  $\mu$ L of the sample was transferred to the TEM grid surface. After 3 minutes, the sample solution was removed from the surface by gently pressing the grid surface on a filter paper. To remove the salt from the buffer 10  $\mu$ L of ddH<sub>2</sub>O was applied in the grid for 1 min. The removal of the ddH<sub>2</sub>O was performed the same way as the sample removal. Subsequently, 10  $\mu$ L of the staining solution was added to the grid. After 1 min the solution was removed, and the grid was stored in an Eppendorf tube.

### 2.2.9. Centrifugation assay

The centrifugation assay was performed for 20  $\mu$ M peptide concentration at three different time points: 0h, 20 min and 7 days. Each time point was prepared in triplicates. Initially, the peptide stock with a concentration of 100  $\mu$ M was prepared by the addition of cold HFiP to a peptide aliquot. Afterwards, a volume correspondent to 1  $\mu$ g was transferred to a 0,5 mL Eppendorf tube. The HFiP was let to evaporate naturally at room temperature. Then, the 1xb was added to have a final concentration of 20  $\mu$ M and the solution was vortexed one time at speed 4. The calibration curve was prepared in a similar way to the samples. The only difference was that the volume of 1xb added was 50  $\mu$ L of 1xb. In this case, the desired masses were: 5, 2,5, 1, 0,5 and 0,25  $\mu$ g. The control, in triplicates, consisted in 50  $\mu$ L of 1xb.

The 20 min and 7 days samples were centrifuge at 19900 g for 20 min. After that, the supernatant was transferred to a new Eppendorf tube, inclusive the triplicates of time 0h. In order to have a final volume of 50  $\mu$ L of 1xb, the correct amount of 1xb was added to the supernatant Eppendorf tubes and the pellet was redissolved in 50  $\mu$ L of 1xb. The BCA solution was prepared in a falcon tube covered with aluminium foil. The ratios of the BCA solutions was 25:24:1 for A:B:C, respectively. After the preparation and mixing



of the BCA solution, 150  $\mu\text{L}$  was transferred to all Eppendorf tubes and mixed. The Eppendorf tubes were incubated for 3h at 37  $^{\circ}\text{C}$ . Then, the Eppendorf tubes were put at -20  $^{\circ}\text{C}$  for 5 min. Lastly, the solutions were transferred to a 96-well sterile plate and the absorbance was measured at 570 nm.

## 2.2.10. Fluorescence titration

Fluorescence is a phenome of electronic de-excitation with the emission of a photon. When an electron absorbs a photon, it can jump to an unoccupied orbital. Afterwards, the electron will return to the lower energy orbital, emitting a photon with a higher wavelength because some energy will be loss in the excited state due to vibrational relaxation. Fluorescence measurements were performed with a JASCO FP-6500 fluorescence spectrophotometer.

### Fluos-peptide (5 nM) + soluble IAPP

To prepare the fluos-peptide stock, previously purified by HPLC, remove with a pipette tip a small amount and dissolved it in 200  $\mu\text{L}$  of HFiP. The solution was vortexed and put it on ice during, approximately 15 min, until the peptide was completely dissolved. Then, the stock solution was filtered with a Millipore filter, previously soaked in HFiP, and the concentration was determined by UV at 432 nm. Afterwards, the concentration of the stock had to be adjusted to 1  $\mu\text{M}$ .

The concentration of the stock of IAPP, previously stored at -4  $^{\circ}\text{C}$ , was determined by UV. After that, the concentration is adjusted to 1 mM. Afterwards, several dilutions were prepared in order to have a final concentration in the Eppendorf tube of 500, 250, 100, 50, 25, 10, 5 ,2,5 and 1  $\mu\text{M}$ . The dilutions were prepared in triplicate. In the cases, where the plateau is not reached higher or lower concentrations had to be prepared.

The measurements were performed from 500 nm to 600 nm, in 1xb buffer with 1% of HFiP using a 10.000 mm cuvette with a final volume of 500  $\mu\text{L}$ . To measure of the fluorescence labelled peptide, 495  $\mu\text{L}$  of 1xb were added to the cuvette and 2,5  $\mu\text{L}$  of the 1  $\mu\text{M}$  stock and HFiP and mixed. To measure the interaction of IAPP with the fluorescence labelled peptide 495  $\mu\text{L}$  of 1xb, 2,5  $\mu\text{L}$  of the fluorescence labelled peptide and IAPP were added to the cuvette and mixed.

### Fluos-IAPP (5 nM) + peptide

This experiment is very similar to the previous one. However, in this case the dilutions were prepared for the peptide stock and the fluorescence labelled peptide concentration had to be adjusted to 1  $\mu\text{M}$ . The measurements were done using the same procedure.

### Fluos-peptide (5 nM) + peptide

In this case the measurements were performed with fluorescence labelled peptide and the several peptide dilutions. The measurements were done using the same procedure.

## 3. Results

### 3.1. Synthesis and purification

#### 3.1.1. Analogs with tags

The solubility of potential drug molecules can be a limitation in the new drug development process since it's necessary to guarantee a certain solubility in order to achieve the desired concentration of the drug in the circulatory system to trigger the desired pharmacological response. Since original peptide solubility was reduced, the first peptide synthesized aimed to increase the solubility through the addition of diamino acid tag.

The first peptide synthesised, peptide 1, consisted in the original sequence linked to the tag 1. This peptide was synthesized in 150 mg RinK resin with a substitution level of 0.45 mmol/g using SPPS technology. The synthesis of first 16 residues was performed in the synthesizer, while the rest of the residues were coupled manually. The synthesis occurred according to the plan, except the coupling of amino acid in position 17, which required an extra coupling since after the second coupling the Chloranil test showed the presence of brown beads instead of colourless beads, which was only visualized after the third coupling. The cleavage of 40 mg of peptide resin using the TFA/H<sub>2</sub>O (95%/5%) cleavage originated 17,37 mg of crude.

The purification of the crude was performed through HPLC, with the Schnell A $\beta$  program, in which the desired peptide was eluted with a retention time of 21,013 min and it was collected in three different fractions, as it shown in figure 3.1. The identification of each fraction was done with MALDI-TOF in acetone matrix. The expected mass of the peptide is 2442 g/mol and the MALDI results showed a m/z = 2466,034 which corresponded to the desired peptide with a sodium atom, [M+Na<sup>+</sup>] as the main component in all fractions, as it is shown in figure 3.2. Since none of the fractions were cleaned, a different purification program had to be used.

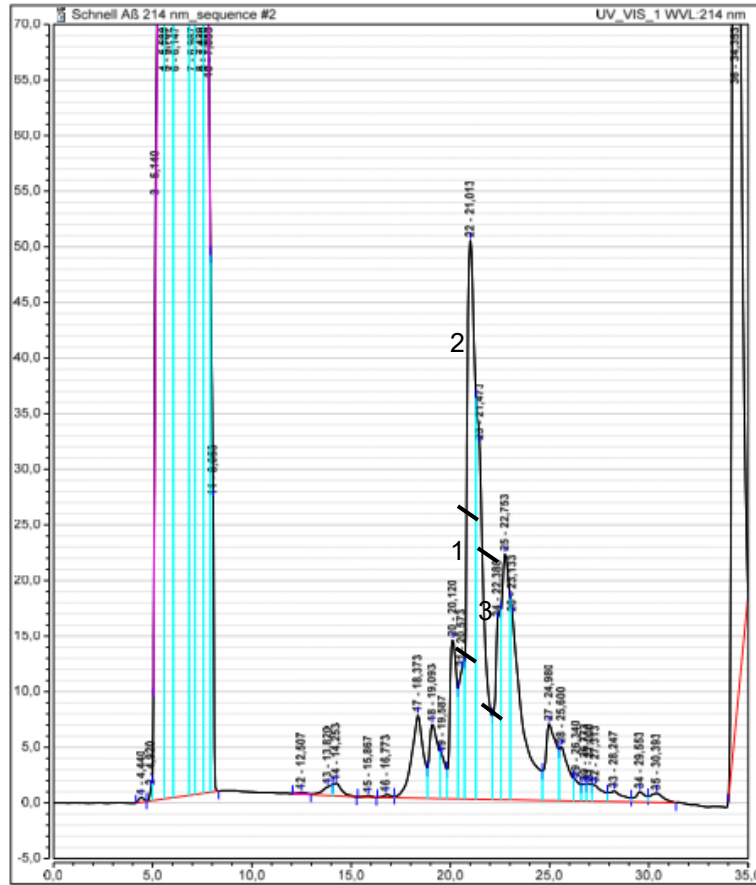


Figure 3.1 – Purification of 500 µg crude, dissolved in 100 µL TFA and 400 µL 80% B, with a Repronil Gold 200 column (C18, 10 µm 250 x8 mm), using Schnell Aβ program. The elution program started with 70% of solution A and 30% of solution B and ended with 30% of solution A and 70% of solution B. The detection of the amine bond was done using a wavelength of 214 nm. The peptide was eluted at a retention time of 21,013 min and the peak was collected in three fractions, fractions 1,2 and 3.

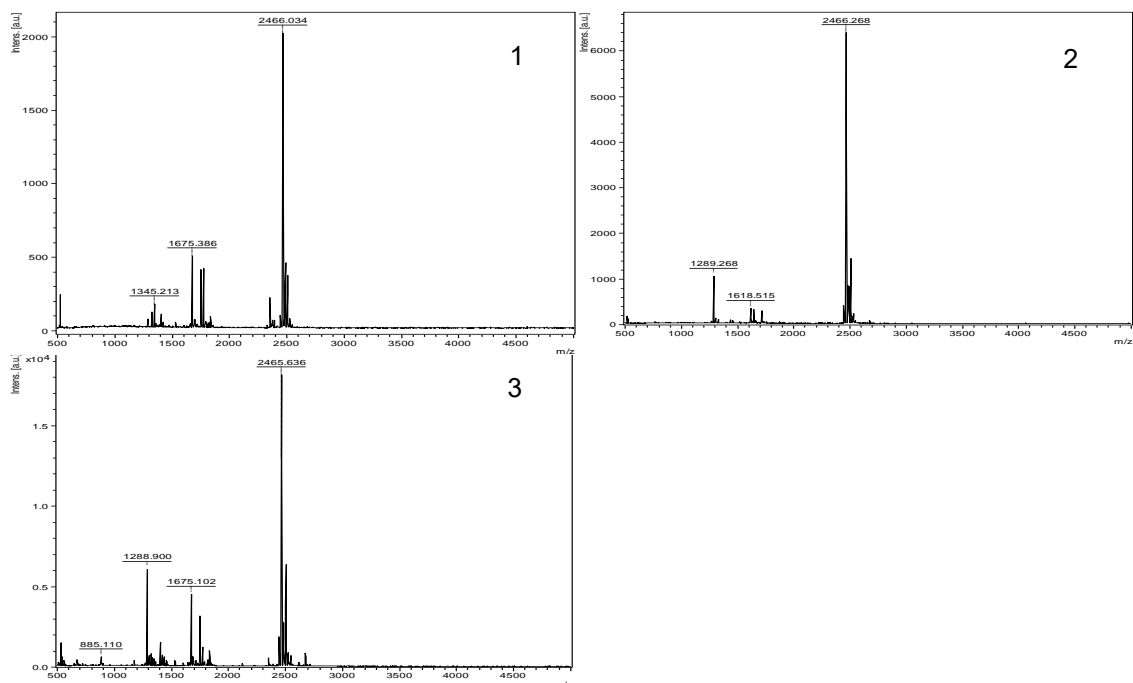


Figure 3.2 – MALDI-TOF results obtained from the three fractions of the purification of the peptide 1 crude, in an acetone matrix. The samples were dissolved in acetone solution constituted by 97% acetone and 0.1% TFA in ddH<sub>2</sub>O. The peptide mass was 2442 g/mol and the main peak obtained in all fraction was 2466 which corresponded to the peptide coupled with the Na<sup>+</sup> ion. The numeration used was the same used for the collected fractions.

The repurification of the uncleaned fractions were performed using the Langsame A $\beta$  program. This program had a slower gradient than the Schnell A $\beta$ , which allowed a better selectivity, i. e., the separation of peptides with similar affinities in two different peaks. With this program the desired peak was eluted at 28,000 min, as it's shown in figure 3.3. The peak was collected in two fractions, the first one from the bottom until the shoulder and the other one was collected after the shoulder. The MALDI-TOF results in figure 3.4 showed a first fraction with a m/z = 2465,79, which corresponded to the desired peptide with a sodium atom, completely clean (the other peaks were matrix) and a second peak, containing the product of interest as well as some impurities.

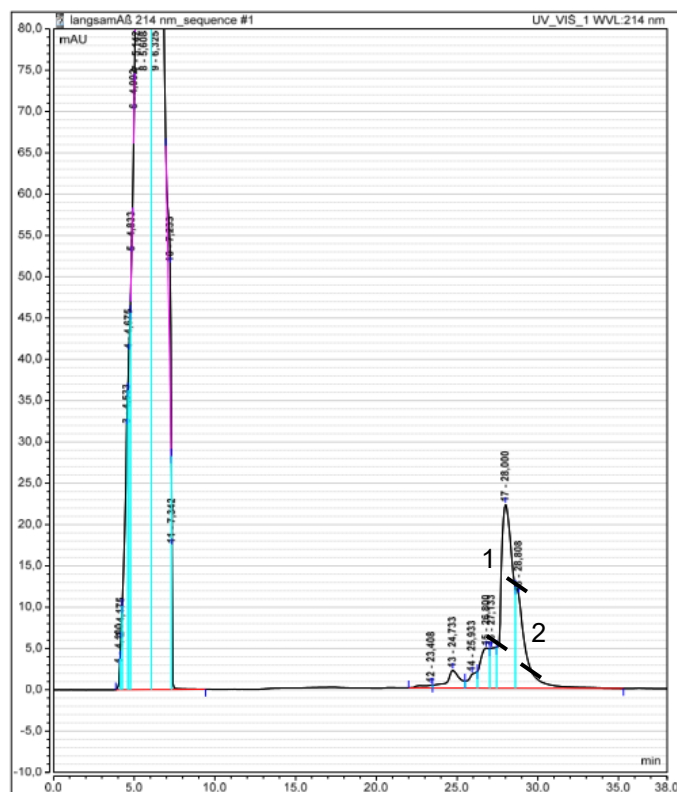


Figure 3.3 – Repurification of 500 µg peptide 1, dissolved in 100 µL TFA and 400 µL 80% B, with a Reprisil Gold 200 column (C18, 10 µm 250 x8 mm), using Langsame Aβ program 214 nm. The elution program started with 70% of solution A and 30% of solution B and ended with 30% of solution A and 70% of solution B. The detection was done at 214 nm. The peptide was eluted at a retention time of 28,00 min and the peak was collected in two different fractions, fractions 1 and 2.

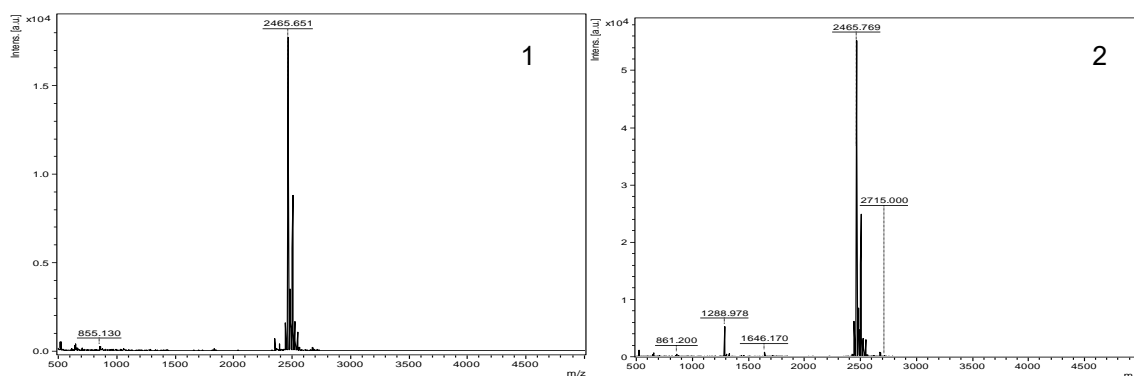


Figure 3.4 – MALDI-TOF results obtained for the repurification of the peptide 1, in an acetone matrix. The samples were dissolved in acetone solution constituted by 97% acetone and 0.1% TFA in ddH<sub>2</sub>O. The peptide mass was 2442 g/mol and the main peak obtained in all fraction was 2465,6 which corresponded to the peptide coupled with the Na<sup>+</sup> ion. The numeration used was the same used for the collected fractions.

The synthesis of the fluorescence labelled peptide 1 was achieved by the coupling the 5(6)-carboxyfluorescein to the N-terminus of the 20 mg of resin. After the cleavage of the 20 mg with TFA/H<sub>2</sub>O (95%/5%), 6,31 mg of peptide was achieved. In this case, the purification was performed with two wavelengths: 214 nm and 433 nm, which corresponded to the wavelength that the amide bond and the fluorophore absorbed, respectively.

Initially, the crude was purified with Schnell A $\beta$  program. The desired labelled peptide was eluted with a retention time of 22,778 min, a higher retention time than the unlabelled peptide, which indicated that the coupling of the carboxyfluorescein was successful since the carboxyfluorescein increased the hydrophobicity of the peptide. The peak was collected in three different fractions designated by 1, 2 and 3, as it was shown in figure 3.5.

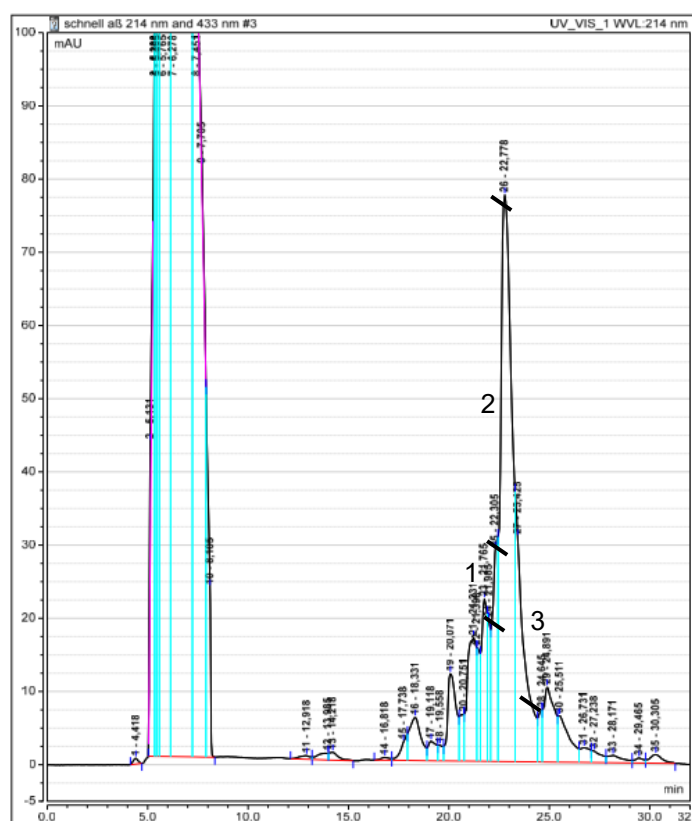


Figure 3.5 – Purification of 500  $\mu$ g fluorescence labelled peptide 1 crude, dissolved in 100  $\mu$ L TFA and 400  $\mu$ L 80% B, with a Reprosil column Gold 200 (C18, 10  $\mu$ m 250 x8 mm), using Schnell A $\beta$  program 214 nm and 433 nm. The elution program started with 70% of solution A and 30% of solution B and ended with 30% of solution A and 70% of solution B. The detection of the fluorescence labelled peptide was done at 214 nm and 433 nm which corresponded to absorption of the amide bond and the fluorophore, respectively. The peptide was eluted at a retention time of 22,778 min and the peak was collected in three different fractions, fractions 1, 2 and 3.

To determine whether the fractions were cleaned, MALDI-TOF in acetone matrix was performed. The fluorescence labelled peptide mass was 2800 g/mol. The results in figure 3.6 showed that, even though, all fractions had the product of interest with a  $m/z$  of 2823  $[M + Na^+]$ , the percentage of impurities were accentuated.

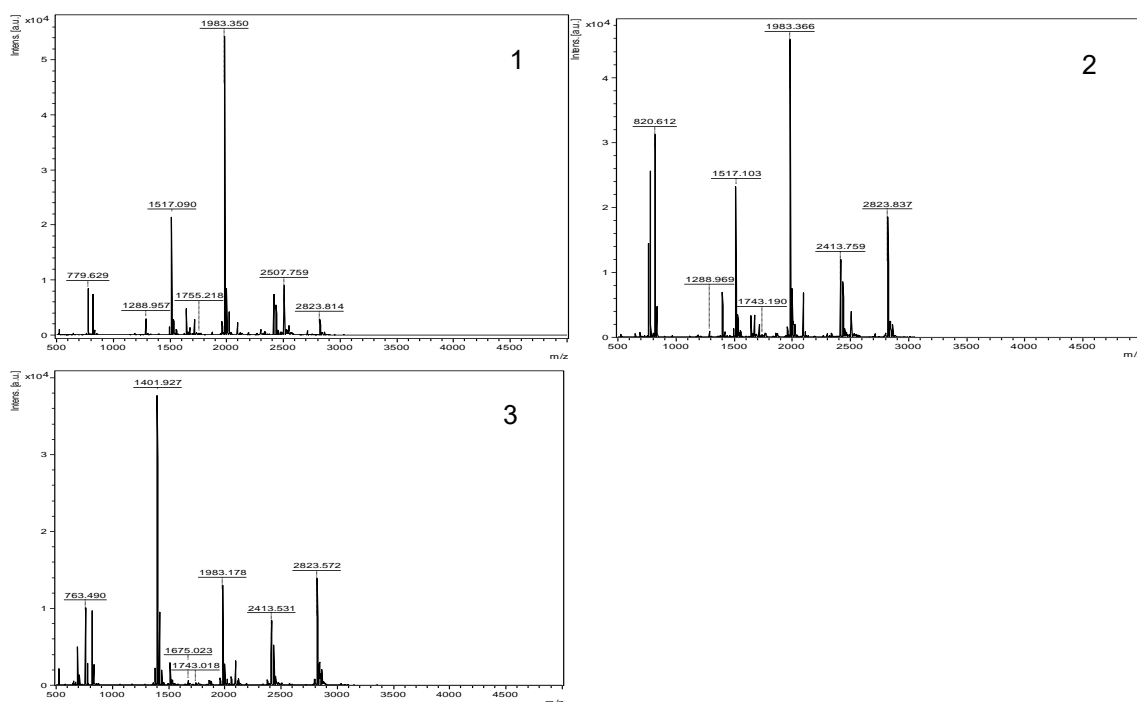


Figure 3.6 – MALDI-TOF results obtained for the purification of the fluorescence labelled peptide 1, in acetone matrix. The samples were dissolved in acetone solution constituted by 97% acetone and 0.1% TFA in ddH<sub>2</sub>O. The peptide mass was 2800 g/mol and the main peak obtained in all fraction was 2823 g/mol which corresponded to the peptide coupled with the Na<sup>+</sup> ion. The numeration used was the same used for the collected fractions.

Afterwards, the fluorescence labelled peptide 1 was repurified with langsame A $\beta$  214 nm and 433 nm program and the peptide was eluted with a retention time of 31,142 min. The peak showed a shoulder in the down part of the peak, which showed an increased in selectivity with this program. Since the purification of the crude showed a higher percentage of impurities, the peak was collected in four different 4 parts, two in the upper and the down part, as it was shown in figure 3.7. The peptide mas was 2800 g/mol and the MALDI results showed the peptide presence with a Na<sup>+</sup> ion – mass of 2823 g/mol – mainly in the down fractions. Moreover, the fraction 4 had the peptide pure.

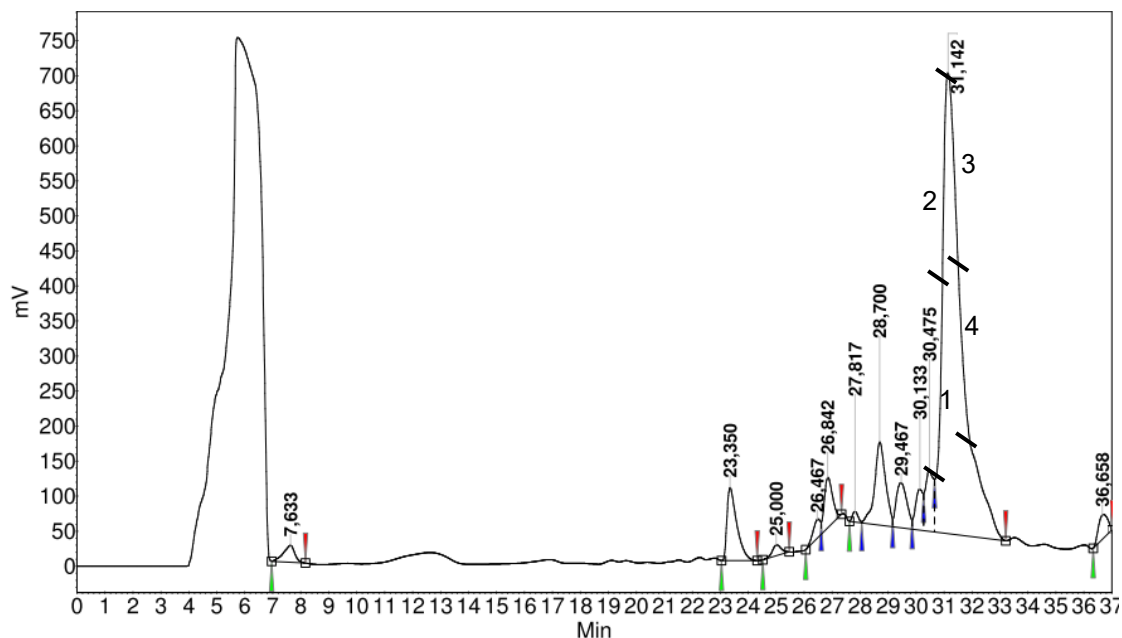


Figure 3.7 – Purification of 500  $\mu\text{g}$  of fluorescence labelled peptide 1 crude dissolved in 100  $\mu\text{L}$  TFA and 400  $\mu\text{L}$  80% B with a Reprosil Gold 200 (C18, 10  $\mu\text{m}$  250 x8 mm) using Langsame A $\beta$  214 nm and 433 nm. The detection was done using two wavelengths: the 214 and 433 nm which corresponded to the wavelength of absorption of the amine bond and the carboxyfluorescein, respectively. The elution program started with 70% of solution A and 30% of solution B and ended with 30% of solution A and 70% of solution B. The peaks with a retention time of 31,142 min was collected in four different parts, which were designated as fractions 1,2,3 and 4.

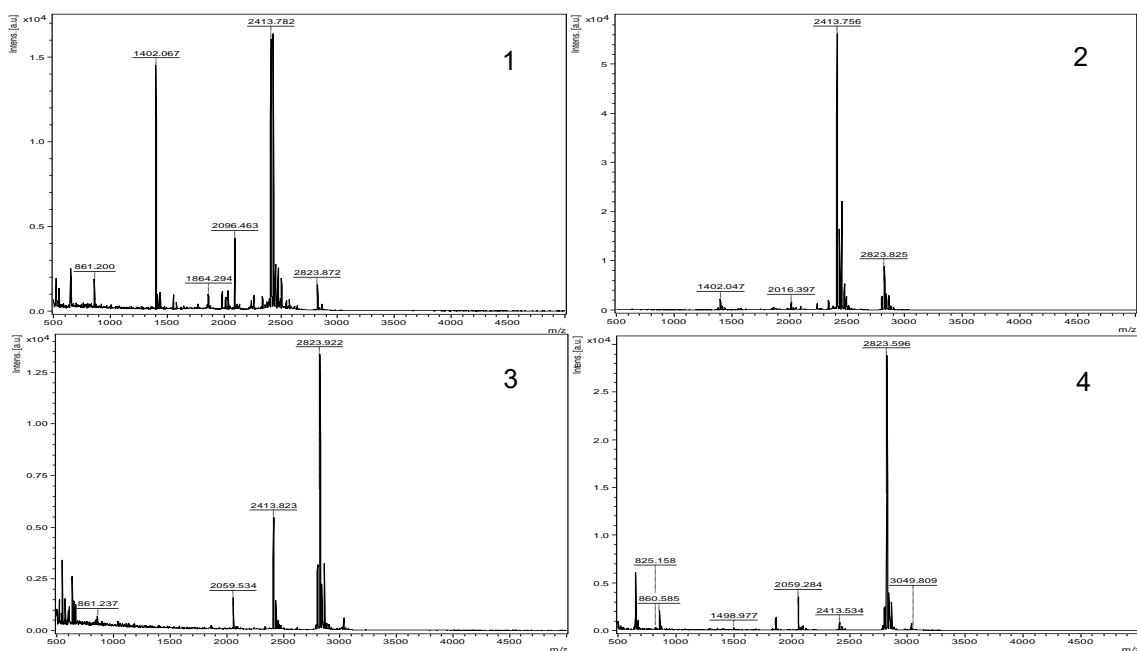


Figure 3.8 – MALDI-TOF results obtained for the purification of the fluorescence labelled peptide 1, in an acetone matrix. The samples were dissolved in acetone solution constituted by 97% acetone and 0.1% TFA in ddH<sub>2</sub>O. The peptide mass was 2800 g/mol and the peak of the peptide had a mass of 2823 g/mol which corresponded to the peptide with a Na<sup>+</sup> [M+ Na<sup>+</sup>]. The peptide was presented in all fractions, whereas in higher amount in fractions 3 and 4.



The other option to increase the peptide solubility was performed by the addition of tag 2 to N-terminus of the peptide A. The peptide 2 was synthesized in 150 mg of Rink resin with a substitution level of 0,45 mmol/g. The first 16 amino acids were synthesised in the synthesizer, while the rest were coupled manually. The coupling of the amino acids were according to the synthesis plan, showed in annex 3. The TFA/H<sub>2</sub>O cleavage of 40 mg of peptide resin originated 17,56 mg of crude. The presence of a by-product made the purification of the desired peptide extremely difficult since both peptides were eluted with similar elution conditions. Several programs were tested and the Langsame Aβ long 214 nm was the only one that enabled the purification of the inhibitor. The peptide was eluted at a retention time 25,858 min, and it was collected in 3 fractions, the upper part of the peak, the down part until the shoulder, as it is shown in detailed in figure 3.9 B, and the rest of the down part, named fractions 1, 2 and 3, respectively. The MALDI results, in figure 3.10 showed a mass of 2408 g/mol that corresponded to the peptide coupled with a Na<sup>+</sup> ion [M + Na<sup>+</sup>] since the peptide mass was 2384 g/mol. Moreover, the fractions 1 and 2 were pure.

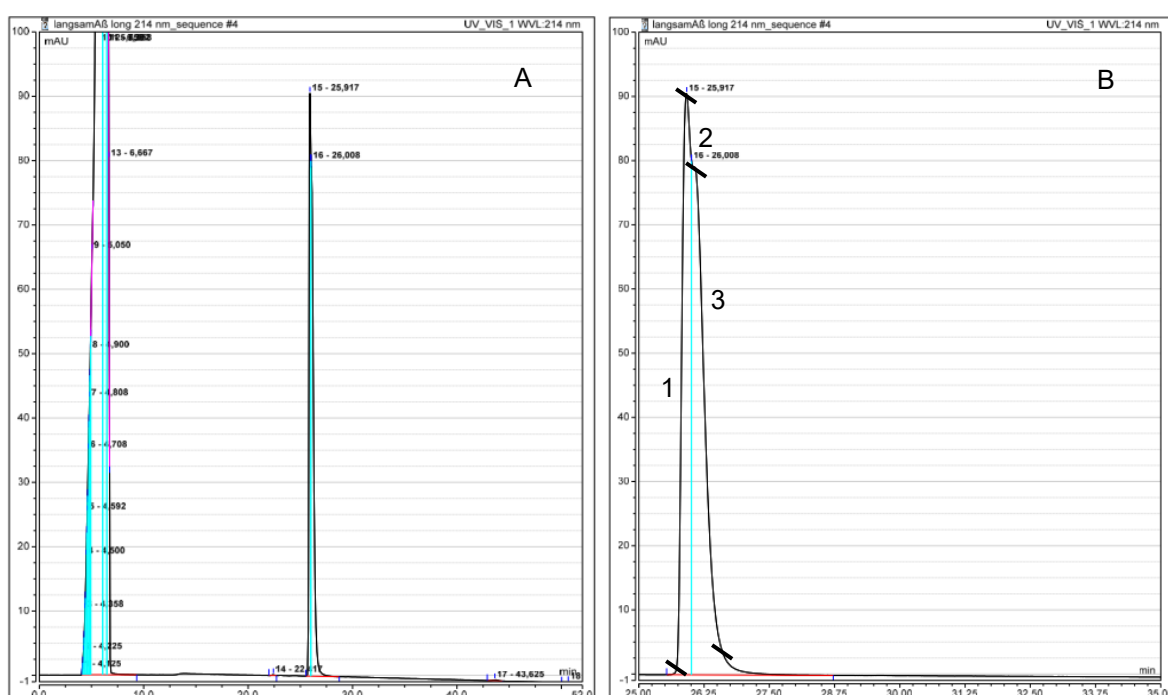


Figure 3.9 – Repurification of 500 µg of peptide 2 crude dissolved in 100 µL TFA and 400 µL 80% B with a Reprisil Gold 200 (C18, 10 µm 250 x8 mm) using Langsame Aβ Long 214 nm. The detection was done using 214 nm which corresponded to the wavelength of absorption of the amine bond. The elution program started with 70% of solution A and 30% of solution B and ended with 30% of solution A and 70% of solution B. The peak with a retention time of 25,858 min was collected three fractions, the upper, the down part until the shoulder and the rest of down part, designated by fractions 1, 2 and 3 respectively. A- The entire chromatogram. B – Detailed view of the peak region, focusing the collected fractions.

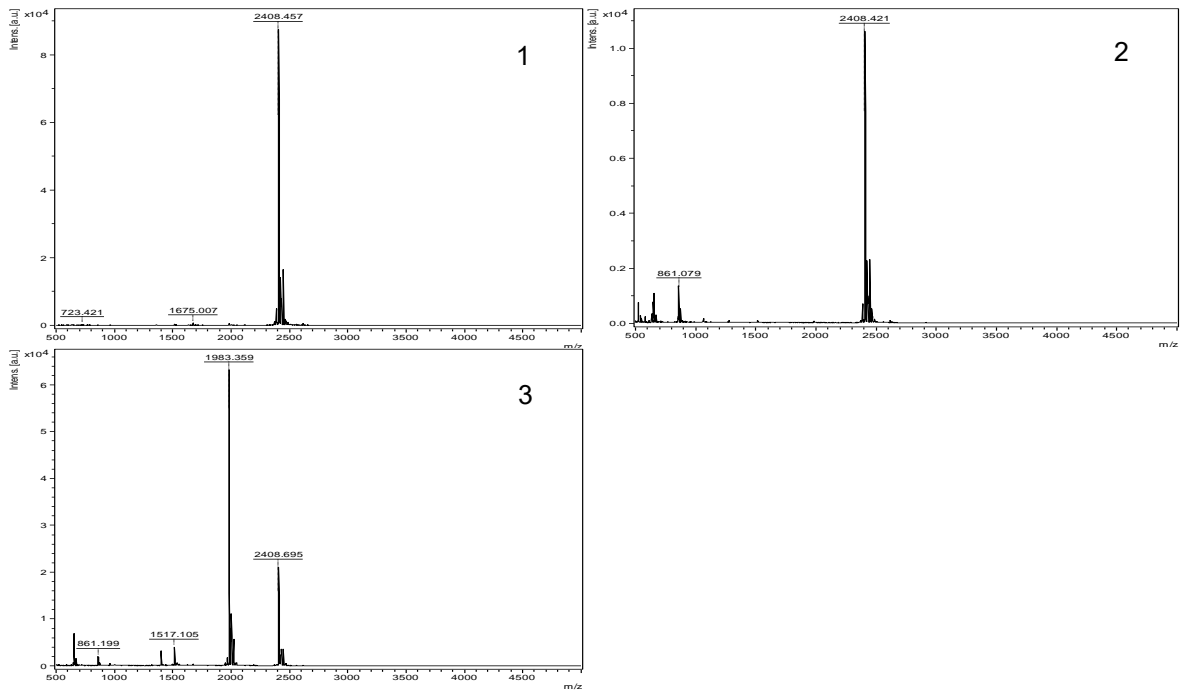


Figure 3.10 – MALDI-TOF results obtained for the purification of peptide 2, in an acetone matrix. The samples were dissolved in acetone solution constituted by 97% acetone and 0.1% TFA in ddH<sub>2</sub>O. The peptide mass was 2384 g/mol and the peak of the peptide had a mass of 2408 g/mol which corresponded to the peptide with a Na<sup>+</sup> [M+Na<sup>+</sup>].

Afterward, the fluorescence labelled peptide 2 was synthesized through the coupling of the carboxyfluorescein to 20 mg of peptide anchored to the resin. The cleavage with TFA/H<sub>2</sub>O (95%/5%) yielded 10,74 mg of crude. The purification of the crude was performed with Schnell A $\beta$  214 nm and 433 nm and the chromatogram is shown in figure 3.11. The peptide was eluted at 24,631 min and was collected in two different fractions, the upper and down parts, designated by 1 and 2. Since, the mass of the fluorescence labelled peptide was 2742 g/mol, it was possible to conclude that the first fraction, obtained by MALDI-TOF in acetone matrix, with a  $m/z = 2766,540 [M + Na^+]$  was cleaned, as it was shown in figure 3.12.

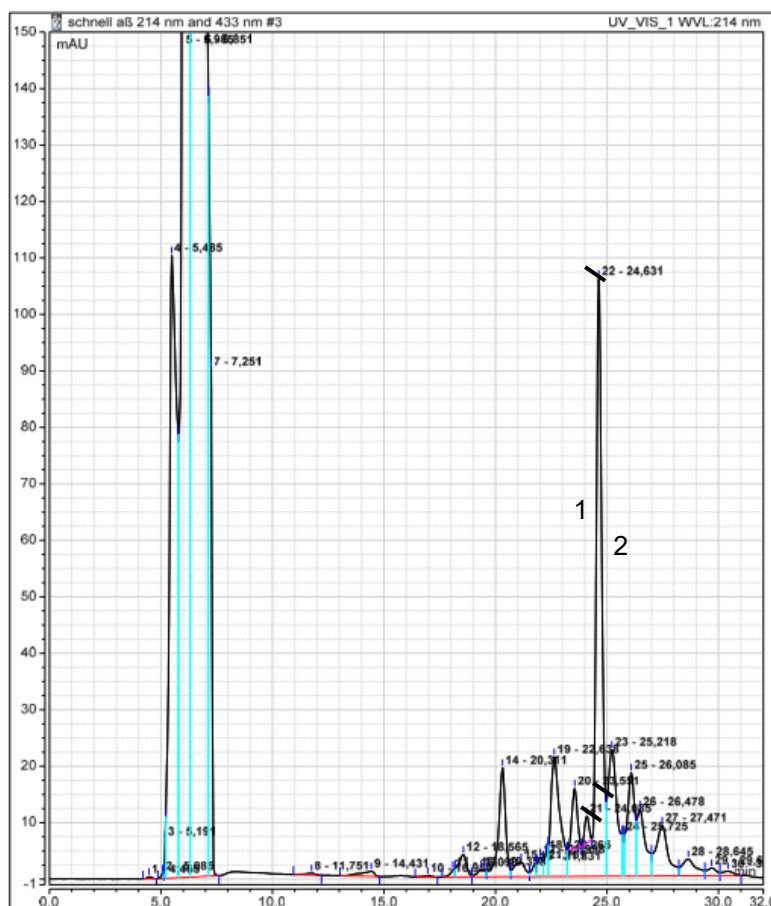


Figure 3.11 – Purification of 500 µg of fluorescence labelled peptide 2 crude dissolved in 100 µL TFA and 400 µL 80% B with a Reprisil Gold 200 (C18, 10 µm 250 x8 mm) using Schnell Aβ 214 nm and 433 nm. The detection was done using two wavelengths: the 214 and 433 nm which corresponded to the wavelength of absorption of the amine bond and the carboxyfluorescein, respectively. The elution program started with 70% of solution A and 30% of solution B and ended with 30% of solution A and 70% of solution B. The peptide was eluted at 24,631 min and the peak was collected in two parts, the upper and the down parts, designated as 1 and 2.

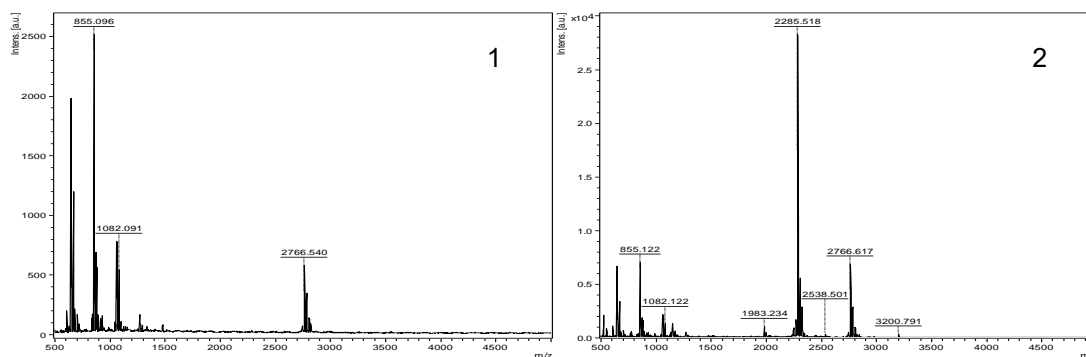


Figure 3.12 - MALDI-TOF results obtained for the purification of the fluorescence labelled peptide 2, in an acetone matrix. The samples were dissolved in acetone solution constituted by 97% acetone and 0,1% TFA in ddH<sub>2</sub>O. The peptide mass was 2742 g/mol and the peak obtained in both fractions was 2766,540 g/mol, which corresponded to the peptide with Na<sup>+</sup> ion [M + Na<sup>+</sup>].

### 3.1.2. Analogs with mutations in specific residues

To increase the inhibitory properties of the peptide A, mutations in the position X were performed. The first substitution was the hydrophobic residue in position X by an aromatic/hydrophobic amino acid. This peptide, named peptide 3, aimed to test how the strength of the hydrophobic core could impact the inhibition properties. The synthesis was performed in 200 mg of Rink resin with a substitution level of 0,41 mmol/g. The coupling of the first 16 amino acids were performed in the synthesizer. The coupling of the rest of the sequence was performed manually. The coupling of residue in position 19 was particularly difficult and it required four extra coupling, in which three of them were performed with an excess of reagents of 6 equivalents for 1h. Furthermore, the coupling of residue in position 18 also required 2 extra coupling. Afterwards, 40 mg of resin was cleaved using the TFA/H<sub>2</sub>O (95%/5%) cleavage and 17,87 mg of crude was obtained.

After the synthesis of the peptide, the programs schnell A $\beta$  and langsame A $\beta$  were tested aiming to understand which program enable a better purification of the desired peptide from the rest of the crude. The peptide was eluted with a retention of 23,935 min and 33,835 min in the Schnell and Langsame A $\beta$  programs, as it was shown in figure 3.13 A and B, respectively. The expected mass of the peptide 3 was 2219 and the MALDI-TOF results showed a m/z of 2243, which corresponded to the peptide with a Na<sup>+</sup> ion [M + Na<sup>+</sup>], in acetone matrix (figure 3.14). The results showed that the langsame A $\beta$  allowed the obtainment of the peptide without impurities, while with the schnell A $\beta$  a repurification step would be required.

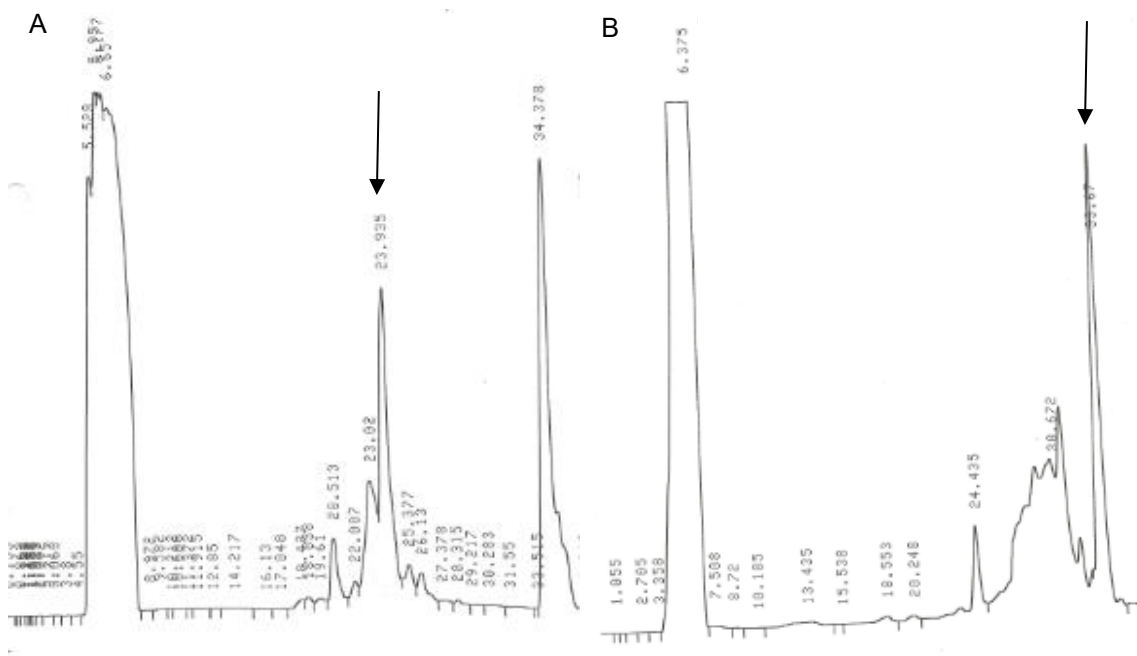


Figure 3.13 – Purification of 500 µg peptide 3 crude dissolved in 100 µL TFA and 400 µL 80% B with a Repronil Gold 200 column (C18, 10 µm 250 x8 mm) using Schnell Aβ (A) and Langsame Aβ (B) and the detection was at 214 nm. A – With the Schnell Aβ the peptide was eluted with a retention time of 23,935 min and it was collected in a single fraction. The program had a duration of 30 min and the gradient conditions was: 90% of solution A and 10% of solution B as the started conditions and 10% of solution A and 90% of solution B as the ended conditions. B – With langsame Aβ the peptide was eluted with a retention time of 33,67 min and it was collected in 1 fraction. The program had a duration of 35 min and the gradient conditions was: 90% of solution A and 10% of solution B as the started conditions and 10% of solution A and 90% of solution B as the ended conditions.

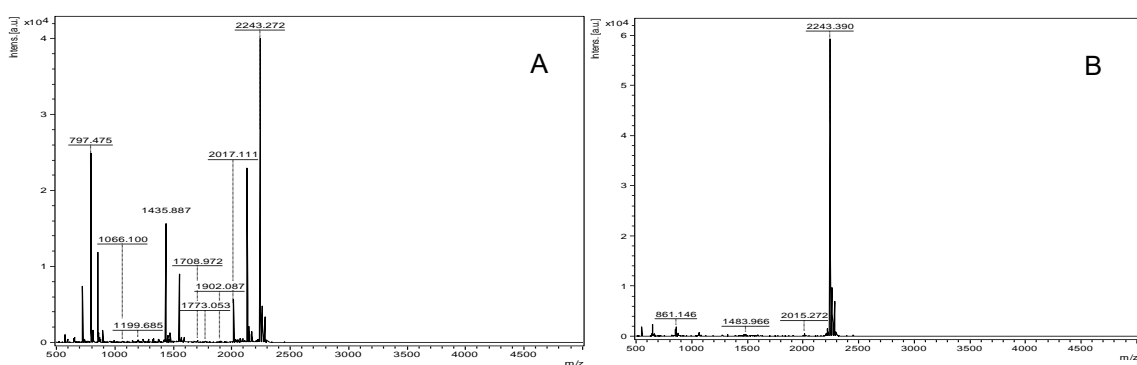


Figure 3.14 - MALDI-TOF results obtained for the purification of the peptide 3, in an acetone matrix. The samples were dissolved in acetone solution constituted by 97% acetone and 0.1% TFA in ddH<sub>2</sub>O. The peptide mass was 2219 g/mol and the main peak main peak obtained in all fraction was 2243 g/mol which corresponded to the peptide coupled with the Na<sup>+</sup> ion [M + Na<sup>+</sup>]. The numeration used was the same used for the programs.

The synthesis of the fluorescence labelled peptide 3 was performed through the coupling of the 5(6)-carboxyfluorescein in 20 mg of peptide resin followed by the cleavage with TFA/H<sub>2</sub>O (95%/5%). As a result, 9,89 mg of crude was obtained. The fluorescence labelled peptide was purified with the langsame Samuel A $\beta$  214 nm and 433 nm and the chromatogram is represented in figure 3.15. Two peaks with a retention time of 44,625 and 45,570 min were collected. The expected mass of the fluorescence labelled peptide was of 2577 g/mol. The MALDI-TOF in acetone matrix showed two cleaned fractions with a m/z = 2577 [M + Na<sup>+</sup>], which corresponded to the two different isomers of 5(6)-carboxyfluorescein, as it was shown in figure 3.16.

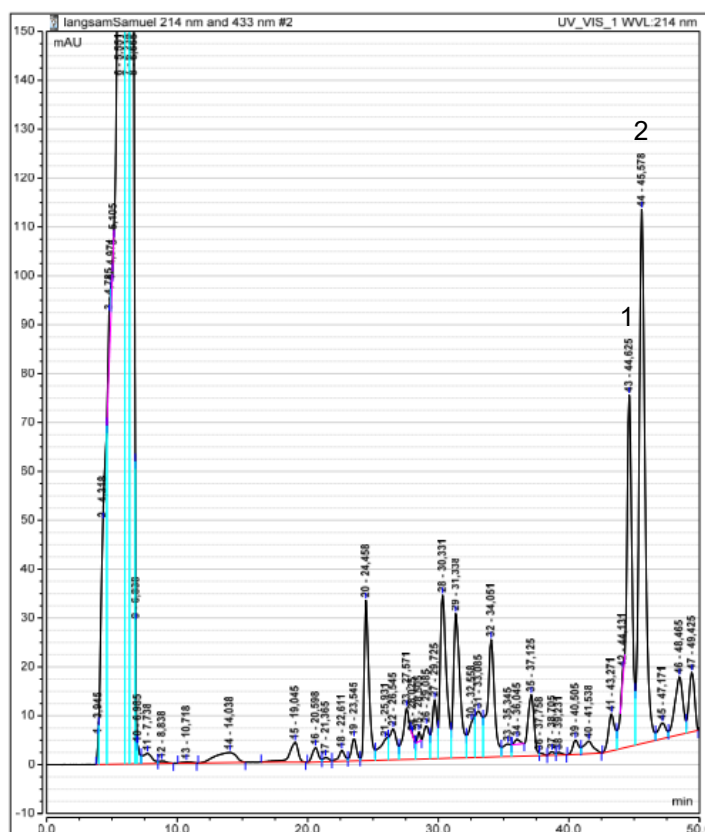


Figure 3.15 – Purification of 500  $\mu$ g of fluorescence labelled peptide 3 crude dissolved in 100  $\mu$ L TFA and 400  $\mu$ L 80% B with a Reprisil Gold 200 column (C18, 10  $\mu$ m 250 x8 mm) using LangsameSamuel A $\beta$  214 nm and 433 nm. The detection was done using two wavelengths: the 214 and 433 nm which corresponded to the wavelength of absorption of the amine bond and the carboxyfluorescein, respectively. The elution program started with 70% of solution A and 30% of solution B and ended with 30% of solution A and 70% of solution B. The peaks with a retention time of 44,625 min and 45,570 min were collected separately and they were designated 1 and 2, respectively.

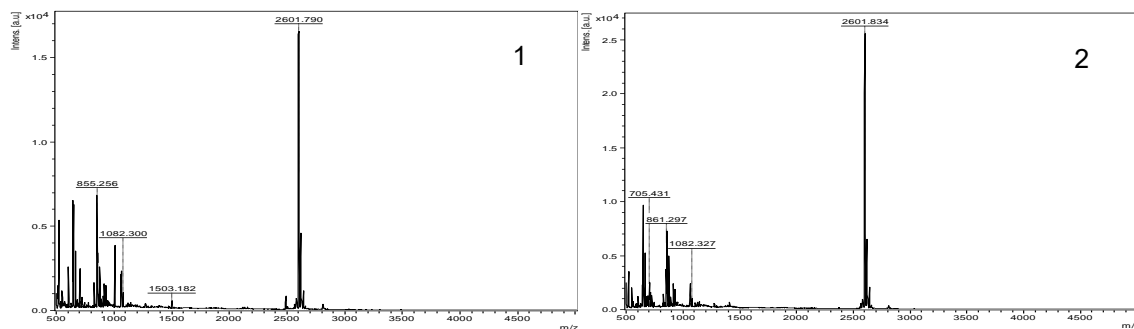


Figure 3.16 - MALDI-TOF results obtained for the purification of the fluorescence labelled peptide 3, in an acetone matrix. The samples were dissolved in acetone solution constituted by 97% acetone and 0.1% TFA in ddH<sub>2</sub>O. The peptide mass was 2577 g/mol and the peak obtained in both fractions was 2601,790 g/mol which corresponded to the peptide with Na<sup>+</sup> ion [M + Na<sup>+</sup>].

The last peptide synthesized, peptide 4, had a charge residue in position X instead of the hydrophobic amino acid. This modification aimed to understand how the incorporation of a polar residue in the hydrophobic core would alter the inhibitory properties of the peptide and simultaneously its solubility. The peptide was synthesized in 200 mg of Rink resin with a substitution level of 0,41 mmol/g. The synthesis was performed manually and went according the synthesis plan, except the coupling of amino acid in position Y, which required an extra coupling. The TFA/H<sub>2</sub>O (95%/5%) cleavage of 40 mg resin yielded 26,41 mg of crude.

Afterwards, the peptide 4 was purified with Schnell A $\beta$  and the peptide was eluted with a retention time of 21,447 min and it was collected in two fractions: the upper and the down parts designated by 1 and 2, as it was shown in figure 3.17. The samples, prepared in acetone matrix, were sent to MALDI to verify whether they were pure or not. The results showed in figure 3.18 demonstrated that the 2<sup>nd</sup> fraction was constituted by the peptide without impurities.

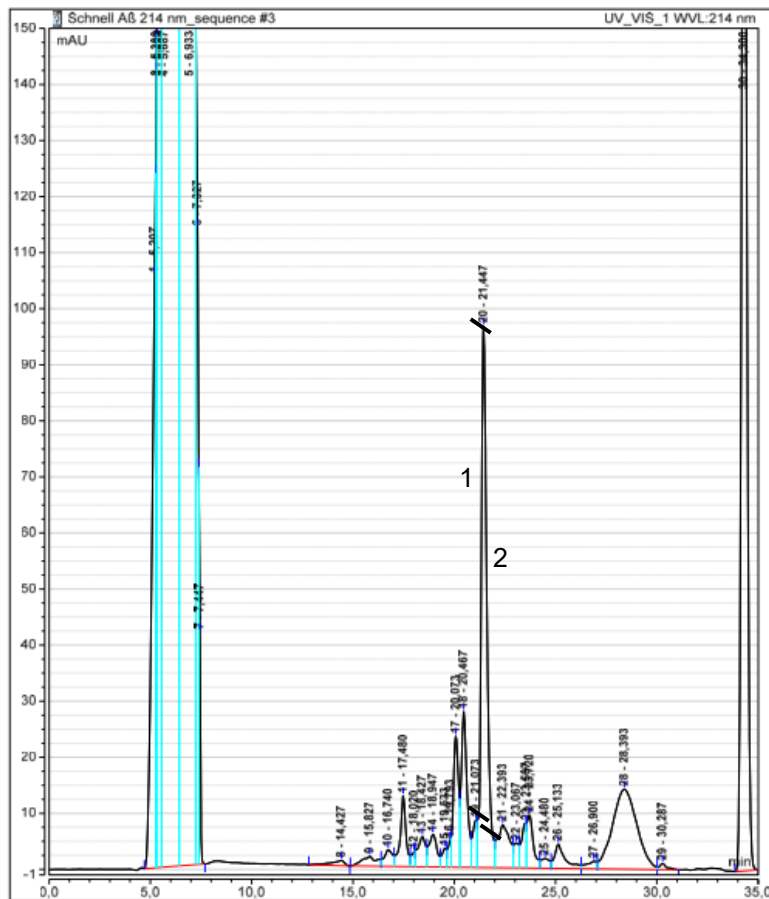


Figure 3.17 – Purification of 500 µg of peptide 4 crude dissolved in 100 µL TFA and 400 µL 80% B with a Repronil Gold 200 column (C18, 10 µm 250 x8 mm) using Schnell Aβ and the detection was at the wavelength of 214 nm. The elution program started with 70% of solution A and 30% of solution B and ended with 30% of solution A and 70% of solution B. The peptide was eluted with a retention time of 21,447 min was collected in two fractions, the upper part and the down part designated by 1 and 2, respectively.

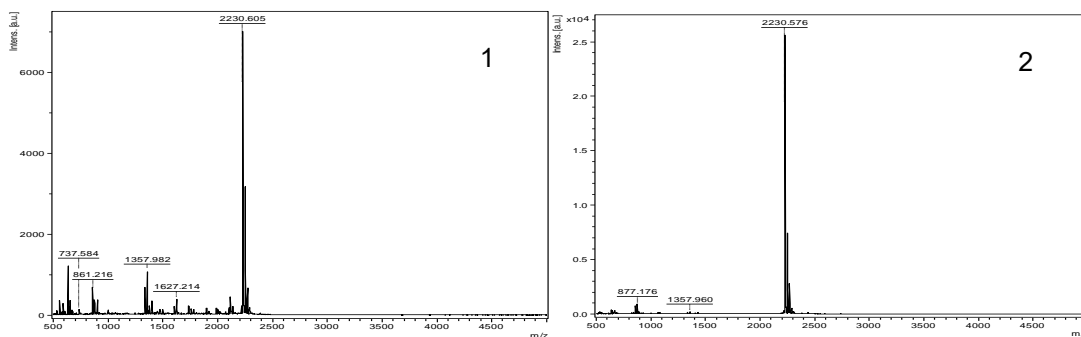


Figure 3.18 - MALDI-TOF results obtained for the purification of the peptide 4, in an acetone matrix. The samples were dissolved in acetone solution constituted by 97% acetone and 0.1% TFA in ddH<sub>2</sub>O. The peptide mass was 2228 g/mol and the peak obtained in both fractions was 2230 g/mol which corresponded to the peptide with a hydrogen [M+H<sup>+</sup>].

Afterwards, the fluorescent labelled peptide 4 was synthesized with the coupling of the 5-(6)-carboxyfluorescein to 20 mg of resin. The standard cleavage protocol yielded 10,46 mg of fluorescence



labelled peptide. The crude was purified with Schnell A $\beta$  program and the chromatogram is shown in figure 3.19. In this case, two peaks were collected, the ones with a retention time of 26,131 and 26,505 min, which were thought to be the two fluorescence labelled peptide isomers. Each peak was collected in two parts, the upper and the down part, and the collected fractions were analysed by MALDI-TOF in acetone matrix. The expected mass of the fluorescence labelled peptide was 2586 g/mol and the results, in figure 3.20, showed that the main component in each fraction had a mass of 2588 g/mol, which corresponded to the peptide with a hydrogen atom  $[M + H^+]$ . This result also confirmed the previous assumption and the small difference in the retention time could be explained by a different conformation of carboxyfluorescein isomers. Moreover, two of the fractions were cleaned, namely, the down part of both peaks, the fraction 2 and 4.

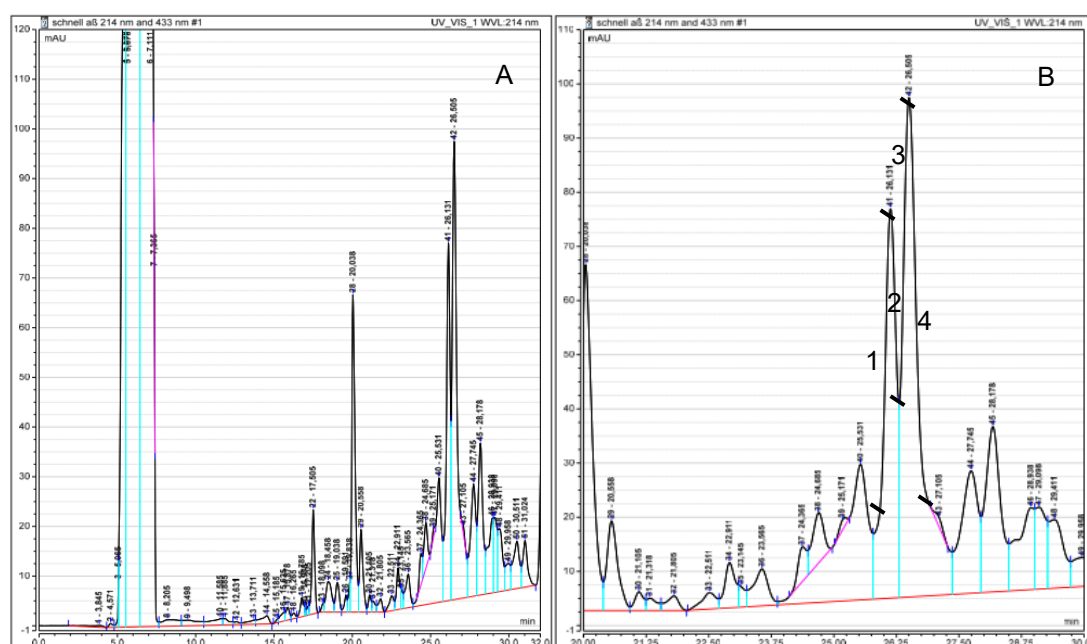


Figure 3.19 – Purification of 500  $\mu$ g of fluorescence labelled peptide 4 crude dissolved in 100  $\mu$ L TFA and 400  $\mu$ L 80% B with a Reprosil Gold 200 column (C18, 10  $\mu$ m 250 x8 mm) using Schnell A $\beta$  214 nm and 433 nm. The detection was done using two wavelengths: the 214 and 433 nm which corresponded to the wavelength of absorption of the amine bond and the carboxyfluorescein, respectively. The elution program started with 70% of solution A and 30% of solution B and ended with 30% of solution A and 70% of solution B. The peaks with a retention time of 26,131 min and 26,505 min were collected and each peak was collected in two fractions, the upper and the down part. The first one corresponded to fractions 1 and 2 and the second peak corresponded to fractions 3 and 4. A- The entire chromatogram. B – Detailed view of the peak, focusing the collected fractions.

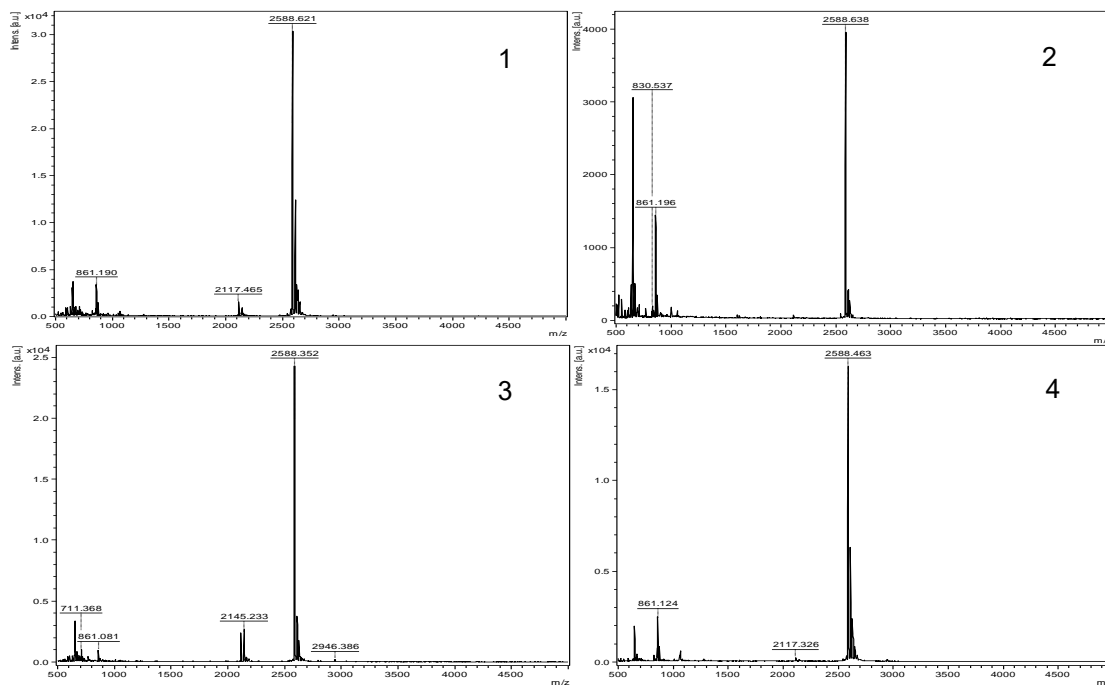


Figure 3.20 - MALDI-TOF results obtained for the purification of the fluorescence labelled peptide 4, in an acetone matrix. The samples were dissolved in acetone solution constituted by 97% acetone and 0.1% TFA in ddH<sub>2</sub>O. The peptide mass was 2586 g/mol and the main peak obtained in all fractions was 2588 g/mol which corresponded to the peptide with a hydrogen [M+H<sup>+</sup>].

In annex 2 there is a resume of the sequence of the synthesized peptides with the respective name. The annex 3 showed the synthesis plan of the synthesized peptides.

### 3.2. Effect of the modifications on the secondary structure and solubility of the analogs

To analyse how the structural modifications affected the secondary structure of the peptides far UV circular dichroism (CD) was performed. Firstly, the measurements were performed using an increase concentration of peptide stock 5 μM, 10 μM, 20 μM, 50 μM and 100 μM inside the cuvette in 1xb buffer containing 1% of HFiP from 250 nm to 195 nm. The increase of the concentration intended to determine the concentration in which the peptide precipitated, and therefore, the solubility of the peptide. Hence, when the peptides started the precipitate the measurements were stopped.

Since the ellipticity measured by the CD machine is dependent on the concentration and on the cuvette length path used, the mean residue ellipticity (MRE) was calculated in order to normalize the results obtained experimentally, using the equation 3.

$$MRE \left( \frac{\text{deg} \cdot \text{cm}^2}{\text{dmol}} \right) = \frac{CD}{c \cdot d \cdot n \cdot 10} \quad (3)$$

where CD is the circular dichroism value obtained,  $c$  the molar concentration in [M],  $d$  the length path of the cuvette in cm,  $n$  the number of amino acids in the protein/peptide and 10 is the conversion from mol to dmol.

The figure 3.21 showed the CD concentration dependence results of all peptides, focusing their secondary structure and solubility in a phosphate buffer with pH=7,4 (1xb) at room temperature.

The figure 3.21 A and B showed the CD spectrum of the control peptides. The peptide B was a peptide with two more residues in the N-terminus than the peptide A and it was used as control for the peptides 1 and 2. The figure 3.21 A showed the secondary structure of the peptide A was  $\beta$ -sheet/  $\beta$ -turn due to the local minimum around 220-230 nm. The different concentration tested showed the peptide started to oligomerized at a concentration of 10  $\mu$ M and precipitated at the highest concentration, 100  $\mu$ M. Thus, the solubility of this peptide was 50  $\mu$ M. The figure 3.21 B showed the results for the peptide B. This peptide showed two local minimums, around 220-230 and 195 nm, which indicated a  $\beta$ -sheet/  $\beta$ -turn and random coil structure. The structure remained the same with the increase of the concentration since the shape of the curves had the same local minimums. It began to oligomerize at 10  $\mu$ M since the MRE decrease in comparison with the lower concentration. However, the precipitation was only visible at 50  $\mu$ M, which was also accompanied by a significant reduction of the MRE. Therefore, the peptide solubility was 20  $\mu$ M (Armiento, Kapurniotu et al. unpublished).

### 3.2.1. Secondary structure and solubility of the analogs with tags

In order to increase the solubility of the peptide A, a tag 1 were added to the N-terminus. In figure 3.21 C, the CD results of the peptide 1 showed that the addition of the tag didn't lead to structural modifications, i. e, the secondary structure of the peptide 1 was the same as the peptide A. Moreover, the curves had the same shape, which meant the peptide structure didn't change with the increase of concentration. The increase of the concentration showed that on the two lowest concentration, 5 and 10  $\mu$ M, the peptide was soluble and didn't oligomerize since the signal increased. However, at 20  $\mu$ M precipitation was observed in the cuvette and due to that, the measurements were stopped. Hence, the addition of the tag 1 decrease solubility of the peptide in comparison with the peptide A.

The figure 3.21 D showed the results obtained for the peptide 2. The addition of tag 2 to the N-terminus of the peptide induced a  $\beta$ -turn structure, local minimum around 230 nm, showing a different structure in comparison to the control peptides. In this case, the peptide started to oligomerized at 20  $\mu$ M and it precipitated at 50  $\mu$ M, showing a solubility of 20  $\mu$ M.

When compared to the peptide B, the peptides 1 and 2 showed a different secondary structure. The structure of the peptide B had  $\beta$ -sheet/  $\beta$ -turn and random coil content, while the structure of the peptides

1 and 2 lost the random coil content. Moreover, the peptide structure altered its solubility and the modification performed in the N-terminus residue didn't increase the solubility. Thus, the residue on the N-terminus of peptide seemed to play an important role in the secondary structure of the analogs.

### 3.2.1. Secondary structure and solubility of analogs with mutations in specific residues

The figure 3.21 E showed the results obtained for the peptide 3. The exchange of the residue at position X for an aromatic residue resulted in a peptide with a  $\beta$ -sheet/ $\beta$ -turn structure since the minimum of the curve was between 220 and 230 nm. The shape of the curve remained the same with the increase of the concentrations. This alteration didn't change the secondary structure of the peptide in comparison with the peptide A. In this case, the increase of the peptide concentration led to oligomerization at 20  $\mu$ M and precipitation at 50  $\mu$ M.

On the other hand, the substitution of the residue at position X for a charged residue led to a different secondary structure, as it is shown in figure 3.21 F. The secondary structure of the peptide 4 had two local minimums around 230 and 195 nm, which meant a  $\beta$ -turn and random coil structure, while the control peptide only had a  $\beta$ -sheet/ $\beta$ -turn structure. The peptide started to oligomerize at 20  $\mu$ M and it precipitated at 100  $\mu$ M, which indicated a solubility of 50  $\mu$ M, the same solubility as the control peptide. The strange shape of the MRE curve for the 100  $\mu$ M was due to the precipitation of the peptide.

Thus, the alteration of the residue in position X enabled a conformational change. However, those alterations didn't manage to increase the solubility of the peptides in comparison with the peptide A.

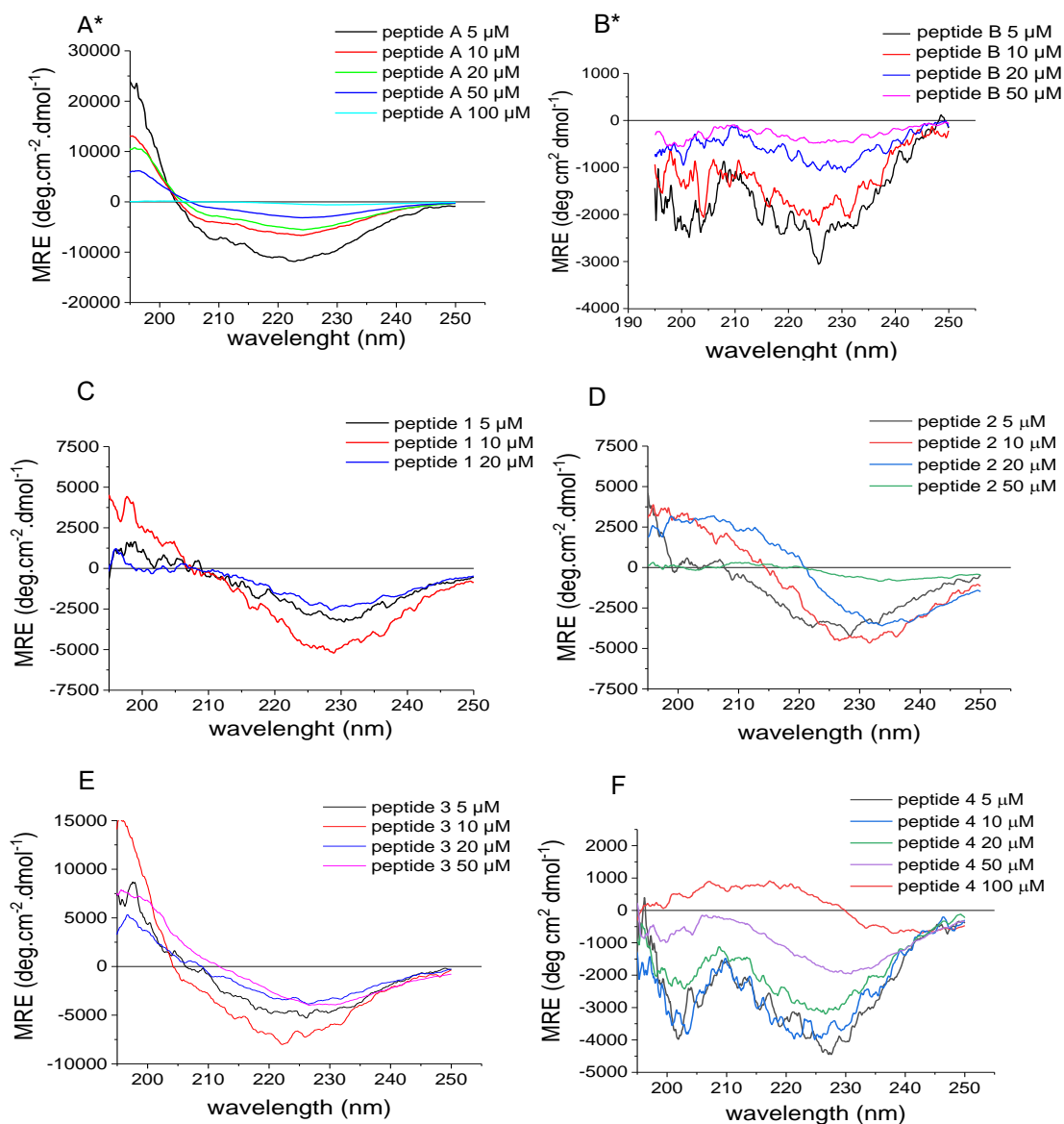


Figure 3.21 – Far UV CD – concentration dependence spectra obtained for all analogs. The peptides were dissolved in 1xb containing 0,5 % HFiP, at room temperature. The determination of the peptide solubility was performed at 5, 10, 20, 50 and 100  $\mu\text{M}$ . The concentrations were tested until visible precipitation was observed in the cuvette. The 5  $\mu\text{M}$  measurement was performed in a 1 cm cuvette, whereas the 10, 20 and 50  $\mu\text{M}$  were performed at a 0,5 cm cuvette. Lastly, the 100  $\mu\text{M}$  concentration was done in a 0,2 cm cuvette. A – peptide A. B – peptide B. C – peptide 1. D – peptide 2. E – peptide 3. F – peptide 4.

\* *Armiento, Kapurniotu et al.* unpublished.

### 3.3. Effect of the interaction between IAPP and the analogs in the secondary structure

Afterwards, the interaction between IAPP and the peptides were performed to analyse if the interaction induced an alteration of conformation. To notice, that the CD results showed an average conformation, so the absence of a structural conformation change didn't mean that the peptides didn't interact. This alteration was tested over time, more specifically, 0h, 5 min, 15 min, 30 min, 1h, 7h and 24h. At 24h, the signal was very low due to deposition of the peptides in cuvettes wall and because of that, another time point was measured after the mixture of the solution. Three different measurements were followed in parallel, namely, the IAPP alone, the peptide alone and the mixture of IAPP and the peptides.

In the figure 3.22 is shown the initial and the final time measurements obtained for the APP, the peptide alone and the mixture of both peptides. Moreover, there were two dash plots represented in each figure. They corresponded to the sum of the IAPP and the peptide alone ellipticity values. As it was mention before, the CD results corresponded the average conformation of the peptides. To analyse if the structure of the mixture was due to a change in the conformation or was simply the average of the conformation of both peptides, the mixture results had to be compared with those plots.

The IAPP structure changed over time. In the beginning the spectrum showed a random coil structure, local minimum around 195 nm. This result was compatible with the hIAPP monomers structure in the experimental conditions used. However, at 24h the IAPP acquired a  $\beta$ -sheet structure, local minimum around 220 nm. This result was used as a control since the IAPP fibrils formation was an indication as the kinetics of the reaction went on according the expected. This result was obtained for all experiments, as it was shown in figure 3.22.

In figure 3.22 A are shown the interaction results for the IAPP and the peptide A. The structure of the peptide A alone was  $\beta$ -sheet/  $\beta$ -turn and it didn't change over time. On the other hand, the structure of the mixture changed. In the beginning the structure of the mixture was  $\beta$ -sheet/ $\beta$ -turn and after 24h it had both random coil and  $\beta$ -sheet/ $\beta$ -turn content. At 0h, the sum curves of IAPP and the peptide A had a different shape compared to the mixture curve at the same time point, showing that the peptides were interacting. At 24h, the sum curve was also different from the mixture curve, which indicated there were a conformational change due to the interaction of both peptides (Armiento, Kapurniotu et al. unpublished).

#### 3.3.1. Interaction between IAPP and the analogs with tags

In the figure 3.22 B are shown the interaction results for the IAPP and the peptide 1. The secondary structure of the peptide 1 was  $\beta$ -sheet/ $\beta$ -turn and it remained the same over time. The mixture of the

IAPP the peptide 1 showed random coil and  $\beta$ -sheet/  $\beta$ -turn content. The sum of the ellipticity of the IAPP and peptide alone at 0h showed the same structure, which meant the structure was the average structure of both peptides in solution. However, at 24h the structure of the mixture showed that the secondary structure of the mixture was random coil, while the sum curve showed a  $\beta$ -sheet structure. Thus, the IAPP and the peptide 1 interact with each other and as a result of that interaction the random coil content increase and the  $\beta$ -sheet content decreased.

The results obtained for the peptide 2 showed  $\beta$ -sheet/ $\beta$ -turn structure and it didn't change over time. The secondary structure of the mixture between IAPP and the peptide 2 showed the presence of random coil and  $\beta$ -sheet/ $\beta$ -turn content. At 0h, the sum of the ellipticity values obtained for the IAPP and the peptide alone showed the same shape as the ellipticity curve of the mixture at the same time point. At 24h, the sum curve showed a  $\beta$ -sheet structure, while the mixture curve showed a random coil structure. Thus, the interaction of the peptides induced a change in the secondary structure of the mixture.

Hence, the addition of the diamino acid tag to the N-terminus of the peptides didn't affect their ability to bind to IAPP. In both cases, the interaction led to the increase of the random coil structure, as it was observed in the interaction of IAPP and the peptide A.

### 3.3.1. Interaction between IAPP and the analogs with mutations in specific residues

The structure of peptide 3 alone was a  $\beta$ -sheet/ $\beta$ -turn structure and it did not change over time. The mixture structure had random coil and  $\beta$ -sheet/  $\beta$ -turn content throughout the entire experiment. At 0h, the sum curve had the same shape as the mixture curve, two minimum locals around 195 nm and 220-230 nm. This result indicated that the conformation was the average conformation of both monomers. At 24h, the results obtained for the sum of both peptides and the mixture showed different shapes and, consequently, different structures. In first case, the curve showed two local minimums around 195 nm and 220-230 nm, while the 24h curve showed a local minimum around 220-230 nm. On the other hand, the mixture ellipticity curves showed the presence of both random coil and  $\beta$ -sheet content. Thus, these results showed the existence of interaction between the IAPP and the peptide 3.

The peptide 4 had a secondary structure with  $\beta$ -sheet/  $\beta$ -turn and random coil content and it didn't change over time. The mixture curve of the peptide and IAPP showed two local minimums at 200 and 220-230 nm. Then, the secondary structure of the peptide was random coil and  $\beta$ -sheet/  $\beta$ -turn. The sum curves at time 0 and 24h showed the same shape, with random coil and  $\beta$ -sheet/  $\beta$ -turn structure. Moreover, the mixture curves and the sum curves showed the same shape, which indicated the absence of a conformation change. The results suggested the lack of interaction between the peptides or the absence of a conformational change due to the interaction of both peptides. To emphasize, the results were not sufficient to conclude weather the peptides interact with each other or not.

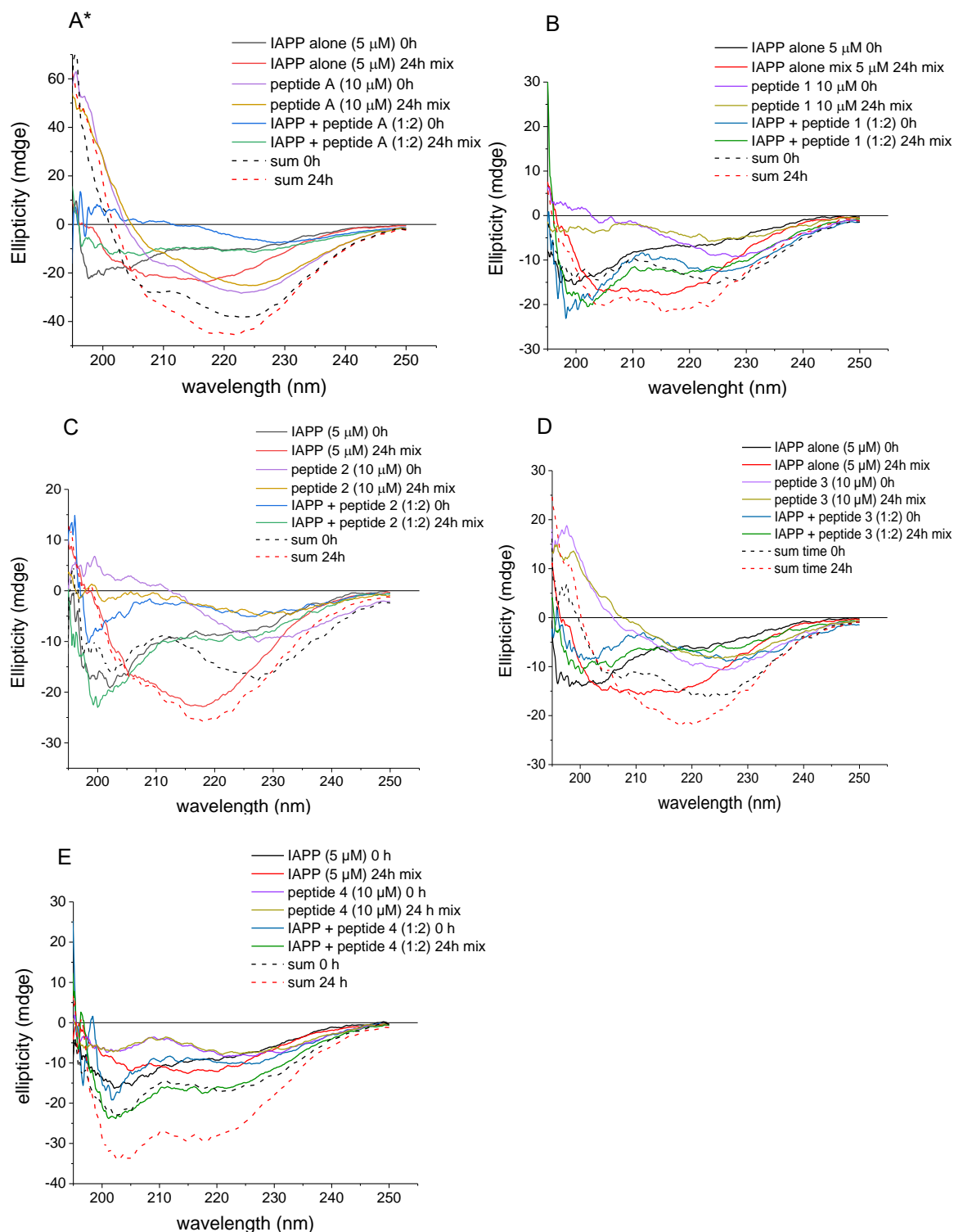


Figure 3.22 – Far UV CD spectra obtained for the interaction of IAPP and the analogs. The peptides were dissolved in 1xb containing 1% HFIP, at room temperature. Three different measurements were measured in parallel: the IAPP alone (5  $\mu$ M), the peptide alone (10  $\mu$ M) and the mixture of both peptides (1:2). The measurements were done in 1 cm cuvettes. The interaction of the peptides was tested over time, more specifically, 0h, 5 min, 15 min, 30 min, 1h, 7h and 24h. A- Interaction between IAPP and the peptide A. B – Interaction of IAPP and peptide 1. C – Interaction of IAPP and peptide 2. D – Interaction of IAPP and peptide 3. E – Interaction of IAPP and peptide 4.

\* Armiento, Kapurniotu et al. unpublished.



Thus, the mutations in the residue in position X led to different results of the interaction of IAPP and the peptide. The addition of an aromatic/hydrophobic residue led to a change in conformation as a result of the interaction. On the other hand, the addition of a charged amino acid did not change apparently the secondary structure of the mixture.

### 3.4. Effect of the modifications in the inhibition of the IAPP fibrillogenesis

The activity of the peptides was tested using ThT assay. In these assays, the thioflavin-T has the ability of binding to fibrils and consequently allowed the determination whether the peptide was capable of inhibiting IAPP fibrillogenesis. The experiments were performed in Eppendorf tubes, where the IAPP (16,5  $\mu\text{M}$ ) and the mixtures of IAPP and the peptides were dissolved in 50 mM  $\text{Na}_2\text{PHO}_4$ , 100 mM NaCl in  $\text{ddH}_2\text{O}$ , pH=7,4 (ThT buffer), containing 0,5% of HFiP. Three different IAPP and peptide ratios were tested. The measurements were performed for 7 days every 24 hours, in triplicates, except the peptides A and C, which were only performed one time.

#### 3.4.1. Inhibitory properties of the analogs with tags

The results obtained for the peptide 1 are shown in the figure 3.23 for the different ratios. The IAPP results, red curve, showed that the fluorescence of IAPP increases after 24h, and it remains elevated during the seven days. Hence, following the correct IAPP kinetics for the experimental conditions used. The grey curve showed the results obtained for the mixture of IAPP and the peptide A in the ratio 1:5. Previous experiments showed that in this ratio the peptide A enabled the inhibition of IAPP fibril formation (Armiento, Kapurniotu et al. unpublished). Thereby, this peptide was used as a control. The figure 3.23 showed that in all the experiments, the fluorescence value of the mixture between IAPP and the peptide 1 increased at 7 days. However, the ratios 1:5 and 1:10 enabled the fibril formation at 24h, as it is shown in figure 3.23 B and C. Overall, the results showed that the peptide was only capable of inhibiting the IAPP fibrils formation for 24h at a minimum concentration of 82,5  $\mu\text{M}$ .

The confirmation of the presence of fibrils was performed by TEM. The results obtained for the mixture of IAPP and peptide 1 in the ratio 1:10 at seven days showed the presence of 90% fibril and 10% of amorphous, as it is shown in figure 3.23 E.

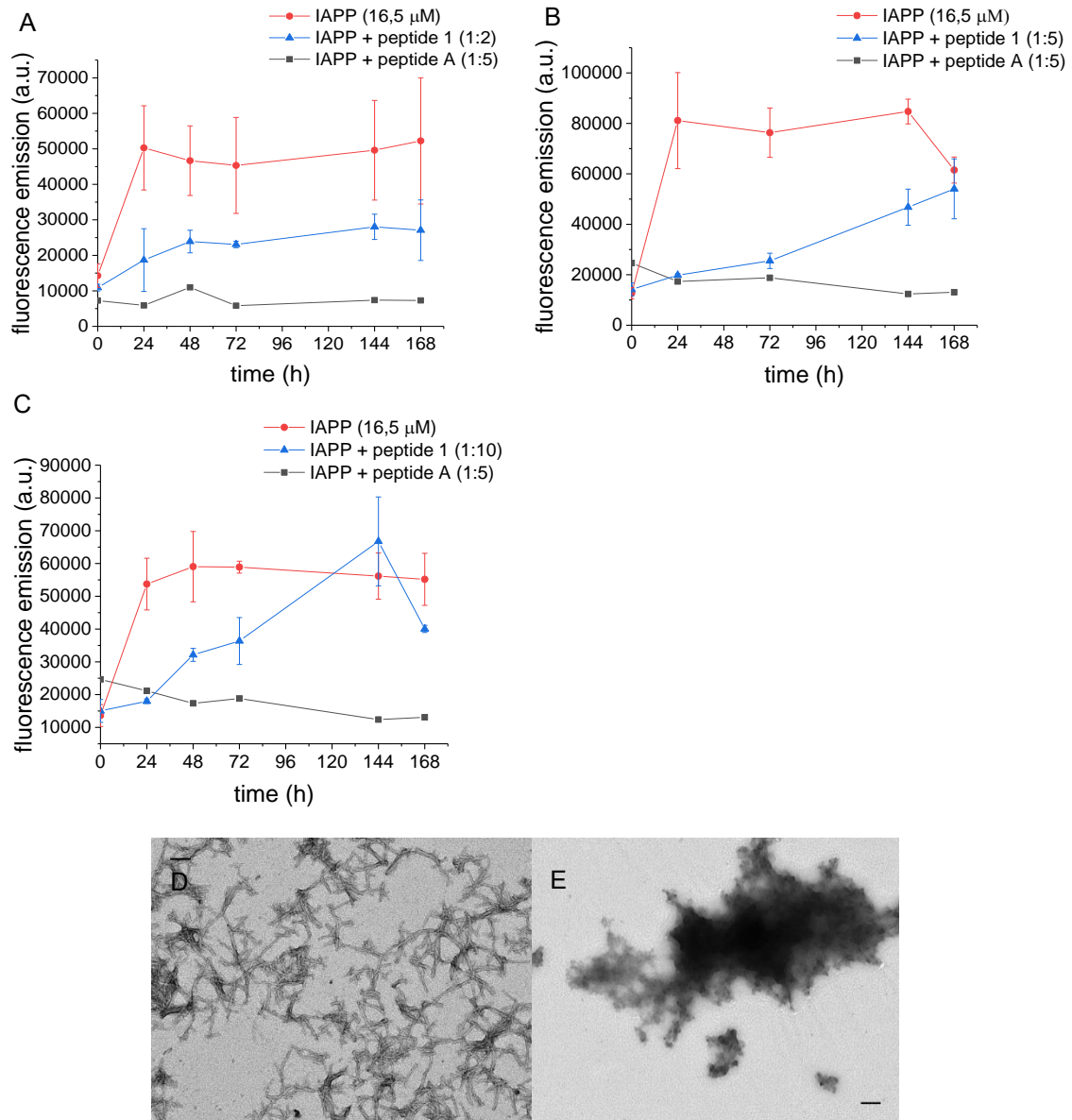


Figure 3.23 – ThT assay of the mixture IAPP with peptide 1 and TEM images. The peptides were dissolved in ThT buffer, containing 0,5 % of HFIP. The Eppendorfs were incubated at 20 °C and experiment was followed through 7 days and the measurements were done every 24h. The IAPP kinetics was represent in red (mean  $\pm$  SD, n =3), the mixture of the IAPP and the peptide 1 were represented in blue (mean  $\pm$  SD, n =3) and the control was represented in grey (n=1). A- IAPP plus peptide 1 in the ratio 1:2. B- IAPP plus peptide 1 in the ratio 1:2 the ratio 1:5. C - IAPP plus peptide 1 in the ratio 1:10. D-E – TEM pictures for the mixture between IAPP and the peptide 1 (1:10) taken for 7 days. D- fibrils. E- amorphous.

The results of the ThT assay for the peptide 2 were represented in figure 3.24. The IAPP kinetics, red curve, showed the ordinary profile with a lag time of 24h. The fibrils formation was observed after 24h with the increase of the fluorescence emission. The peptide A was used as control at a concentration of 85,5  $\mu$ M and the kinetics was represented as a grey curve in figure 3.24. The results of the inhibitory

properties of the peptide showed that both ratios 1:2 and 1:5 inhibit the IAPP fibrils formation. Hence, the minimum concentration required to inhibit the IAPP fibrillogenesis was 33  $\mu\text{M}$ . However, the TEM grids for the mixture IAPP plus peptide showed the presence on fibrils on both ratios. For the ratio 1:2 and 1:1 the percentage of fibrils and amorphous aggregates was 70%-30% and 50%-50%, respectively. This result was inconsistent with the ThT assay.

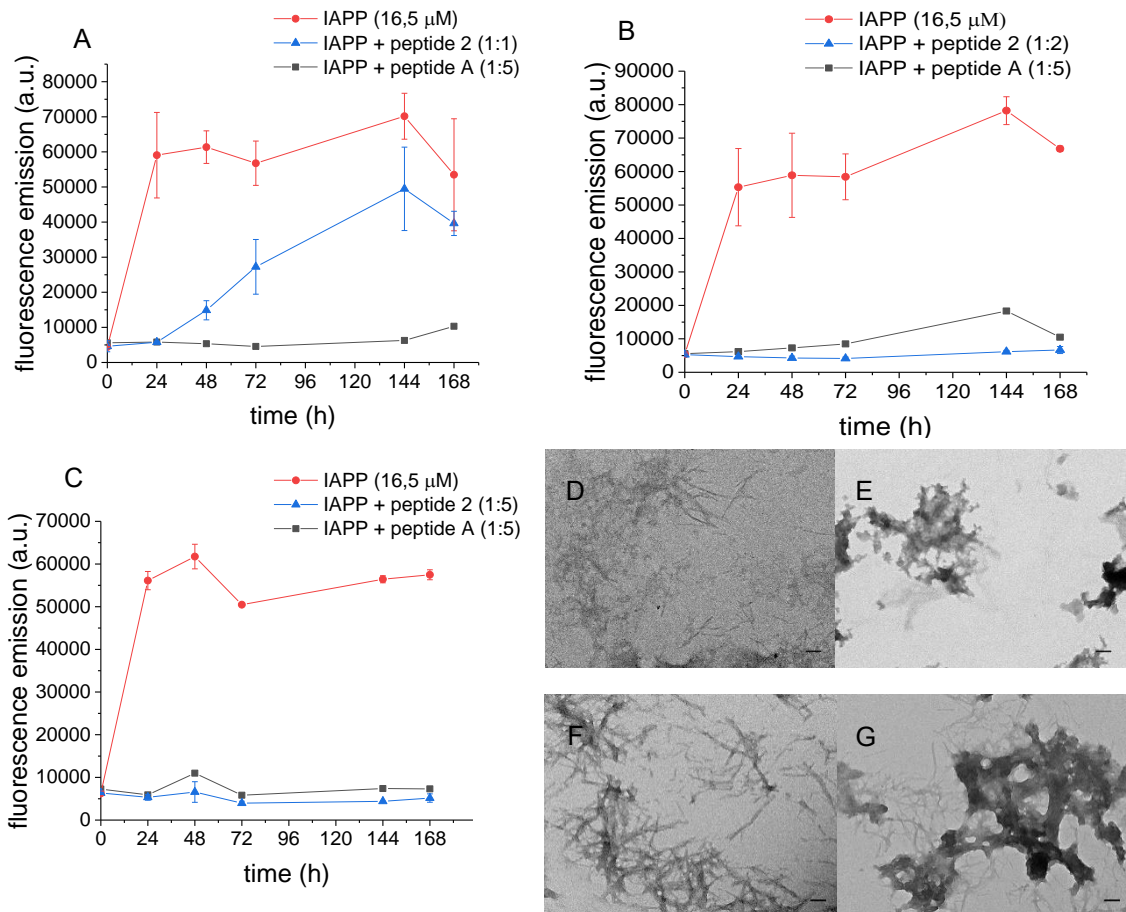


Figure 3.24– ThT assay of the mixture IAPP with peptide 2 and TEM images. The peptides were dissolved in ThT buffer, containing 0,5 % of HFiP. The Eppendorfs were incubated at 20 °C and experiment was followed through 7 days and the measurements were done every 24h. The IAPP kinetics was represent in red (mean  $\pm$  SD, n =3), the mixture of the IAPP and the peptide 2 were represented in blue (mean  $\pm$  SD, n =3) and the control was represented in grey (n =1). A- IAPP plus peptide 2 in the ratio 1:1. B- IAPP plus peptide 2 in the ratio 1:2 C- IAPP plus peptide 2 in the ratio 1:5. D-E – TEM pictures for the mixture between IAPP and the peptide 2 (1:2) taken for 7 days. D- fibrils. E- amorphous. F-G – TEM pictures for the mixture between IAPP and the peptide 2 (1:1) taken for 7 days. F- fibrils. G- amorphous.

### 3.4.2. Inhibitory properties of the analogs with mutations in specific residues

The ThT results of the inhibition of IAPP by the peptide 3 are summarized in the figure 3.25, as well as the peptide alone. The results showed that the IAPP alone, red curve, followed the normal kinetic profile with a lag time of 24h. The control, mixture of IAPP and peptide A in the ratio 1:5, inhibited the IAPP fibril formation, as expected (Armiento, Kapurniotu et al. unpublished). The mixture between IAPP and the peptide 3 increased significantly at 24h, indicating that the peptide was not able to inhibit the fibrils formation with a concentration of 82,5  $\mu\text{M}$ . Since the ThT assay measures the binding of ThT dye to the fibrils, the analysis of the peptide alone was performed in order to understand if the peptide also forms fibrils which contributes to the increasing of the fluorescence. The confirmation of the presence of fibrils was performed with TEM, showed in figure 3.25 C-E. The results are showed the presence of 60% of fibrils and 40% of amorphous and amorphous for the IAPP plus peptide 3 and for the peptide 3 alone, respectively. The ThT experiment of the peptide 3 was only tested at a ratio of (1:5) since at this concentration the peptide was already oligomerizing, so would be counterproductive to increase the peptide concentration. On the other hand, since the peptide cannot inhibit the fibrils formation the decrease of concentration wouldn't be effective.

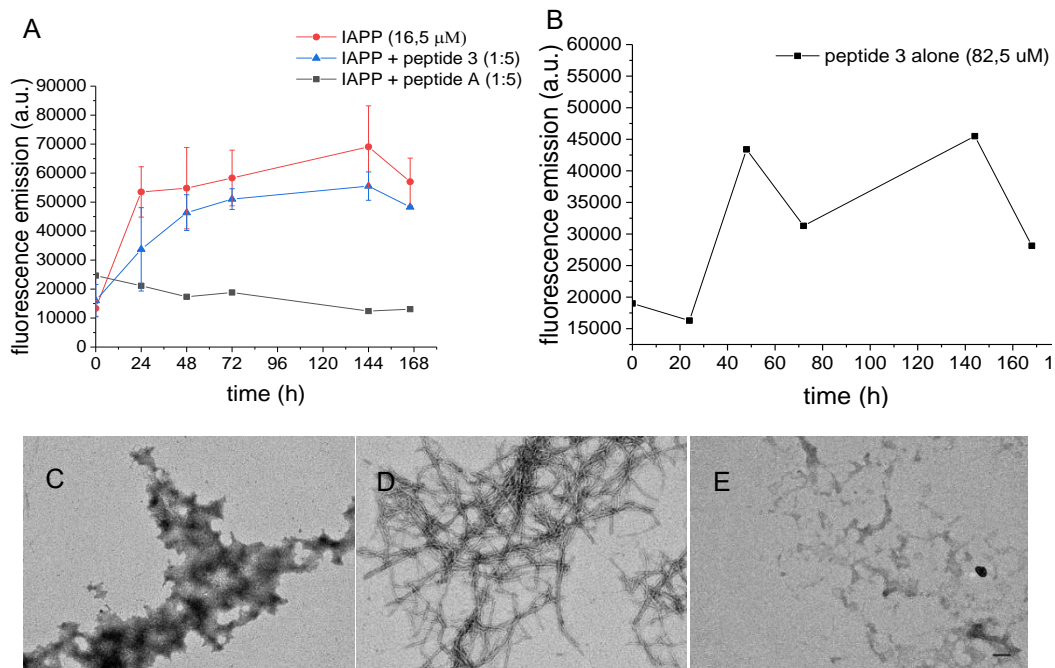


Figure 3.25 – ThT assay of the mixture between IAPP and the peptide 3 and TEM images. The peptides were dissolved in ThT buffer, containing 0,5 % of HFIP. The Eppendorfs were incubated at 20 °C and experiment was followed through 7 days and the measurements were done every 24h. The IAPP kinetics was represent in red (mean  $\pm$  SD, n =3), the mixture of the IAPP and the peptide 3 were represented in blue (mean  $\pm$  SD, n =3) and the control was represented in grey (n =1). A- IAPP plus peptide 3 in the ratio 1:5. B- peptide alone at 82,5  $\mu\text{M}$  (n=1). C-D – TEM pictures for the mixture between IAPP and the peptide 3 (1:5) taken for 7 days. C- amorphous. D- fibrils. E – TEM pictures of the peptide 3 alone (82,5  $\mu\text{M}$ ) taken for 7 days. It showed amorphous aggregates.

The results obtained for the peptide 4 are represented in figure 3.26. The IAPP curve is represented in red and showed the normal kinetics profile with a lag time of 24h. The mixture between IAPP and the peptide 4 was tested in two different ratios, the 1:5 and the 1:2. Initially, the ratio 1:5 was tested and the peptide enabled the inhibition of IAPP fibril formation since the fluorescence values remained low during the 7 days. Afterwards, the ratio 1:2 was tested and in this case the peptide concentration did not prevent the IAPP fibril formation. Thus, the peptide 4 needed to be present with a concentration of 82,5  $\mu\text{M}$  in order to inhibit IAPP fibrillogenesis. In both cases, the control (peptide A) was able to inhibit the IAPP fibril formation in the ratio (1:5) (Armiento, Kapurniotu et al. unpublished). In this case, another peptide was tested, the peptide C, which differed from the peptide A in the C-terminus residue. This peptide did not inhibit the IAPP fibrillogenesis (Armiento, Kapurniotu et al. unpublished). The TEM grid performed at 7 days for the ratio 1:5 was empty. On the other hand, the TEM grid performed for the ratio 1:2 showed the presence of 30% of fibrils and 70% of amorphs. The amount of fibrils obtained was lower than the expected based on the ThT assay.

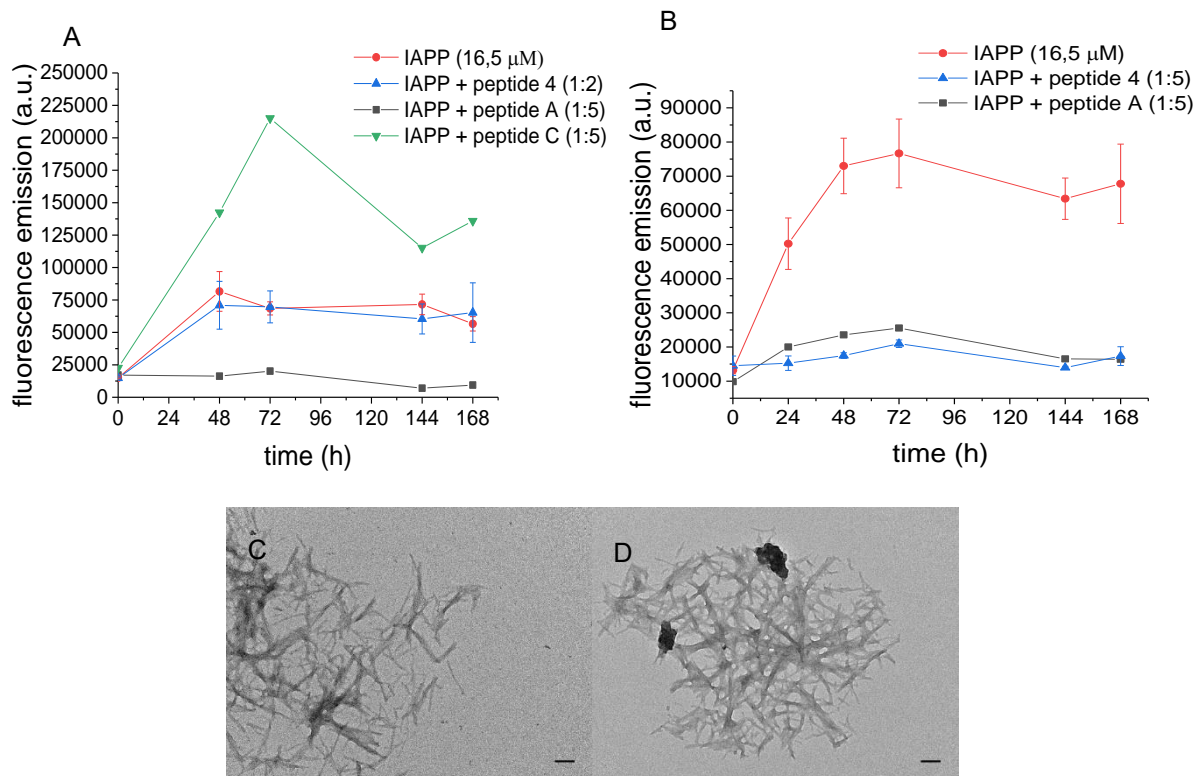
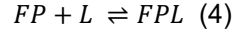


Figure 3.26 – ThT assay of the mixture IAPP with peptide 4 and TEM images. The peptides were dissolved in ThT buffer, containing 0,5% of HFIP. The Eppendorfs were incubated at 20 °C and experiment was followed through 7 days and the measurements were done every 24h. The IAPP kinetics was represent in red (mean  $\pm$  SD, n =3), the mixture of the IAPP and the peptide 4 were represented in blue (mean  $\pm$  SD, n =3). The control was represented in grey (n =1) and the mixture between IAPP and the peptide C was represented in green (n =1). A- IAPP plus peptide 4 in the ratio 1:2. B- IAPP plus peptide 4 in the ratio 1:5. C-D– TEM pictures for the mixture between IAPP and the peptide 4 (1:2) taken for 7 days. C- fibrils. D- amorphous.

### 3.5. Effect of the modifications on the self-assembly and binding of the analogs to IAPP

The fluorescence titration consisted in the determination of binding constant between two molecules. Overall, the dissociation equilibrium was described in equation 4.



where FP, L and FPL was the fluorescence labelled peptide, the ligand and the complex, respectively. The apparent dissociation constant,  $app. K_D$ , defined as an equilibrium constant between the monomeric and the oligomeric form was calculated by equation 5:

$$app. K_D = \frac{[FP] \cdot [L]}{[FPL]} \quad (5)$$

The fluorescence titration was performed with a fluorescence labelled peptide (with 5(6)-carboxyfluorescein) at 5 nM and increasing concentrations of the other peptide in triplicates. The constant determined were: the binding of the fluorescence labelled peptide to the IAPP, the binding of the fluorescence labelled IAPP to the peptide and the self-assembly of the peptide (binding of the fluorescence labelled peptide to the peptide).

The experimental results were fitted using a dose-response curve, suitable to analyse the response that one molecule generated in another system. The curve had a rectangular hyperbola shape. This curve is defined by four parameters: the minimum (bottom) and the maximum (top), responses, the slope and the  $IC_{50}$ <sup>153</sup>. This last parameter is defined as the concentration at which the response obtained was half of the maximum response. Therefore, this parameter consisted in the dissociation constant.

The high affinity constant,  $K_D < 100$  nM, was recalculated with GraFit Erithacus Software. The equation used aimed to determine the quadratic solution of equation 5. In this condition, the fluorescence is described by equation 6<sup>153</sup>.

$$F = F_{min} + (F_{max} - F_{min}) \cdot \frac{\sqrt{\frac{[FP] + [L] + K_D}{2} - \frac{([FP] + [L] + K_D)^2 - [FP] \cdot [L]}{4}}}{[L]} \quad (6)$$

where  $F_{min}$  and  $F_{max}$  corresponded to the minimum and the maximum fluorescence. [FP] and [L] were the fluorescence labelled peptide and the ligand concentrations, respectively.

The first constant measured the binding between the monomeric form of the peptide to IAPP oligomers. The second constant measured the binding between the monomeric IAPP and the peptide oligomers. The last constant measured the self-assembly propensity of the peptide, i.e the affinity of the peptide to

oligomerize. The table 3.1 summarized the dissociation constant obtained for the three experiments and the dose-response curves were represented in annex 4.

Table 3.1 – Apparent  $K_d$  mean values ( $\pm$  SD) obtained for three different experiments: the determination of the binding affinity between the fluorescence labelled peptide and IAPP; the binding affinity between the fluorescence IAPP and the peptide and the binding activity between the fluorescence labelled peptide and the peptide. The experiments were performed in triplicates and used 5 nM of the fluorescence labelled peptide with the increase concentration of the peptides in 1xb (10 mM phosphate buffer, pH=7,4) containing 1% HFIP at room temperature.

	App. $K_d$ Fluorescence labelled peptide + IAPP (nM)	App. $K_d$ Fluorescence labelled IAPP + peptide (nM)	App. $K_d$ Fluorescence labelled peptide + peptide (nM)
Peptide A	n.b.* [a]	26,3 $\pm$ 5,9*	65,9 $\pm$ 26,3*
Peptide B	$\approx$ 9*	28,4 $\pm$ 6,7*	5,0 $\pm$ 0,7*
Peptide 1	24,5 $\pm$ 3,57	66,3 $\pm$ 33,4	39,6 $\pm$ 4,3
Peptide 2	47,6 $\pm$ 5,4	103 $\pm$ 2 (24,0 $\pm$ 4,2)	49,6 $\pm$ 8,6
Peptide 3	167 $\pm$ 18	25,7 $\pm$ 14,2	99,5 $\pm$ 19,7
Peptide 4	56,8 $\pm$ 20,3	37,6 $\pm$ 17,3	31,9 $\pm$ 10,7

\* Armiento, Kapurniotu et al. unpublished. [a] n.b. – no binding

The fluorescent spectroscopy titration results of peptide A showed that the peptide oligomers bound to the IAPP monomers and it was able to oligomerize. However, the peptide A monomers were not able to bind to the IAPP oligomers. On the other hand, the peptide B was able to bind to itself, to the IAPP monomers and its oligomers also bound to the IAPP monomers. In both cases, the dissociation constant revealed a high affinity of the fluorescence labelled peptide to the unlabelled peptide (Armiento, Kapurniotu et al. unpublished).

The peptides 1 and 2 had strong binding to the IAPP monomers and oligomers. Moreover, they both have a higher propensity to oligomerize since the self-assembly dissociation constant values were low. To notice that the dissociation constant obtained through the titration of the fluorescence labelled IAPP with peptide 2 dilutions showed 2 values. The first value corresponded to the value calculated with GraFit, while the other one was the one obtained through the Origin. The significant differences could be explained by the high dispersion of the points in the upper plateau. Hence, the GraFit fit considered that the upper plateau wasn't reached in the dilution 1:100, and consequently, the dissociation constant was higher than it was supposed. Thereby, the second value will be taken in account for the analyses of the results. The peptide 1 and 2 enabled to bind with high affinity to the IAPP oligomers. The rest of the dissociation constants were similar to the ones from the peptide A. The peptides 1, 2 and B differed only in the residue in the N-terminus. The peptides showed a similar binding affinity of the fluorescence labelled IAPP to the peptide. On the other hand, the peptide B had a higher affinity to bind to oligomeric IAPP and to self-assembly.

The peptide 3 and 4 were able to bind to the IAPP monomers, oligomers and to oligomerize with a high affinity. However, the peptide 3 self-assembly constant value was the double of the peptide 4, which meant the peptide 3 had a lower propensity to oligomerize in comparison with peptide 4. Moreover, the peptide 3 monomers affinity towards the IAPP oligomers was 10 times lower than the peptide 4.

In comparison with the peptide A, the peptide 3 and 4 were allowed to bind to the IAPP monomers. The others dissociation constants were similar, excepted for the dissociation constant value for the self-assembly of the peptide 3, which was the double of the peptide A. Thus, the peptide 3 had a less propensity to oligomerize rather than the peptide A.

### 3.6. Determination of the solubility by a centrifugation assay

The solubility of the peptides 3 and 4 was further analysed by a centrifugation assay. This assay consisted in the centrifugation of a sample with different incubation times to understand what was the amount of peptide that precipitated and the amount which remained in solution. After the centrifugation of the samples, the supernatant was transferred to another Eppendorf tube and the pellet was redissolved in 1xb. The quantification of the peptide in each fraction was done by BCA. This assay was performed in triplicates for three different time points: 0h, 20 min and 7 days.

Initially the correlation between the fluorescence emission and the peptide mass was determined as it is showed in figure 3.27.

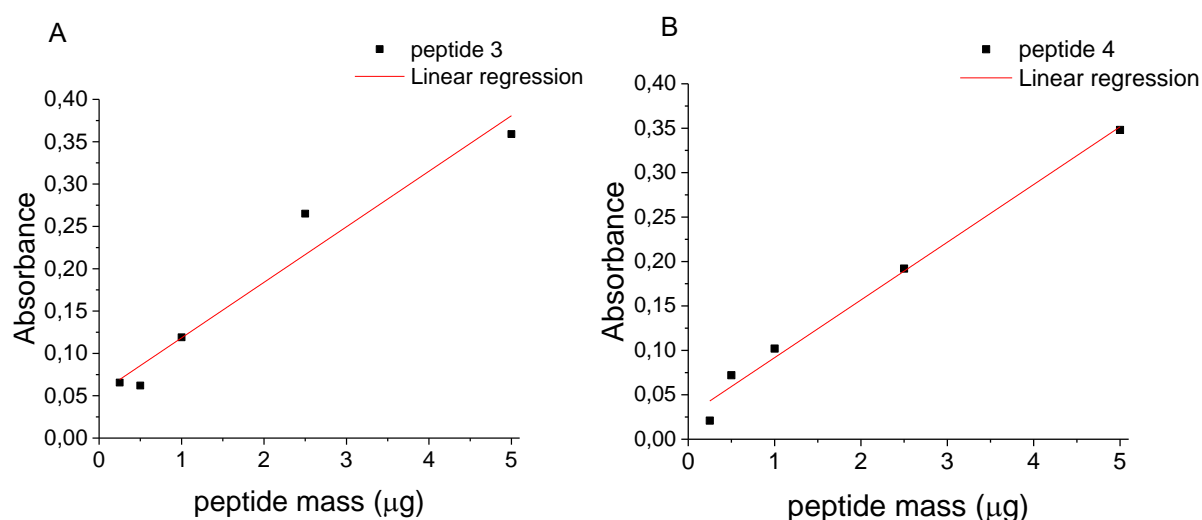


Figure 3.27 - Correlation between the fluorescence emission in arbitrary units (a.u.) and the peptide mass in µg. The determination was performed by BCA. To the peptides previously dissolved in 50 µL of 1xb, at room temperature, were added 150 µL of BCA solution. The samples were incubated at 37 °C during 3h. A – Linear correlation between the absorbance at 570 nm and the peptide 3 mass. The equation of the linear regression was  $y = 0,0656x + 0,0528$ ,  $r^2 = 0,95$ . B – A – Linear correlation between the absorbance at 570 nm and the amounts of peptide 4. The equation of the linear regression was  $y = 0,0650x + 0,0268$ ,  $r^2 = 0,98$ .



With the calibration curve equations and the samples absorbance, the amount of peptide in  $\mu\text{g}$  was calculated for the pellet and supernatant samples. Since the initial mass is known, the percentage of soluble peptide was calculated by the ratio between the calculated mass and the initial mass. The percentage of soluble peptide in the three different time points for peptide 3 and 4 were represented in figure 3.28.

The results showed that both peptides precipitated at  $20\ \mu\text{M}$ . The figure 3.28 A showed that peptide 3 is presented on the pellet fraction. At time 0h, the sum of the peptide in the pellet and the supernatant was inferior than 100%. At time 20 min and 7 days the percentage of the peptide in the pellet was 100%. In the figure 3.24 B the majority of the peptide 4 was in the pellet fraction. However, at 0h 10% of the peptide was still soluble.

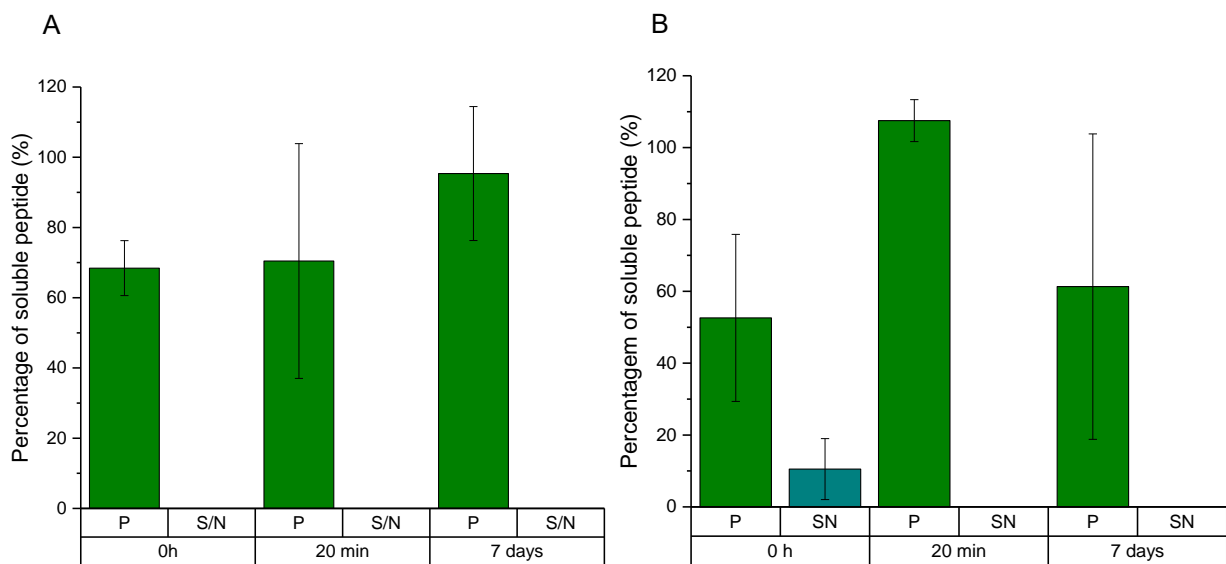
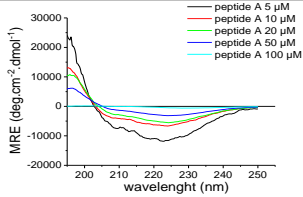
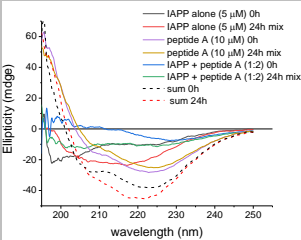
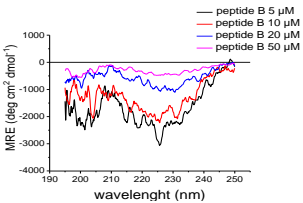
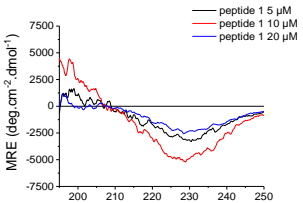
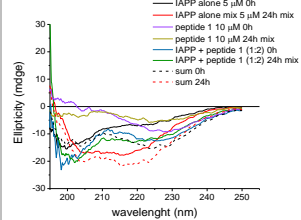


Figure 3.28 – Centrifugation assay performed with  $20\ \mu\text{M}$  of peptide. The peptide was dissolved in 1xb at room temperature. The measurements were performed at three different time points: 0h, 20 min and 7 days. The peptide soluble in the pellet and supernatant fractions were determined by BCA assay. Data shown are the mean value from 3 assays  $\pm$  SD. A – Results obtained for the peptide 3. B – Results obtained for the peptide 4.

Table 3.2 – Summary of the experiments performed for the analogs.

	Secondary structure	Interaction of peptide + IAPP	ThT <sup>[a]</sup>	TEM	Binding affinities			Centrifugation assay <sup>[a]</sup>
					Fluos-IAPP + peptide <sup>[a]</sup>	Fluos-peptide + IAPP <sup>[a]</sup>	Self – assembly <sup>[a]</sup>	
Peptide A*			(1:2) –  (1:5) +	100% fibrils	n.b.	26,3 ± 5,9	65,9 ± 26,3	
Peptide B*			(1:2) +  (1:5) +	70% fibrils + 30% amorphs	≈ 9	28,4 ± 6,7	5,0 ± 0,7	
Peptide 1			(1:2) –  (1:5) –  (1:10) –	90% fibrils + 10% amorphs	24,5 ± 3,57	66,3 ± 33,4	39,6 ± 4,3	

Peptide 2			<p>(1:1) –</p> <p>(1:2) +</p> <p>(1:5) +</p>	<p>50% fibrils</p> <p>+ 50% amorphs</p>	<p><math>47,6 \pm 5,4</math></p>	<p><math>103 \pm 2</math> (<math>24,0 \pm 4,2</math>)</p>	<p><math>49,6 \pm 8,6</math></p>		
Peptide 3			<p>(1:5) –</p>	<p>60% fibrils</p> <p>+ 40% amorphs</p>	<p><math>167 \pm 18</math></p>	<p><math>25,7 \pm 14,2</math></p>	<p><math>99,5 \pm 19,7</math></p>	<p>Precipitate at 20 μM</p>	
Peptide 4			<p>(1:2) –</p> <p>(1:5) +</p>	<p>30% fibrils</p> <p>+ 70% amorphs</p>	<p><math>56,8 \pm 20,3</math></p>	<p><math>37,6 \pm 17,3</math></p>	<p><math>31,9 \pm 10,7</math></p>	<p>Precipitate at 20 μM</p>	

\*(Armiento, Kapurniotu et al. unpublished).

[a] Mean value  $\pm$  SD, (n=3)

## 4. Discussion

### 4.1. Synthesis and purification

The synthesis of the peptides was performed using the SPPS technology. The Fmoc/tBu approach was chosen due to the orthogonality of this process, which simplified the synthesis process since the different protective group could be removed using different experimental conditions.

The monitoring of the several steps through the Kaiser or Chloranil test allowed the confirmation whether the step was successfully done or not. Nevertheless, this test was only qualitative which only gave an indication whether the coupling was successfully performed or not. Depending on the coupled amino acid and its position, different coupling conditions were used, namely the coupling reagents, the number of equivalents used and the time of the reaction. The hardest coupling was performed with HATU as a coupling agent, while the rest were performed with HBTU or a combination of both; where the first coupling step was used with HATU and the rest with HBTU. As the number of residues anchored in the resin increased, the number and the time of couplings were increased since the coupling reaction became more difficult. The synthesis plans of the four peptides are described in detailed in annex 3. After the coupling of each amino acid, the resin was acetylated to prevent the growth of truncated sequences.

The synthesis of peptide 1 was performed according to the synthesis plan. Also, the synthesis of the peptide 2 went according to the synthesis plan. However, the MALDI results showed the presence of a truncated sequence. The Chloranil test performed after the coupling on one phenylalanine showed the presence of colourless beads, as it was expected. Since the Chloranil test is a qualitative test, it may haven't worked properly in this case. To overcome this problem, the number of equivalents, the time of coupling or the number the couplings could be increased to improve the coupling. The synthesis of the peptide 3 became difficult after the amino acid at sequence position 4 and in order to function, the number of equivalents and the time of coupling have to be increased. A possible explanation may be that the sequence started to fold on the resin and the N-terminus was less available to react. The synthesis of the peptide 4 went according to the synthesis plan except the coupling of the amino acid in position W.

Overall, the coupling of the residue in position W was difficult and required, at least, one extra coupling step. This coupling step was difficult since was preceded by a methylated residue, which could cause steric hindrance and make the coupling more difficult.

The purification of the peptides was performed using different programs. Initially the peptides were purified with the program Schnell A $\beta$ . This program is the program with the bigger gradient and consequently, the lowest selectivity. However, since the peptides 1, 2 and 3 had by-products which were eluted with similar conditions as the peptide of interested, other programs had to be used. The

repurification of those peptides were achieved using programs with a smaller gradient during a longer period of time in order to achieve a higher selectivity. For the peptides 1 and 3, the langsame A $\beta$  program was enough to purify the peptide. For the peptide 2, the presence of a truncated segment in the amino acid at position W required the purification with Langsame long A $\beta$  since the purification was more complicated. A possible explanation was that since the by-product and the peptide 2 differed only in 2 amino acids, the conformation and hydrophobicity of the peptides were very similar. Therefore, it was more complicated to separate the peptides in two different peaks.

## 4.2. Effect of the modifications on the secondary structure and solubility of the analogs

### 4.2.1. Secondary structure and solubility of the analogs with tags

The secondary structure of the synthesised peptides was analysed by far-UV circular dichroism and compared with the structure of peptide A and B in order to understand how the alterations affected the peptides conformation. The figure 4.1 showed how the addition of the tags effected the secondary structure of the analogs.

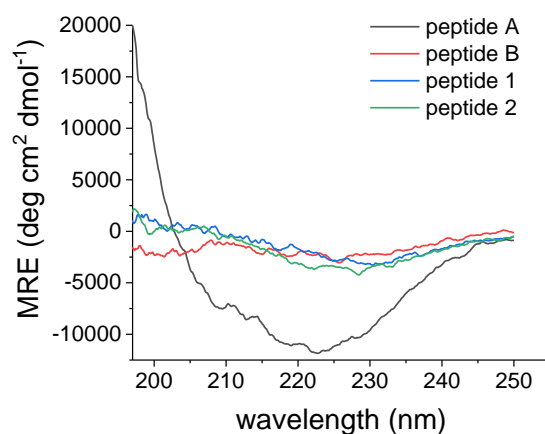


Figure 4.1 – Comparison of the secondary structures of the analogs A and B and the analogs with tags at 5  $\mu$ M.

The attempts to increase the peptide solubility were based on the addition of tags to the N-terminal of the peptide. Initially, tag 1 was added. The first tag aimed to increase the random coil content of the peptide and consequently their solubility. The peptide 1 showed a mixture of a  $\beta$ -sheet and  $\beta$ -turn structure, while the peptides A and B showed the presence of  $\beta$ -sheet/  $\beta$ -turn structure and random coil and  $\beta$ -sheet/  $\beta$ -turn content, respectively. Thus, the addition of the tag 1 didn't change its secondary structure, when compared with the peptide A. However, in comparison in the peptide B, the peptide 1 lost the random coil content. The solubility of the peptide was 20  $\mu$ M, while the solubility of peptide A and B was 100 and 50  $\mu$ M, respectively. The unexpected decreased of the solubility could be explained by the establishment of non-covalent interactions between the peptide extremities.

To test this hypothesis, the tag 2 was added to the N-terminus of the peptide. The secondary structure of this peptide was the  $\beta$ -sheet/  $\beta$ -turn, the same as the peptide A. The CD concentration dependence experiment showed that the peptide precipitated at 50  $\mu$ M. The increase of the solubility corroborated the hypothesis. However, the peptide solubility was inferior to the solubility of the peptide A and the same as peptide B.

Thus, the addition of amino acids to the N-terminal of the peptide didn't increase the peptide solubility in comparison to peptide A. This result seemed to suggest that the decrease of the peptide size was responsible for the increase of the solubility.

#### 4.2.2. Secondary structure and solubility of the analogs with mutations in specific residues

The figure 4.2 summarized the different secondary structures of the analogs with the mutation in position 31.

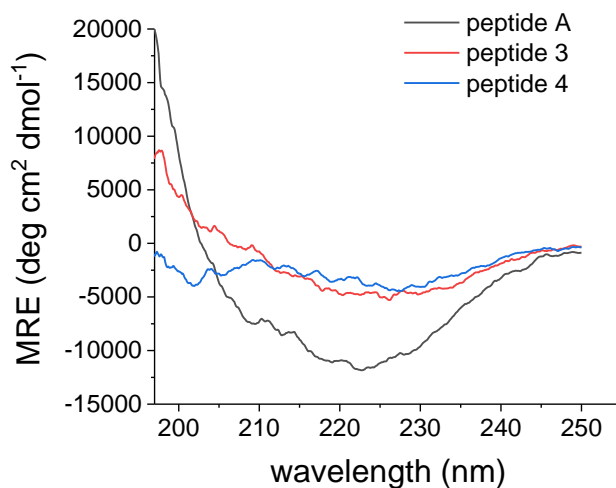


Figure 4.2 – Comparison of the secondary structure of the analog A and the analogs with mutations in position 31 at 5  $\mu$ M.

The first peptide aimed to understand how the increase of the hydrophobicity of the peptide A would affect its properties. This was accomplished by the modifications of residue in position X for an aromatic residue. The increase of the aromatic/hydrophobic interactions could explain the stabilization of the  $\beta$ -sheet/  $\beta$ -turn structure. The solubility of the peptide 3 decrease in comparison with the peptide A since the peptide 3 precipitated at 50  $\mu$ M, while the peptide A precipitated at 100  $\mu$ M. This result was predictable due to the increase of the peptide hydrophobicity.

On the other hand, the introduction of a charged residue in position X could affect both the peptide conformation and the solubility. The secondary structure of the peptide showed the presence of both  $\beta$ -sheet/  $\beta$ -turn and random coil content. The mutation in position X enabled the appearance of random

coil since the incorporation of the charged residue destabilize core structure. Nevertheless, this modification was not enough to increase the peptide solubility.

### 4.3. Effect of the modifications in the inhibition of the IAPP fibrillogenesis

The ThT assay was performed to analyse the peptides activities. Different ratios were tested to determine the lowest ratio where the peptide inhibit the IAPP fibrils formation.

#### 4.3.1. Inhibitory properties of the analogs with tags

The peptide 1 was not able to inhibit the IAPP fibrils formation for 7 days. However, it was able to inhibit at a ratio 1:5 for 24h. On the other hand, the peptide A and B were able to inhibit the IAPP fibrils formation for 7 days with the ratios of 1:5 and 1:2, respectively. Thus, the addition of tag 1 destroyed the ability to inhibit the IAPP fibrillogenesis.

The substitution of tag 1 for tag 2 prevented the IAPP fibrils formation with a ratio of 1:2. In comparison with the peptide A and B, the addition of those amino acids allowed the increase and maintenance of the peptide activity, respectively. Thus, this result together with the previous one demonstrated the importance of the N-terminus position (in peptide 2) in the inhibitory properties of the peptide.

The confirmation of the ThT experiments by TEM indicated contradictory results for the peptide 2. The amount of fibrils was higher in the ratio 1:5 than in the ratio 1:2. It had been proven that the ThT bound to IAPP fibrils and as a result the ThT emitted fluorescence. However, for the ratio 1:5 the fluorescence emission remained low. Further tests are required in order to find out the reason for the discrepancy between ThT and TEM results.

#### 4.3.2. Inhibitory properties of the analogs with mutations in specific residues

The activity of the peptide 3 appeared to decrease significantly since this peptide couldn't inhibit the IAPP fibrils formation for 24h. The peptide alone showed the formation of amorphous aggregates, and for that reason, the higher ratio wasn't tested. This result showed that the increase of the hydrophobicity destroyed the peptide activity.

On the other hand, the peptide 4 was capable of inhibiting the IAPP fibrils formation for 7 days at a ratio of 1:5, as the peptide A. Therefore, the addition of polar did not affect its activity. A possible explanation could be that this modification did not affect the interactions between the peptide and IAPP.

Overall, the shortest peptides, the peptide 3,4 and A had a lower activity rather than the longest peptides. This suggested that those positions were important in the peptide ability to inhibit the IAPP fibril formation.

#### 4.4. Effect of the interaction between IAPP and the analogs in the secondary structure

The other CD experiment measured the secondary structure of the IAPP alone, the peptide alone and the mixture between IAPP and the peptide over time. It aimed to understand whether there was an alteration in peptides conformation due to the interaction of both peptides.

The figure 4.3 showed a detailed view of the two local minimums, around 197 nm and 230 nm in figure 4.3 A and B, respectively.

Over time, the mixtures of the peptides showed with the increase or appearance of random coil content due to the interaction of IAPP and the peptides since the ellipticity values at time 7h are lower than the values at time 0h. To notice that main alterations occurred between the initial time point and the 1h. Afterwards the ellipticity value remained approximately the same showing that the interaction occurred within the first hour. The peptide 4 was the only peptide where theoretical sum of IAPP and the peptide alone ellipticity had the same shape. Thus, this result did not mean that the peptides did not interact. A detailed viewed of the random coil structure showed the increased of the random coil content demonstrating the interaction of both peptides. The interaction of the peptide and IAPP was also confirmed by the fluorescence titration.

On the other hand, the  $\beta$ -sheet content of the peptides decreased over 7 hours. Interestingly, the peptides whose inhibitory properties remained for 7 days, showed an increase in the  $\beta$ -sheet content within the first hour followed by a decreased of  $\beta$ -sheet content. This result suggested that the  $\beta$ -sheet structure could be a transitional structure from the peptides interaction. This transitional structure may be important for the inhibitory properties of the peptides.



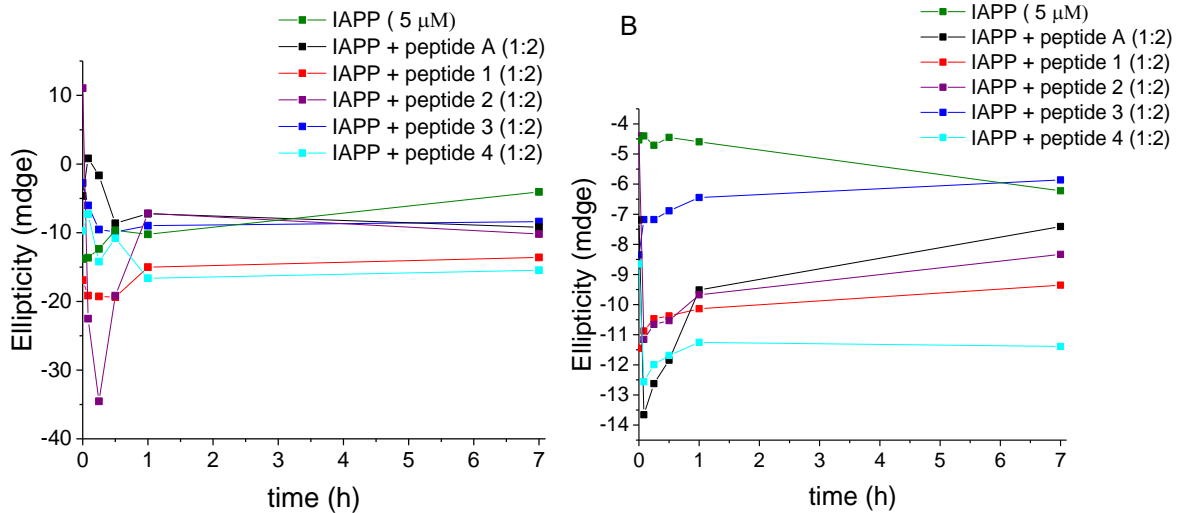


Figure 4.3 – Representation of the two local minimums obtained from the IAPP and the peptide mixture. The mixtures were measured at 0h, 5 min, 15 min, 30 min, 1h and 7h in 1xb containing 1% HFIP at room temperature. A – Representation of the 197 nm minimum. B – Representation of the 230 nm region.

Furthermore, there was not a relationship between the change in the secondary structure and the peptides activity since alteration in conformation was visible in all the peptides, the ones which inhibited and did not inhibit the IAPP fibrillogenesis.

## 4.5. Effect of the modifications on the analogs self-assembly and the binding affinity of the analogs to IAPP

Afterwards, the dissociation constants for the interactions of the 4 peptides with IAPP or themselves were determined. These dissociations constants aimed to understand if the peptides were able to bind to IAPP and the self- assembly propensity.

The peptide A bound only to IAPP in the monomeric form. Thereby, this binding was determinant for the inhibitory properties of this peptide.

### 4.5.1. Addition of tags

The figure 4.4 showed the differences of the three dissociation constant for the analogs A, B, 1 and 2.

The addition of the tags allowed the binding with high affinity of the monomeric form of the peptide to oligomeric IAPP. Thus, the N-terminus of the peptides B, 1 and 2 were important to the binding of the peptide to oligomeric IAPP. This could be due to the establishment of non-covalent interactions between

those residues and the oligomeric IAPP. The rest of the apparent dissociation constants didn't change in comparison to the peptide A.

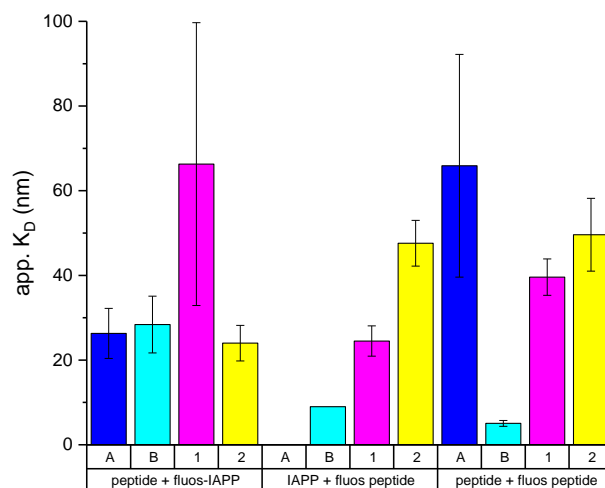


Figure 4.4 – Comparison of binding affinities of the synthesized analogs 1 and 2 with the control peptides, A and B. Mean value  $\pm$  SD (n=3) of apparent  $K_D$  estimated for the analogs with the tags.

#### 4.5.2. Mutations in specific residues

The peptides 3 and 4 differed only in the amino acid in position X in comparison with peptide A. This alteration changed mainly the ability of the peptides monomers to bind to IAPP oligomers, as it is shown in figure 4.5. The peptides A and 3 had hydrophobic residues in position X, while the peptide 4 had a polar residue. The peptides A and 3 were not able to bind to IAPP or with a low affinity, respectively. On the other hand, the peptide 4 bound with a high affinity to IAPP oligomers. Thereby, the polarity of the residue in this position changed the ability of the peptide to bind to IAPP oligomers.

Overall, the values demonstrated the absence of correlation between the peptides binding affinities and their activity.

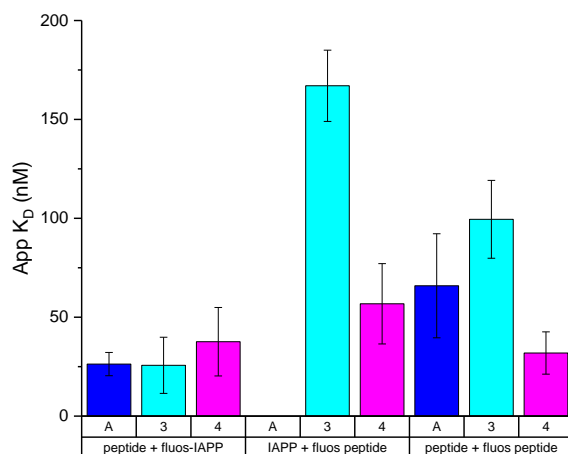


Figure 4.5 – Comparison of binding affinities of the synthesized analogs 3 and 4 with the peptide A. Mean value  $\pm$  SD (n=3) of apparent  $K_D$  estimated for the analogs with mutation in specific residues.

#### 4.6. Determination of the solubility by a centrifugation assay

The solubility of the peptides 3 and 4 were analysed by the centrifugation assay. The determination of the protein on the pellet and the supernatant by BCA allowed to calculate the amount of the peptide which precipitated. The results obtained in this assay were contradictory with the CD-concentration dependence results. At 20  $\mu$ M, the peptides 3 and 4 were present in the pellet, which meant that both precipitated, while the CD results showed precipitation at 50  $\mu$ M and 100  $\mu$ M for the peptides 3 and 4, respectively. The differences could be explained by non-specific binding of the peptide to the Eppendorf tube walls. In this case, the different surface of the Eppendorf tube and the cuvettes could alter the peptide propensity to bind it. Moreover, the peptide 4 showed around 10%, while the 20 min (which corresponded to the time 0h with centrifugation) did not show any soluble peptide. This result suggested that the centrifugation step may induce precipitation. Thus, the driving force in both time points were different. A possible solution was to perform the assay without the centrifugation assay to analysed if the peptide precipitated completely after 7 days.

Moreover, the presence of HFiP in the CD assay could also contribute to solubilization of the peptide. Therefore, the centrifugation assay should be repeated with the 1% of HFiP, the same conditions as the CD concentration dependence assay, to understand whether the presence of HFiP affect the peptide solubility.

To notice, the big error bars obtained for some point measurements, such as the 7<sup>th</sup> day in the peptide 4, were due to pipetting mistakes. Since the BCA is sensitive to the peptide concentration, small volumes variations will affect the final results, especially in this case, where small amount of peptide was used.

Additional more detailed information is to be found in the supplementary discussion in annex 5.

## 5. Conclusion and future perspective

The increase number of patients with diseases associated with amyloid fibrils have increased on the last decade and the outlook is to continue to grow in the next years, namely the T2D and neurodegenerative diseases, such as the Alzheimer's disease<sup>65</sup>. The optimization of the properties of designed peptides was mandatory to increase their potency, selectivity or pharmacokinetics parameters.

This work attempted to optimize the solubility and the inhibitory properties of designed peptides through the addition of diamino acid tags to N-terminus region and through mutations in the core structure of peptide A. The addition of two amino acids to the N-terminal region did not change the secondary structures of the peptide in comparison with the peptide A. However, the peptides solubility was inferior. The inhibitory properties of the peptides tested by ThT assay and TEM showed contradictory results for the peptide 2. This was the only inhibitor which was capable of inhibit the IAPP fibrillogenesis at a lower ratio than the peptide A. The peptide B, a longer version of peptide A, had the same size as the peptide 1 and 2. In comparison with this peptide, the secondary structure changed, with the loss of the random coil structure. The solubility and inhibitory capacity of peptide 2 were similar to the values obtained for the peptide B, while the peptide 1 displayed a lower solubility and loss the ability to inhibit IAPP fibrillogenesis. The different tags did not change the binding affinity to IAPP.

The differences between the tags provided new insights regarding the importance of the N-terminus amino acid and how the establishment of non-covalent interactions would affect the properties of the peptides.

Afterwards, the mutations in amino acid in the hydrophobic core, more specifically, in position X were performed to test how those alterations affected the activity of the peptide. Initially, the hydrophobic residue at position X was substituted by an aromatic one. This substitution did not alter the peptide conformation in comparison with peptide A but decreased its solubility. Furthermore, the peptide ability to inhibit the IAPP fibrils formation was destroyed with this substitution. On the other hand, the change of the residue at position X by a polar charged residue led to the appearance of random coil content. Despite the random coil structure, the solubility of the peptide 4 was similar to the solubility of the peptide A. The centrifugation assay to determine the solubility of the peptides provided different results from the CD – concentration dependence results. Moreover, the activity of peptide was the same as the peptide A. Thereby, this alteration did not increase the inhibitory properties of the peptides. Both peptides were able to bind with high affinity to the IAPP monomers and to self-assembly. These alterations were also compatible with the ability of the peptides to bind to oligomeric IAPP.

After the biophysical characterization of the peptides, *in vitro* test should be performed to understand if the cells were able to survive to the toxicity of IAPP in the presence of the peptides 2 and 4. An interesting possibility would be to add the tag 2 to the peptide 4 to understand if we could maintain the solubility of the peptide and increase its activity. Moreover, single mutations in other positions using charged polar residues should also be performed to understand which could be the best mutant. Double mutations

could also be tested in order to increase the solubility, but they must be performed carefully not to destroy the hydrophobic core.

In conclusion, the addition of the tags to the N-terminus of the peptide A did not increase the peptide solubility, but the activity of the peptide 2 was higher than the peptide A. On the other hand, the mutations in position X led to the loss and remain of the peptide function for the peptide 3 and 4, respectively. Thus, the substitution with a polar charged amino acid led to similar properties as the peptide A, with the increase of the random coil content. This feature was interesting since it could allow the optimization of the peptide solubility. However, the results demonstrated that longer peptides displayed a higher activity rather than the shorter peptides, but a lower solubility. Therefore, the optimal size must be pursued in order to optimize the peptides properties.

## 6. References

1. Dobson, C. M. Protein folding and misfolding. *Nature* **426**, 884–890 (2003).
2. Bukau, B. & Horwich, A. L. The Hsp70 and Hsp60 chaperone machines. *Cell* **92**, 351–366 (1998).
3. Hartl, F. Molecular Chaperones in the Cytosol: from Nascent Chain to Folded Protein. *Science* (80-. ). **295**, 1852 (2002).
4. Hammond, C. & Helenius, A. Quality control in the secretory pathway. *Isr. Med. Assoc. J.* **8**, 238–42 (2006).
5. Kaufman, R. J. *et al.* The unfolded protein response in nutrient sensing and differentiation. *Nat. Rev. Mol. Cell Biol.* **3**, 411–421 (2002).
6. Coop, G. M. *The Cell, 2nd edition A Molecular Approach.* (2000).
7. Chiti, F. & Dobson, C. M. Protein Misfolding, Amyloid Formation, and Human Disease: A Summary of Progress Over the Last Decade. *Annu. Rev. Biochem.* **86**, 27–68 (2017).
8. Dobson, C. M., Sali, A. & Karplus, M. Protein folding: A perspective from theory and experiment. *Angew. Chemie - Int. Ed.* **37**, 868–893 (1998).
9. Wolynes, P. G., Onuchic, J. N. & Thirumalai, D. Navigating the Folding Routes. **267**, (1995).
10. Dill, K. A. & Chan, H. S. From Levinthal to pathways to funnels. *Nat. Struct. Biol.* **4**, 10–19 (1997).
11. Fersht, A. R. Transition-state structure as a unifying basis in protein-folding mechanisms: Contact order, chain topology, stability, and the extended nucleus mechanism. *Proc. Natl. Acad. Sci.* **97**, 1525–1529 (2000).
12. Gregersen, N., Bross, P., Vang, S. & Christensen, J. H. Protein Misfolding and Human Disease. *Annu. Rev. Genomics Hum. Genet.* **7**, 103–124 (2006).
13. Hartl, F. U. & Hayer-Hartl, M. Converging concepts of protein folding in vitro and in vivo. *Nat. Struct. Mol. Biol.* **16**, 574–581 (2009).
14. Maurizi, M. R. & Li, C. C. AAA proteins: in search of a common molecular basis. International Meeting on Cellular Functions of AAA Proteins. *EMBO Rep.* **2**, 980–5 (2001).
15. Manuscript, A. & Non-folding, U. P. *NIH Public Access.* **1804**, (2011).
16. Dyson, H. J. & Wright, P. E. Intrinsically unstructured proteins and their functions. *Nat. Rev. Mol. Cell Biol.* **6**, 197–208 (2005).
17. Tartaglia, G. G. *et al.* Prediction of Aggregation-Prone Regions in Structured Proteins. *J. Mol. Biol.* **380**, 425–436 (2008).
18. Knowles, T. P. J., Vendruscolo, M. & Dobson, C. M. The amyloid state of proteins in human diseases. *Nat. Rev. Mol. Cell Biol.* **15**, 384–396 (2014).
19. Christian Wasmer,\* Adam Lange,\* Hélène Van Melckebeke,\* Ansgar B. Siemer,† Roland Riek, B. H. M. Amyloid Fibrils of the HET-s(218–289) Prion Form a b Solenoid with a Triangular Hydrophobic Core. **319**, 1523–1527 (2008).
20. Paravastu, A. K., Leapman, R. D., Yau, W.-M. & Tycko, R. Molecular structural basis for polymorphism in Alzheimer's  $\beta$ -amyloid fibrils. *Proc. Natl. Acad. Sci.* **105**, 18349–18354 (2008).
21. Eisenberg, D. & Jucker, M. The amyloid state of proteins in human diseases. *Cell* **148**, 1188–1203 (2012).
22. Knowles, T. P. *et al.* Roles of intermolecular forces in defining material properties of protein

- nanofibrils. *Science* (80-. ). **318**, 1900–1903 (2007).
23. Chalovich, J. M. & Eisenberg, E. The amyloid state of proteins in human diseases. *Magn Reson Imaging* **31**, 477–479 (2013).
  24. Sawaya, M. R. *et al.* Atomic structures of amyloid cross- $\beta$  spines reveal varied steric zippers. *Nature* **447**, 453–457 (2007).
  25. Ritter, C. *et al.* 3D structure of Alzheimer ' s amyloid- beta ( 1 – 42 ) fibrils. (2005).
  26. Morris, A. M., Watzky, M. A. & Finke, R. G. Protein aggregation kinetics, mechanism, and curve-fitting: a review of the literature. *Biochim. Biophys. Acta* **1794**, 375–397 (2009).
  27. Analytical, A. N. *et al.* An Analytical Solution to the Kinetics of Breakable Filament Assembly. **4**, 1533–1538 (1987).
  28. Cohen, S. I. A. *et al.* Proliferation of amyloid- 42 aggregates occurs through a secondary nucleation mechanism. *Proc. Natl. Acad. Sci.* **110**, 9758–9763 (2013).
  29. Karamanos, T. K., Kalverda, A. P., Thompson, G. S. & Radford, S. E. Progress in Nuclear Magnetic Resonance Spectroscopy Mechanisms of amyloid formation revealed by solution NMR. **89**, 86–104 (2015).
  30. Koudinov, A. R. & Berezov, T. T. Alzheimer ' s amyloid-beta ( A b ) is an essential synaptic protein , not neurotoxic junk. 71–79 (2004).
  31. Ittner, L. M. *et al.* Dendritic function of tau mediates amyloid- $\beta$  toxicity in alzheimer's disease mouse models. *Cell* **142**, 387–397 (2010).
  32. Manuscript, A. Synapses and Alzheimer ' s disease. 1–18 (2013). doi:10.1101/cshperspect.a005777.Synapses
  33. Barage, S. H. & Sonawane, K. D. Amyloid cascade hypothesis: Pathogenesis and therapeutic strategies in Alzheimer's disease. *Neuropeptides* **52**, 1–18 (2015).
  34. Henry W. Querfurth, M.D., Ph.D., and Frank M. LaFerla, P. . Mechanisms of Alzheimer's Disease. *N. Engl. J. Med.* **362**, 329–344 (2010).
  35. Coulson, E. J., Paliga, K., Beyreuther, K. & Masters, C. L. What the evolution of the amyloid protein precursor supergene family tells us about its function. *Neurochem. Int.* **36**, 175–184 (2000).
  36. Duce, J. A. *et al.* Iron-Export Ferroxidase Activity of  $\beta$ -Amyloid Precursor Protein is Inhibited by Zinc in Alzheimer's Disease. *Cell* **142**, 857–867 (2010).
  37. Turner, P. R., O'Connor, K., Tate, W. P. & Abraham, W. C. *Roles of amyloid precursor protein and its fragments in regulating neural activity, plasticity and memory. Progress in Neurobiology* **70**, (2003).
  38. Priller, C. *et al.* Synapse Formation and Function Is Modulated by the Amyloid Precursor Protein. *J. Neurosci.* **26**, 7212–7221 (2006).
  39. Lu, P. *et al.* Europe PMC Funders Group Three-dimensional structure of human  $\gamma$  -secretase. *Nature* **512**, 166–170 (2015).
  40. Haass, C. & Selkoe, D. J. Soluble protein oligomers in neurodegeneration: Lessons from the Alzheimer's amyloid  $\beta$ -peptide. *Nat. Rev. Mol. Cell Biol.* **8**, 101–112 (2007).
  41. Reitz, C. & Mayeux, R. Alzheimer disease: Epidemiology, Diagnostic Criteria, Risk Factors and

- Biomarkers. *Biochem Pharmacol.* **88**, 640–651 (2014).
42. Wolfe, M. S. *et al.* Two transmembrane aspartates in presenilin-1 required for presenelin endoproteolysis and gamma-secretase activity. *Nature* **398**, 513–517 (1999).
  43. De Strooper, B. *et al.* Deficiency of presenilin-1 inhibits the normal cleavage of amyloid precursor protein. *Nature* **391**, 387–390 (1998).
  44. Holtzman, D. M. *et al.* Apolipoprotein E isoform-dependent amyloid deposition and neuritic degeneration in a mouse model of Alzheimer's disease. *Proc. Natl. Acad. Sci.* **97**, 2892–2897 (2000).
  45. Karran, E., Mercken, M. & Strooper, B. De. The amyloid cascade hypothesis for Alzheimer's disease: An appraisal for the development of therapeutics. *Nat. Rev. Drug Discov.* **10**, 698–712 (2011).
  46. Nelson, P. T. *et al.* Correlation of Alzheimer Disease Neuropathologic Changes With Cognitive Status: A Review of the Literature. *J. Neuropathol. Exp. Neurol.* **71**, 362–381 (2012).
  47. Miller, E. C. *et al.* Tau phosphorylation and tau mislocalization mediate soluble A $\beta$  oligomer-induced AMPA glutamate receptor signaling deficits. *Eur. J. Neurosci.* **39**, 1214–1224 (2014).
  48. Chen, G. F. *et al.* Amyloid beta: Structure, biology and structure-based therapeutic development. *Acta Pharmacol. Sin.* **38**, 1205–1235 (2017).
  49. O'Nuallain, B., Shivaprasad, S., Kheterpal, I. & Wetzel, R. Thermodynamics of A $\beta$ (1-40) amyloid fibril elongation. *Biochemistry* **44**, 12709–12718 (2005).
  50. Booth, D. R. *et al.* Instability, unfolding and aggregation of human lysozyme variants underlying amyloid fibrillogenesis. *Nature* **385**, 787–793 (1997).
  51. Mroczko, B., Groblewska, M., Litman-Zawadzka, A., Kornhuber, J. & Lewczuk, P. Amyloid  $\beta$  oligomers (A $\beta$ Os) in Alzheimer's disease. *J. Neural Transm.* **125**, 177–191 (2018).
  52. Shankar, G. M. *et al.* Amyloid- $\beta$  protein dimers isolated directly from Alzheimer's brains impair synaptic plasticity and memory. *Nat. Med.* **14**, 837–842 (2008).
  53. Spires, T. L. Dendritic Spine Abnormalities in Amyloid Precursor Protein Transgenic Mice Demonstrated by Gene Transfer and Intravital Multiphoton Microscopy. *J. Neurosci.* **25**, 7278–7287 (2005).
  54. Xiao, Y. *et al.* HHS Public Access. **22**, 499–505 (2015).
  55. Schütz, A. K. *et al.* Atomic-resolution three-dimensional structure of amyloid b fibrils bearing the osaka mutation. *Angew. Chemie - Int. Ed.* **54**, 331–335 (2015).
  56. Colvin, M. T. *et al.* Atomic Resolution Structure of Monomorphic A $\beta$ <sub>42</sub> Amyloid Fibrils. *J. Am. Chem. Soc.* **138**, 9663–9674 (2016).
  57. Tycko, R. NIH Public Access. **154**, (2014).
  58. Bertini, I., Gonnelli, L., Luchinat, C., Mao, J. & Nesi, A. A new structural model of A $\beta$  fibrils. *J. Am. Chem. Soc.* **133**, 16013–16022 (2011). 40
  59. Scheidt, H. A., Morgado, I., Rothmund, S. & Huster, D. Dynamics of amyloid  $\beta$  fibrils revealed by solid-state NMR. *J. Biol. Chem.* **287**, 2017–2021 (2012).
  60. Tarus, B., Straub, J. E. & Thirumalai, D. Dynamics of Asp23-Lys28 salt-bridge formation in A $\beta$ <sub>10-35</sub> monomers. *J. Am. Chem. Soc.* **128**, 16159–16168 (2006).



61. Gremer, L. *et al.* Fibril structure of amyloid- b (1 – 42) by cryo – electron microscopy. *Science* (80-. ). **358**, 116–119 (2017).
62. Zraika, S. *et al.* Toxic oligomers and islet beta cell death: Guilty by association or convicted by circumstantial evidence? *Diabetologia* **53**, 1046–1056 (2010).
63. Shaw, J. E., Sicree, R. A. & Zimmet, P. Z. Global estimates of the prevalence of diabetes for 2010 and 2030. *Diabetes Res. Clin. Pract.* **87**, 4–14 (2010).
64. Zimmet, P., Alberti, K. G. M. M. & Shaw, J. Global and societal implications of the diabetes epidemic. *Nature* **414**, 782–787 (2001).
65. Chen, L., Magliano, D. J. & Zimmet, P. Z. The worldwide epidemiology of type 2 diabetes mellitus - Present and future perspectives. *Nat. Rev. Endocrinol.* **8**, 228–236 (2012).
66. Westermark, P. Quantitative studies on amyloid in the islets of Langerhans. *Ups. J. Med. Sci.* **77**, 91–94 (1972).
67. Clark, A. *et al.* Islet amyloid, increased A-cells, reduced B-cells and exocrine fibrosis: quantitative changes in the pancreas in type 2 diabetes. *Diabetes Res.* **9**, 151–159 (1988).
68. Hyaline Degeneration of Islands of Langerhans. (1901).
69. Zhao, H. L. *et al.* Prevalence and clinicopathological characteristics of islet amyloid in chinese patients with type 2 diabetes. *Diabetes* **52**, 2759–2766 (2003).
70. Butler, A. E. *et al.* Beta-cell deficit and increased beta-Cell apoptosis in humans with type 2 diabetes. *Diabetes* **52**, 102–10 (2003).
71. Fonseca, V. A. Defining and characterizing the progression of type 2 diabetes. *Diabetes Care* **32 Suppl 2**, (2009).
72. Höppener, J. W., Ahrén, B. & Lips, C. J. Islet amyloid and type 2 diabetes mellitus. *N. Engl. J. Med.* **343**, 411–419 (2000).
73. Christmanson, L., Rorsman, F., Stenman, G., Westermark, P., Betsholtz, C. The human islet amyloid polypeptide (IAPP) gene. *Febs* **267**, 160–166 (1990).
74. Cao, P. *et al.* Islet amyloid: From fundamental biophysics to mechanisms of cytotoxicity. *FEBS Lett.* **587**, 1106–1118 (2013).
75. Press, M., Jung, T., König, J., Grune, T. & Höhn, A. Protein aggregates and proteostasis in aging: amylin and  $\beta$ -cell function. *Mech. Ageing Dev.* 0–1 (2018). doi:10.1016/j.mad.2018.03.010
76. Cooper, G. J. *et al.* Purification and characterization of a peptide from amyloid-rich pancreases of type 2 diabetic patients. *Proc. Natl. Acad. Sci.* **84**, 8628–8632 (1987).
77. Westermark, P. *et al.* Amyloid fibrils in human insulinoma and islets of Langerhans of the diabetic cat are derived from a neuropeptide-like protein also present in normal islet cells. *Proc. Natl. Acad. Sci.* **84**, 3881–3885 (1987).
78. Hull, R. L., Westermark, G. T., Westermark, P. & Kahn, S. E. Islet amyloid: A critical entity in the pathogenesis of type 2 diabetes. *J. Clin. Endocrinol. Metab.* **89**, 3629–3643 (2004).
79. Jaikaran, E. T. A. S. & Clark, A. Islet amyloid and type 2 diabetes: From molecular misfolding to islet pathophysiology. *Biochim. Biophys. Acta - Mol. Basis Dis.* **1537**, 179–203 (2001).
80. Larson, J. L. & Miranker, A. D. The mechanism of insulin action on islet amyloid polypeptide fiber formation. *J. Mol. Biol.* **335**, 221–231 (2004).

81. Lutz, T. A. Control of energy homeostasis by amylin. *Cell. Mol. Life Sci.* **69**, 1947–1965 (2012).
82. Montane, J., Klimek-Abercrombie, A., Potter, K. J., Westwell-Roper, C. & Bruce Verchere, C. Metabolic stress, IAPP and islet amyloid. *Diabetes, Obes. Metab.* **14**, 68–77 (2012).
83. Hull, R. L., Westermark, G. T., Westermark, P. & Kahn, S. E. Islet amyloid: a critical entity in the pathogenesis of type 2 diabetes. *J. Clin. Endocrinol. Metab.* **89**, 3629–3643 (2004).
84. Clark, A. & Nilsson, M. R. Islet amyloid: A complication of islet dysfunction or an aetiological factor in Type 2 diabetes? *Diabetologia* **47**, 157–169 (2004).
85. Wazen, R. M. *et al.* The role of aromatic interactions in amyloid formation by islet amyloid polypeptide. **8**, 1385–1395 (2014).
86. Dunkelberger, E. B. *et al.* Deamidation accelerates amyloid formation and alters amylin fiber structure. *J. Am. Chem. Soc.* **134**, 12658–12667 (2012).
87. Nilsson, M. R., Driscoll, M. & Raleigh, D. P. Low levels of asparagine deamidation can have a dramatic effect on aggregation of amyloidogenic peptides: Implications for the study of amyloid formation. *Protein Sci.* **11**, 342–349 (2009).
88. Kajava, A. V., Baxa, U., Wickner, R. B. & Steven, A. C. A model for Ure2p prion filaments and other amyloids: the parallel superpleated beta-structure. *Proc. Natl. Acad. Sci. U. S. A.* **101**, 7885–7890 (2004).
89. Kajava, A. V., Aebi, U. & Steven, A. C. The parallel superpleated beta-structure as a model for amyloid fibrils of human amylin. *J. Mol. Biol.* **348**, 247–252 (2005).
90. Wiltzius, J. E. D. J. W. *et al.* Atomic structure of the cross- $\beta$  spine of islet amyloid polypeptide ( amylin ). *Insulin* 1467–1474 (2008). doi:10.1110/ps.036509.108.The
91. Manuscript, A. & Magnitude, S. NIH Public Access. **31**, 1713–1723 (2013).
92. Luca, S., Yau, W. M., Leapman, R. & Tycko, R. Peptide conformation and supramolecular organization in amylin fibrils: Constraints from solid-state NMR. *Biochemistry* **46**, 13505–13522 (2007).
93. Akter, R. *et al.* Islet Amyloid Polypeptide: Structure, Function, and Pathophysiology. *J. Diabetes Res.* **2016**, (2016).
94. Laybutt, D. R. *et al.* Endoplasmic reticulum stress contributes to beta cell apoptosis in type 2 diabetes. *Diabetologia* **50**, 752–763 (2007).
95. Casas, S. *et al.* Impairment of the Ubiquitin-Proteasome Pathway Is a Downstream Endoplasmic Reticulum Stress Response Induced By Extracellular Human Islet Amyloid Polypeptide and Contributes To Pancreatic. *Diabetes* **56**, 2284–2294 (2007).
96. Gurlo, T. *et al.* Evidence for proteotoxicity in  $\beta$  cells in type 2 diabetes: Toxic islet amyloid polypeptide oligomers form intracellularly in the secretory pathway. *Am. J. Pathol.* **176**, 861–869 (2010).
97. Formation, A. *et al.* Islets and Pancreas and Human Pancreas Is Not. **52**, 1102–1111 (2010).
98. Parks, J. K., Smith, T. S., Trimmer, P. A., Bennett, J. P. J. & Parker, W. D. J. Neurotoxic Abeta peptides increase oxidative stress in vivo through NMDA-receptor and nitric-oxide-synthase mechanisms, and inhibit complex IV activity and induce a mitochondrial permeability transition in vitro. *J. Neurochem.* **76**, 1050–1056 (2001).

99. Gupta, D. & Leahy, J. L. Islet amyloid and type 2 diabetes: Overproduction or inadequate clearance and detoxification? *J. Clin. Invest.* **124**, 3292–3294 (2014).
100. Watada, H. & Fujitani, Y. Minireview: Autophagy in Pancreatic  $\beta$ -Cells and Its Implication in Diabetes. *Mol. Endocrinol.* **29**, 338–348 (2015).
101. Rajamäki, K. *et al.* P38 $\delta$  MAPK: A novel regulator of NLRP3 inflammasome activation with increased expression in coronary atherogenesis. *Arterioscler. Thromb. Vasc. Biol.* **36**, 1937–1946 (2016).
102. Masters, S. L. *et al.* Activation of the NLRP3 inflammasome by islet amyloid polypeptide provides a mechanism for enhanced IL-1 $\beta$  2 in type 2 diabetes. *Nat. Immunol.* **11**, 897–904 (2010).
103. Zhang, S., Liu, J., Dragunow, M. & Cooper, G. J. S. Fibrillogenic Amylin Evokes Islet beta-Cell Apoptosis through Linked Activation of a Caspase Cascade and JNK1. *J. Biol. Chem.* **278**, 52810–52819 (2003).
104. Trikha, S. & Jeremic, A. M. Clustering and internalization of toxic amylin oligomers in pancreatic cells require plasma membrane cholesterol. *J. Biol. Chem.* **286**, 36086–36097 (2011).
105. Janson, J., Ashley, R. H., Harrison, D., McIntyre, S. & Butler, P. C. The mechanism of islet amyloid polypeptide toxicity is membrane disruption by intermediate-sized toxic amyloid particles. *Diabetes* **48**, 491–498 (1999).
106. Milanesi, L. *et al.* Direct three-dimensional visualization of membrane disruption by amyloid fibrils. *Proc. Natl. Acad. Sci.* **109**, 20455–20460 (2012).
107. Engel, M. F. M. *et al.* Membrane damage by human islet amyloid polypeptide through fibril growth at the membrane. *Proc. Natl. Acad. Sci.* **105**, 6033–6038 (2008).
108. Manuscript, A. Spectroscopy of Membrane Nanotubes. **1768**, 2026–2029 (2007).
109. Knight, J. D., Hebda, J. A. & Miranker, A. D. Conserved and Cooperative Assembly of Membrane-Bound  $\alpha$ -Helical States of Islet Amyloid Polypeptide. *Biochemistry* **45**, 9496–9508 (2006).
110. Seeliger, J., Weise, K., Opitz, N. & Winter, R. The effect of A $\beta$  on IAPP aggregation in the presence of an isolated  $\beta$ -cell membrane. *J. Mol. Biol.* **421**, 348–363 (2012).
111. Li, L. & Hölscher, C. Common pathological processes in Alzheimer disease and type 2 diabetes: A review. *Brain Res. Rev.* **56**, 384–402 (2007).
112. Andreetto, E. *et al.* Identification of hot regions of the A $\beta$ -IAPP Interaction interface as high-affinity binding sites in both cross- and self-association. *Angew. Chemie - Int. Ed.* **49**, 3081–3085 (2010).
113. Shim, S.-H. *et al.* Two-dimensional IR spectroscopy and isotope labeling defines the pathway of amyloid formation with residue-specific resolution. *Proc. Natl. Acad. Sci.* **106**, 6614–6619 (2009).
114. Mazor, Y., Gilead, S., Benhar, I. & Gazit, E. Identification and characterization of a novel molecular-recognition and self-assembly domain within the islet amyloid polypeptide. *J. Mol. Biol.* **322**, 1013–1024 (2002).
115. Tenidis, K. *et al.* Identification of a penta- and hexapeptide of islet amyloid polypeptide (IAPP) with amyloidogenic and cytotoxic properties. *J. Mol. Biol.* **295**, 1055–1071 (2000).
116. Petkova, A. T. *et al.* A structural model for Alzheimer's  $\beta$ -amyloid fibrils based on experimental constraints from solid state NMR. *Proc. Natl. Acad. Sci. U. S. A.* **99**, 16742–7 (2002).

117. Luo, J., Wärmländer, S. K. T. S., Gräslund, A. & Abrahams, J. P. Cross-interactions between the Alzheimer disease amyloid- $\beta$  peptide and other amyloid proteins: A further aspect of the amyloid cascade hypothesis. *J. Biol. Chem.* **291**, 16485–16493 (2016).
118. O’Nuallain, B., Williams, A. D., Westermark, P. & Wetzel, R. Seeding Specificity in Amyloid Growth Induced by Heterologous Fibrils. *J. Biol. Chem.* **279**, 17490–17499 (2004).
119. Ono, K. *et al.* Exogenous amyloidogenic proteins function as seeds in amyloid  $\beta$ -protein aggregation. *Biochim. Biophys. Acta - Mol. Basis Dis.* **1842**, 646–653 (2014).
120. Moreno-Gonzalez, I. *et al.* Molecular interaction between type 2 diabetes and Alzheimer’s disease through cross-seeding of protein misfolding. *Mol. Psychiatry* **22**, 1327–1334 (2017).
121. Wilson, M. E. *et al.* Peripheral Hyperinsulinemia Promotes Tau Phosphorylation In Vivo. *Hybridoma* **54**, 3343–3348 (2005).
122. Zhao, W.-Q., Chen, H., Quon, M. J. & Alkon, D. L. Insulin and the insulin receptor in experimental models of learning and memory. *Eur. J. Pharmacol.* **490**, 71–81 (2004).
123. Watson, G. S. & Craft, S. Modulation of memory by insulin and glucose: neuropsychological observations in Alzheimer’s disease. *Eur. J. Pharmacol.* **490**, 97–113 (2004).
124. Holscher, C. Synaptic plasticity and learning and memory: LTP and beyond. *J. Neurosci. Res.* **58**, 62–75 (1999).
125. Schubert, M. *et al.* Insulin receptor substrate-2 deficiency impairs brain growth and promotes tau phosphorylation. *J. Neurosci.* **23**, 7084–7092 (2003).
126. Zhao, A. Z. *et al.* Leptin induces insulin-like signaling that antagonizes cAMP elevation by glucagon in hepatocytes. *J. Biol. Chem.* **275**, 11348–11354 (2000).
127. Eldar-Finkelman, H., Schreyer, S. A., Shinohara, M. M., LeBoeuf, R. C. & Krebs, E. G. Increased glycogen synthase kinase-3 activity in diabetes- and obesity-prone C57BL/6J mice. *Diabetes* **48**, 1662–1666 (1999).
128. Farris, W. *et al.* Insulin-degrading enzyme regulates the levels of insulin, amyloid beta-protein, and the beta-amyloid precursor protein intracellular domain in vivo. *Proc. Natl. Acad. Sci. U. S. A.* **100**, 4162–4167 (2003).
129. Kurochkin, I. V. Insulin-degrading enzyme: embarking on amyloid destruction. *Trends Biochem. Sci.* **26**, 421–425 (2001).
130. Gasparini, L. & Xu, H. Potential roles of insulin and IGF-1 in Alzheimer’s disease. *Trends Neurosci.* **26**, 404–406 (2003).
131. Yamagishi, S., Nakamura, K., Inoue, H., Kikuchi, S. & Takeuchi, M. Serum or cerebrospinal fluid levels of glyceraldehyde-derived advanced glycation end products (AGEs) may be a promising biomarker for early detection of Alzheimer’s disease. *Med. Hypotheses* **64**, 1205–1207 (2005).
132. Takeuchi, M. & Yamagishi, S. TAGE (toxic AGEs) hypothesis in various chronic diseases. *Med. Hypotheses* **63**, 449–452 (2004).
133. Hudson, S. A., Ecroyd, H., Dehle, F. C., Musgrave, I. F. & Carver, J. A. (-)-Epigallocatechin-3-Gallate (EGCG) Maintains  $\kappa$ -Casein in Its Pre-Fibrillar State without Redirecting Its Aggregation Pathway. *J. Mol. Biol.* **392**, 689–700 (2009).
134. Ehrnhoefer, D. E. *et al.* EGCG redirects amyloidogenic polypeptides into unstructured, off-

- pathway oligomers. *Nat. Struct. Mol. Biol.* **15**, 558–566 (2008).
135. Goyal, D., Shuaib, S., Mann, S. & Goyal, B. Rationally Designed Peptides and Peptidomimetics as Inhibitors of Amyloid- $\beta$  (A $\beta$ ) Aggregation: Potential Therapeutics of Alzheimer's Disease. *ACS Comb. Sci.* **19**, 55–80 (2017).
  136. Fosgerau, K. & Hoffmann, T. Peptide therapeutics: Current status and future directions. *Drug Discov. Today* **20**, 122–128 (2015).
  137. Yan, L.-M., Tatarek-Nossol, M., Velkova, A., Kazantzis, A. & Kapurniotu, A. Design of a mimic of nonamyloidogenic and bioactive human islet amyloid polypeptide (IAPP) as nanomolar affinity inhibitor of IAPP cytotoxic fibrillogenesis. *Proc. Natl. Acad. Sci. U. S. A.* **103**, 2046–51 (2006).
  138. Andreetto, E. *et al.* A Hot-Segment-Based Approach for the Design of Cross-Amyloid Interaction Surface Mimics as Inhibitors of Amyloid Self-Assembly. *Angew. Chemie - Int. Ed.* **54**, 13095–13100 (2015).
  139. Spanopoulou, A. *et al.* Designed Macrocyclic Peptides as Nanomolar Amyloid Inhibitors Based on Minimal Recognition Elements. *Angew. Chemie Int. Ed.* (2018). doi:10.1002/anie.201802979
  140. Sewald, N. & Jakubke, H.-D. *Peptides: Chemistry and Biology.* (2002). doi:10.1002/352760068X
  141. Marrese, M., Guarino, V. & Ambrosio, L. Atomic Force Microscopy: A Powerful Tool to Address Scaffold Design in Tissue Engineering. *J. Funct. Biomater.* **8**, 7 (2017).
  142. Raj, A. Spectroscopy for the Biological Sciences. *Mcgill J. Educ.* **39**, 221–223 (2004).
  143. Ranjbar, B. & Gill, P. Circular dichroism techniques: Biomolecular and nanostructural analyses- A review. *Chem. Biol. Drug Des.* **74**, 101–120 (2009).
  144. Doderio, V. I., Quirolo, Z. B. & Sequeira, M. A. Biomolecular studies by circular dichroism. *Front. Biosci. (Landmark Ed.)* **16**, 61–73 (2011).
  145. Kelly, S. M., Jess, T. J. & Price, N. C. How to study proteins by circular dichroism. *Biochim. Biophys. Acta* **1751**, 119–139 (2005).
  146. Manavalan, P. & Johnson, W. C. J. Variable selection method improves the prediction of protein secondary structure from circular dichroism spectra. *Anal. Biochem.* **167**, 76–85 (1987).
  147. Kelly, S. M. & Price, N. C. The use of circular dichroism in the investigation of protein structure and function. *Curr. Protein Pept. Sci.* **1**, 349–384 (2000).
  148. Ban, T., Hamada, D., Hasegawa, K., Naiki, H. & Goto, Y. Direct observation of amyloid fibril growth monitored by thioflavin T fluorescence. *J. Biol. Chem.* **278**, 16462–16465 (2003).
  149. LeVine, H. 3rd. Stopped-flow kinetics reveal multiple phases of thioflavin T binding to Alzheimer beta (1-40) amyloid fibrils. *Arch. Biochem. Biophys.* **342**, 306–316 (1997).
  150. Levine, H. Thioflavine T interaction with synthetic Alzheimer's disease  $\beta$ -amyloid peptides: Detection of amyloid aggregation in solution. *Protein Sci.* **2**, 404–410 (1993).
  151. Naiki, H., Higuchi, K., Hosokawa, M. & Takeda, T. Fluorometric determination of amyloid fibrils in vitro using the fluorescent dye, thioflavin T1. *Anal. Biochem.* **177**, 244–249 (1989).
  152. Voropai, E. S. *et al.* Spectral properties of thioflavin T and its complexes with amyloid fibrils. *J. Appl. Spectrosc.* **70**, 868–874 (2003).
  153. Motulsky, H. & Christopoulos, A. Fitting Dose Response Curves. *Fitting Model. to Biol. data using linear nonlinear Regres. . A Pract. Guid. to curve fitting* (2002).